ABSTRACT

ALVAREZ, JOSE SANTOS. Factors Affecting Growth of *Pinus radiata* in Chile. (Under the direction of Dr H. Lee Allen).

The Chilean forestry industry is based on hundreds of thousands of hectares of *Pinus radiata* plantations that have been established in a variety of soil and climate conditions. This approach has resulted in highly variable plantation productivity even when the best available technology was used. Little information is known about the ecophysiology basis for this variability.

We explored the spatial and temporal variation of stand growth in Chile using a network of permanent sample plots from Modelo Nacional de Simulación de Pino radiata. We hypothesized that the climate would play an important role in the annual variations in productivity.

To answer these questions we developed the following projects:

1. Determination of site resource availability from historical data from automatic weather stations (rainfall, temperatures) and a geophysical model for solar irradiation,
2. Determination of peak annual leaf area index (LAI) for selected permanent sample plots using remote sensing technologies,
3. Analysis of soil, climate, canopy and stand factors affecting the *Pinus radiata* plantation growth and the use efficiency of site resources.

For project 1, we estimated solar irradiation using the *r.sun*, Hargreaves-Samani (HS), and Bristow-Campbell (BC) models and validated model estimates with observations from weather stations. Estimations from a calibrated *r.sun* model accounted for 94 % of the variance ($r^2 = 0.94$) in monthly mean measured values. The r.sun model performed quite well for a wide range of Chilean conditions when compared with the HS and BC models. Our estimates of global irradiation may be improved with better estimates of cloudiness as they

become available. Our model was able to provide spatial estimates of daily, weekly, monthly and yearly solar irradiation.

For project 2, we estimated the inter-annual variation of LAI (Leaf Area Index), using remote sensing technologies. We determined LAI using Landsat Thematic Mapper (TM) data covering a 5 year period (2005-2009) for a network of permanent sample plots in *Pinus radiata* plantations in Chile. In 2009, we calculated LAI from ground measurements using LI-COR LAI-2000 and TRAC instruments on each one hectare plot. These values of LAI were regressed against Simple Ratio (SR), Normalized Difference Vegetation Index (NDVI) and Reduced Simple Ratio (RSR), derived from the TM 2009 data. Linear relationships were strong with R^2 values of 0.65 for SR, 0.61 for NDVI and 0.67 for RSR. Using the RSR relationship, LAI values were estimated for the network of permanent sample plots of *Pinus radiata* plantations over the whole period.

For project 3, we examined environmental factors affecting growth rates of *Pinus radiata* in Chile. Water availability (as affected by precipitation, soil water holding capacity, and potential evapotranspiration) appeared to be the factor most limiting to leaf area and growth. Maximum growing season temperature also negatively affected growth. Sites with highest productivities had the lowest annual water deficits and the most productive sites used water and light more efficiently. Good sites produced 1.6 as compared to 0.49 kg of wood per m^3 of evapotranspired water for less productive sites. In addition, productive stands produced 0.5 as compared to 0.31 g of wood per MJ for less productive sites.

Factors Affecting Growth of *Pinus radiata* in Chile

by

José Santos Álvarez

A dissertation submitted to the Graduate Faculty of
North Carolina State University
in partial fulfillment of the
requirements for the degree of
Doctor in Philosophy

Forestry

Raleigh, North Carolina

2010

APPROVED BY:

_____	_____
H. Lee Allen Committee Chair	Conghe Song
_____	_____
Jose L. Stape	Bronson P. Bullock

DEDICATION

To my lovely wife Dina, my sons Ignacio and Sebastian and my daughter Maria Paz

BIOGRAPHY

Jose Alvarez was born in Los Angeles, Chile. During his teen years, he discovered the importance of education to improve the quality of life of the people. He was an enthusiastic reader of books and scientific magazines. He graduated with a BS in Forest Engineering from University of Concepcion in 1987 and went to work as research forester for CMPC Company where he spent the last 20 years. He married Dina in October 1989. While with CMPC, he developed his career in Research and Development working in several areas including harvesting and transportation, GIS and forest mensuration, and finally silviculture, where he could develop the most interested and exciting scientific challenges. He also taught classes in GIS, Financing and Silviculture and Operational Research at the University of Concepcion and Catholic University of Concepcion. He completed his Master in Agricultural Economics at Catholic University in Santiago. In 2006, Jose spent one year at NCSU working as a visitor scholar doing analysis of experiments for the Forest Nutrition Cooperative. During the same year he decided to apply for a PhD in Forestry under direction of Dr H. Lee Allen. Dr Allen has been one of Jose's great friends as well as a scientific mentor.

ACKNOWLEDGEMENTS

I really want to thank my family, especially my wife who has been the most relevant friend and supporter to afford very complicate and stressful challenges. Thanks my older son Ignacio, whose silence and difference changed my life forever. Thanks also my two other kids, Sebastian and Maria Paz, for their strength to understand and to share with us big changes in our lives. All my family makes me happy every single day.

Lee Allen, my friend, academic and scientific tutor, thanks for the opportunity to be here after several years of conversations and no little effort, thanks finally for believing in me. With you Lee, I will have a permanent spiritual debt. Blessings for you, Sunny, Rachel and Chris.

Thanks to my advisors Dr Jose Stape, Dr Conghe Song (UNC-Chapel Hill), and Dr Bronson Bullock.

I really want to thank my dear friends and colleagues at NCSU, VT and UDEC including Jose Luis Zerpa, Alicia Peduzzi, Leandra Blevins, Tim Albaugh, Jesus Espinoza, Cristián Montes, Rafael Rubilar and Omar Carrero and my friends and all life colleagues from Forestal Mininco, Daniel Contesse, Fernando Dunn, Patricio Santibáñez, Jean Pierre Lasserre, Patricio Tapia, Francisco Rodriguez, Luis de Ferrari, Jose Albistur, Oscar Mardones and many others for their support and encouragement. Thanks to Dr Miguel

Espinosa, my friend at Universidad de Concepcion, who always encouraged me to follow in the line of intellectual challenges. Special thanks for my friend Jaime Rodriguez from Masisa.

I want to express special gratitude to Andrea Avaria, who worked very hard to measure plots and LAI in the field. Additional thanks to the team of Modelo Nacional de Simulación of Pino radiata, especially Dr. Pedro Real and Cristián Higuera. Special thanks also to Marcelo Miranda and Catalina Gertsmann from Pontificia Universidad Católica de Chile. Thanks for NCSU-VT-UDEC Forest Nutrition Cooperative.

Finally, I want to thank CONICYT-Chile for supporting my studies in the US.

TABLE OF CONTENTS

Chapter 3. FACTORS AFFECTING THE GROWTH OF RADIATA PINE PLANTATIONS IN CHILE

LIST OF TABLES

LIST OF FIGURES

INTRODUCTION

Chapter 1. SOLAR ESTIMATION IN CENTRAL CHILE

Chapter 3. FACTORS AFFECTING THE GROWTH OF RADIATA PINE PLANTATIONS IN CHILE

INTRODUCTION

Factors Affecting the Growth of Radiata Pine Plantations in Chile

The problem

To meet the demand for wood by the Chilean forestry industry, hundreds of thousands of hectares of *Pinus radiata* plantations have been established during the last 20 years. Plantations were first established on highly eroded soils as this land was less expensive. More recently plantations have been established on more productive soils such as recent volcanic ashes. This approach generated a mosaic of conditions where the plantation productivity is highly variable, even where the best available technology was used.

The network of 193 permanent sample plots (PSP) of the Modelo Nacional de Simulación de Pino radiata (Insigne Model, Real 2006) provides a valuable data set representing the range of conditions where *Pinus radiata* grows in Chile (Figure 1).

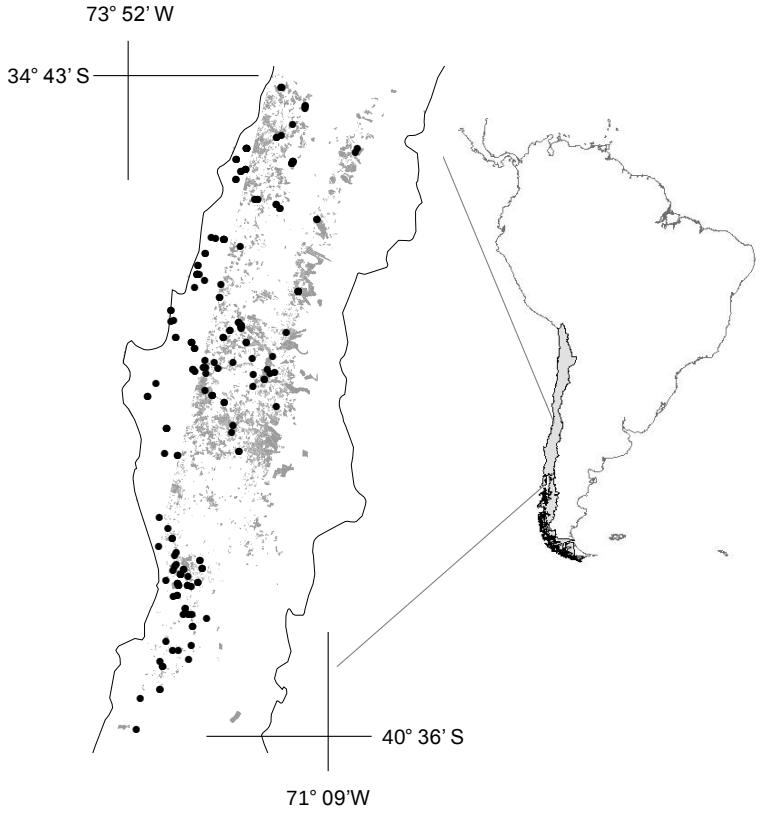

Figure 1. Location permanent sample plots of Insigne model and distribution of *Pinus radiata* plantations in Chile.

We use a subset of these plots to explore the sensitivity of stand growth to changes in growth-limiting factors (Figures 2 and 3). Mean growth sensitivity corresponds to the difference between two adjacent stand volume growth for a specific plot divided by the mean of the two increments, averaged over the entire time series (2005 to 2008). A plot with a high mean sensitivity is hypothesized to have experienced more growth limitation due to environmental factors, such as climate (Fritts 1976, Holman 2006).

$$Mean\_sensitivity = \sum_{i=1}^{4} abs\left[\frac{(x_i - x_{i-1})}{((x_i + x_{i-1})/2)}\right]/(n-1)$$

Where,

x_i = Current annual increment year *i*

x_{i-1} = Current annual increment previous year

n = years

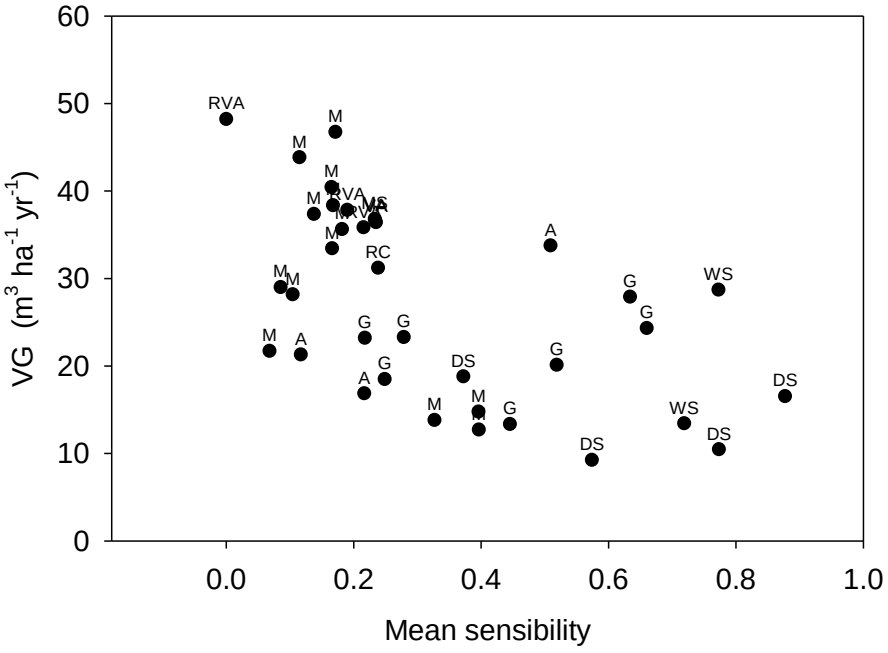

Figure 2. Sensitivity of permanent sample plots of Pinus radiata based on mean sensitivity and average current annual volume increment (VG: Volume growth, [m3 ha-1 yr-1]) during the time period 2005-2008. (A: Aluvial [Inceptisol]; DS: Dry Sand [Andisol]; G: Granitic [Alfisol]; M: Metamorphic [Ultisol]; MS: Marine Sediments [Alfisol]; RC: Red Clay [Alfisol]; RVA: Recent Volcanic Ash [Andisol, Ultisol] ; WS: Wet Sands [Mollisol]).

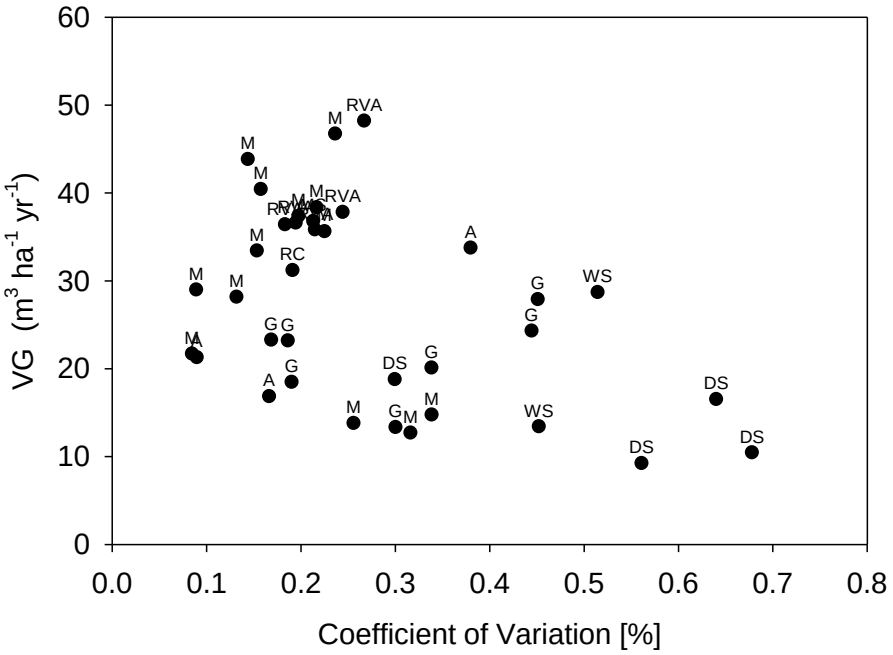

Figure 3. Sensitivity of permanent sample plots of Pinus radiata based on coefficient of variation and average current annual volume increment (VG: Volume growth, [m3 ha-1 yr-1]) during the time period 2005-2008. (A: Aluvial [Inceptisol]; DS: Dry Sand [Andisol];]; G: Granitic [Alfisol]; M: Metamorphic [Ultisol]; MS: Marine Sediments [Alfisol]; RC: Red Clay [Alfisol]; RVA: Recent Volcanic Ash [Andisol, Ultisol] ; WS: Wet Sands [Mollisol]).

Dry sandy soils had the highest mean sensitivity and recent volcanic ash soils had less sensitivity than red clay and vertisols. Similarly, dry sandy soils showed higher coefficient of variations and lower growth than volcanic ash and metamorphic soils.

This exploratory analysis provided ideas about the spatial and temporal variation of stand growth in Chile, and we can hypothesize that the climate could explain an important part of the changes in annual productivity, however we don't know exactly what resources are most important:

- Is the rainfall amount and distribution the most limiting factor?,

- Is minimum or maximum temperatures variations?,
- Incoming radiation?,
- Nutrient availability?.

Additionally, we can ask questions at a regional scale:

- Which plantations are using more efficient water, light and nutrients?,
- Is it financially profitable to establish plantations on dry sites?,
- Is it environmentally better to increase the area of fast growing plantations on dry or wet sites?,

To answer these questions we developed the following steps:

1. Determination of site resource availability from historical data from automatic weather stations (rainfall, temperatures) and a geophysical model for solar irradiation,
2. Determination of peak annual Leaf Area Index (LAI) for selected permanent sample plots using remote sensing technologies,
3. Analysis of soil, climate, canopy and stand factors affecting the *Pinus radiata* plantation growth and the use efficiency of site resources.

References

Fritts, H.C. 1976. Tree Rings and Climate. Academic press, London.

Holman, M.L. and D.L. Petersen. 2006. Spatial and temporal variability in forest growth in the Olympic Mountains, Washington: sensitivity to climatic variability. Can. J. For. Res. 36: 92-104.

Real, P. 2006. National Growth and Yield Simulation Project: example of cooperation among private sector and research institutes. The Second International Symposium on Plant Growth Modeling, Simulation, Visualization and Applications. November 13-17, 2006, Beijing, P.R. China.

CHAPTER 1

Estimation of Solar Irradiation in Central Chile

Abstract

Monthly global solar irradiation for the central region of Chile was estimated using the *r.sun* model and validated with observations from automatic weather stations. We analyzed the performance of the results of global irradiation with Hargreaves-Samani (HS) and Bristow-Campbell (BC) models. Estimations from a calibrated *r.sun* model accounted for 94 % of the variance ($r^2 = 0.94$) in monthly mean measured values. The models performed very well for a wide area of Chilean conditions when we compared them with the HS and BC models. Our estimates of global irradiation may be improved with further calibration with ground measurements and better estimates of cloudiness as they become available. Our model was able to provide spatial estimates of daily, weekly, monthly and yearly solar irradiation.

1. Introduction

Favorable soil and climatic conditions in the central southern region of Chile favor production of numerous crops including wheat, fruits and timber. Crop productivity is highly correlated with climatic conditions (solar irradiation, rainfall amount and distribution, and temperature). This area generally has a Mediterranean climate, with dry summers. However climatic conditions can vary dramatically over short distances due to the effects of the Pacific Ocean and the Coastal and Andes ranges. To predict productivity under these conditions, climate data are essential. Several process-based models such as 3-PG (Landsberg and Waring 1997; Coops et al. 1998; Tickle et al. 2001; Sands 2002; Almeida et al. 2004; Stape et al. 2004), Biomass (McMurtrie 1990), Cabala (Battaglia et al. 2004), and Maestro (Wang and Jarvis 1990), use climate, soil and physiological parameters as input variables. For all these models, solar irradiation is the driver variable.

Process-based models have not been widely used in Chile due to the lack solar irradiation data. Several efforts have been undertaken to predict global radiation in Chile (Yilmaz et al. 2007; Meza and Varas 2005) but only for specific locations and not over wide regions. Because of this gap, between the need for and availability of the irradiation data, several options have been developed to predict solar irradiation with mechanistic models using recorded meteorological data (Kermel 1988; Bindi 1991; Muneer 2000; Coops 2000; Ball 2004; Almeida 2003), remote sensors (Cano 1986; Diabate 1989; Garatuza-Payan 2001; Suri and Hofierka 2004; Lefevre et al. 2007), or geophysical calculations using the solar constant and the discount of transmissivity through the atmosphere (Suri and Hofierka 2004; Ball 2004). Latter models have been used in Europe (Hofierka and Suri 2002; Romero et al. 2008), specific locations in Chile (Yilmaz et al. 2007), and the United States (Ball 2004).

During the last two decades, due to the availability of more powerful computer hardware and geographical information systems (GIS), there has been significant progress in the

development of irradiation models (Suri and Hofierka 2004). These models provide rapid, cost-efficient and accurate estimation of solar irradiation over large territories, considering surface inclination, aspect and shadowing effects (Hofierka and Suri 2002).

Solar Analyst developed under ArcMap GIS, generates an upward-looking hemispherical view shed for each cell of the digital elevation model (DEM). It then generates sun-maps and sky-maps to rapidly calculate direct and diffuse radiation. This model is appropriate for the study of solar irradiation in DEMs and for short periods (Romero et al. 2008). This model is not flexible for transmissivity calculations and diffuses proportion (Hofierka and Suri 2002).

A relatively new approach, called ***r.sun*** model (Suri and Hofierka 2004) and implemented under an open source GRASS GIS environment (Neteler and Mitasova 2008), provided a more flexible and spatially explicit tool to estimate solar irradiation. This open source implementation allows for future improvements and applications.

The term irradiance is used to consider the solar power (instantaneous energy) falling on unit area per unit time [W m^{-2}]. The term irradiation is used to consider the amount of solar energy falling on unit area over a stated time interval [Wh m^{-2}] (Hofierka and Suri 2002).

The interaction of solar radiation with the earth's atmosphere and surface is determined by:

a. the earth's geometry, revolution and rotation (declination, latitude, solar hour angle);
b. terrain (elevation, surface inclination and orientation, shadows);
c. and atmospheric attenuation (scattering, absorption) by:
    - Gases (air molecules, ozone, CO_2, and O_2)
    - Solid and liquids particles (aerosols, including non-condensed water),
    - Clouds (condensed water)

The first group of factors determines the available extraterrestrial radiation. This radiation input to the earth's is modified by the terrain topography (slope and aspect), as well as shadowing effects of neighboring terrain features. The elevation determines the attenuation of radiation by the thickness of the atmosphere.

The extraterrestrial solar radiation path through the atmosphere is attenuated by several atmospheric constituents, namely gases, liquid and solid particles and clouds.

The attenuation by gas elements describes clear and dry (Rayleigh) atmosphere and is given by its relative optical air mass and optical thickness. The attenuation by solid and liquid particles is described by the Linke turbidity (T_{LK}). It indicates the optical density of hazy and humid atmosphere in relation to a clean and dry atmosphere. The values of turbidity factor differ spatially in a similar degree of magnitude and these differences are correlated with the terrain elevation. It also increases with an intensity of industrialization and urbanization.

Clouds are the strongest attenuates and their determination requires great deal of information regarding instantaneous thickness, position and number of layers of clouds, as well their optical properties (Hofierka and Suri 2002).

The ***r.sun*** model estimates global radiation under clear-sky conditions from the sum of its beam, diffuse and reflected components. While the calculation of the beam component is quite straightforward, the main difference between various models is in treatment of the diffuse component. This component depends on climate and regional terrain conditions and somehow is often the largest source of estimation error (Hofierka and Suri 2002).

Overcast radiation can be calculated from the clear-sky values by application of a factor parameterizing the attenuation caused by cloudiness. The clear-sky index (K_c) represents the

ratio between global irradiation under overcast (G_h) and cloud free (G_{hc}) conditions on a horizontal surface and its values range between 0.25 to 1.00:

$$K_c = G_h / G_{hc}$$

In addition to ***r.sun*** model, there are several other mechanistic models that predict solar irradiation (Ball 2004).

To calculate the solar irradiation on the earth's surface it will necessary to follow several steps, first calculating the extraterrestrial radiation and next reducing this value through some modifiers related day of the year, distance from the atmosphere to the ground and composition of the air (e.g. dust, aerosols, water).

The first step is to determine the extraterrestrial radiation (R_a, in [MJ m^{-2} day^{-1}]), which may be calculated for any given day of the year and latitude, according equations from Duffie and Beckman (1980).

$$R_a = \left(\frac{24 * 60}{\pi}\right) G_{sc} d_r [\omega_s \sin\delta \sin\emptyset + \cos\emptyset \cos\delta \sin\omega_s]$$

Where:

G_{sc} = Solar constant = 0.082 [MJ m^{-2} min^{-1}]

d_r = correction for eccentricity of Earth's orbit around the sun on day *i* of the year:

$$d_r = 1 + 0.033\ cos\left(\frac{2\pi}{365} i\right)$$

ω_s = sunrise hour angle [radians] :

$$\omega_s = cos^{-1}(-\tan\emptyset \tan\delta)$$

δ = declination of the sun above the celestial equator in radians on day *i* of the year:

$$\delta = 0.409 \sin\left(\frac{2\pi}{365} i - 1.39\right)$$

Φ = latitude [radians]

φ = Latitude in radians converted from latitude (*L*) in degrees:

$$\varphi = \frac{\pi L}{180}$$

Following this calculation we can obtain the incoming solar radiation on the ground (R_s):

$$R_s = R_a * T_t$$

Where R_s is the solar radiation at the Earth's surface [MJ m^{-2} day^{-1}], R_a is the extraterrestrial radiation and T_t is the atmospheric transmissivity.

Different models have been developed to calculate T_t, based mostly on empirical coefficients, temperatures differentials, cloudiness, or daily sunshine hours (Ball 2004).

Hargreaves and Samani (1982) for instance developed a simple model for estimating R_s. They propose that T_t for a given day was proportional to the square root of the difference between maximum temperature (T_{max}) and minimum temperature (T_{min}).

Following this work, Annandale et al. (2002) proceed to modify the model to include a correction for altitude (z, in [m]) such that:

$$T_t = k_{Rs}\ (1 + 2.7E - 5z)\ (T_{max} - T_{min})^{0.5}$$

Another alternative method for estimating T_t was developed by Bristow and Campbell (1984), where transmissivity was calculated as follows:

$$T_t = A[1.0 - exp(-B(T_{max} - T_{min})^C)]$$

Where T_t is atmospheric transmittance, A is the maximum atmospheric transmittance expected at the elevation of the site (characteristic of the location, and depends also on pollution), ($T_{max} - T_{min}$) is the daily range of temperature and B and C are empirical coefficients when T_t reaches the maximum atmospheric transmittance (A) based on daily temperature range. Values of these coefficients are 0.7 for A, range between 0.004 to 0.010 for B and 2.4 for C (Meza and Varas 2000). The same authors adjusted site specific values for B in different locations in Chile.

Thornton and Running (1999) developed a sensitivity analysis for the estimation of coefficients for different sites in North America. These adjustments improved the quality of daily estimations to within ± 2.4 [MJ m^{-2} day^{-1}] on 40 sites with different soil and climate conditions.

The aim of this paper is to estimate solar irradiation for central regions of Chile using the ***r.sun*** model and to compute the three components of potential solar irradiation (direct, diffuse and reflected) for clear sky and overcast conditions. Specific objectives are: a) to evaluate methods to predict solar irradiation for the study area; b) to evaluate the performance of these models for 15 sites representing a range of climate, elevation and geographic locations.

The present work was initiated to develop a more robust approach to estimate and validate solar irradiation estimates and provide surface maps with monthly estimates of solar irradiation that can be used as inputs into process based growth models.

2. Methods

Our study area included the Central-South region of Chile located between 34°43'S and 40°36' S (Figure 1). The landscape includes the coastal range (mean elevation 550 m), central valley and piedmont of the Andes Mountains. The height of the coastal range greatly influences in the climate on the Central Valley (Santibañez 2003). Within our study area, there are 224 weather stations, which record hourly precipitation and temperature data. Few stations have global radiation measurements and 11 stations make observations of cloudiness (oktas), measured three times a day (0800, 1400 and 2000 hours).

For interpolation processes, we used a 30 m resolution Digital Elevation Model (DEM) which was obtained from a forestry company in Chile. To speed-up calculations and because

the cloudiness data was at a low resolution, the DEM's spatial resolution was decreased to 500 m. Slope and aspect maps were obtained using the GRASS open source GIS tool (Neteler and Mitasova 2008).

All raster data were integrated in GIS using the Universal Tranverse Mercator projection (World Geodetic System of 1984 datum zone 18 S). The raster resolution was 500x500 m^2. The ground albedo was considered as a constant 0.2. We selected 185 representative points in the study area to allow for more efficient spatial interpolation.

Using the ***r. sun*** model, we estimated clear-sky global irradiation for a horizontal surface using the following steps (Figure 2):

- Calculation and spatial interpolation of Linke turbidity index.
- Construction of clear-sky map using the ***r.sun*** model (Suri 2004).
- Calculation and spatial interpolation of clear-sky index and computation of raster maps for global irradiation on a horizontal surface.
- Validation with observed data.

Linke turbidity

Linke turbidity is an index which represents the amount of aerosols and dust in the atmosphere (Diabate 2003). This index varies seasonally and spatially, especially around more industrialized areas. However, there is a global network of observations and it is possible to obtain adequate values for different places around the world.

In our study area, Linke turbidity measurements were obtained for 185 locations. The monthly averages of the Linke turbidity factor were re-interpolated from the global database (Remund et al. 2003), available at the SoDa service (http://www.soda-is.com) (Wald 2000). The accuracy of the data from this source is reported to RMSE = 0.7 T_{LK} units. The position

of input points is defined using x,y,z values, where the z value represents the elevation derived from the digital terrain model. The interpolated results are very sensitive to the correct selection of parameters for tension, smoothing and z-value conversion factor. We used the ***v.vol.rst*** procedure of GRASS (see ***v.vol.rst*** manual page, Neteler and Mitasova 2008) and Mitasova (1993). Using this methodology, 12 monthly raster maps of T_{LK} values were prepared (Figure 3).

The model ***r.sun*** was parameterized for Chilean conditions using the characteristics of slope, aspect, Linke turbidity and cloudiness. A 0.5 hour time step was considered satisfactory for daily estimations of solar irradiation. Declination values for each month were set according to the ***r.sun*** model using the middle of the month (15^{th} day). The distance for the shadowing calculation was set to 0.7 and the albedo value to 0.2.

The clear-sky index (K_c) was calculated from a subset of daily and monthly measurements of oktas in the study area. In order to increase the number of spatial locations with cloudiness (oktas), we fitted linear regressions between oktas against rainfall, minimum and maximum temperature and elevation for 78 different locations. These monthly linear models presented strong R^2 (over 0.7) and also statistical significance for the parameters of each model (α = 0.05).

With these data (78 observations), we built monthly raster maps of cloud index. From the oktas values, we obtained the K_c index for every month according the models proposed by Kasten and Czeplak (1980), Beyer et al. (1997), and Davies (1995, cited by Foyo-Moreno 2001). Based in observed data, we found that Davies model has better performance for Chilean conditions (analysis not included). The Kasten and Czeplak model showed higher values of K_c than the Davies model.

The Kasten and Czeplak model has the following empirical equation:

$$K_c = 1 - 0.75\left(\frac{C}{8}\right)^{3.4}$$

Where C is cloudiness expressed in okta.

Following a procedure similar to what we used for Linke turbidity interpolation, we used ***v.vol.rst*** for spatial interpolation of the clear-sky solar irradiation (Figure 4). To obtain monthly values, we imposed in the ***r.sun*** model the specific calculation for the 15th day of each month, from January to December.

Model validation

Using the Hargreaves-Samani (HS) and Bristow-Campbell (BC) models, we calculated R_n for 15 representative sites of gradient (north to south) in order to compare with the results from ***r.sun*** (Table 1). We had observations of global solar irradiation since 1997 for these locations. We included elevation for our calculations obtained from the DEM. Values of R_a were calculated for the 15th day of each month using standard geometric procedures (Allen et al. 1998), and the transmissivity (T_t) was calculated using the specific procedures for HS and BC models. Using both values, we obtained the global radiation (R_n) for each location. We developed a Microsoft Excel spreadsheet that calculates R_a , T_t, and R_n for any location (latitude and elevation), and any day of the year (1 – 365). Climatic data (T_{max} and T_{min}) was obtained for different networks of weather stations in the research area. We used the average values for the last 10 years of observations.

We used linear regression to compare observed and modeled values, using the Proc Reg procedure of SAS (v. 9.3, SAS Inst., Cary, NC). Significant terms were obtained with $p < 0.05$.

3. Results

We determined global solar irradiation for horizontal surfaces for central southern regions of Chile.

Clear sky indexes were obtained under the Davies model. Figures 4 (clear sky solar irradiation) and 5 (overcast solar irradiation) presents results for four representative months (March, June, September, and December) to encompass low and high temperatures and vegetation development. Values varied during the year and were very low during the winter season (June). Summer season (December) values were highest and fall (March) and spring (September) season values were intermediate. The presence of clouds is more prevalent during the spring and fall seasons, especially in the coast and south. In the north, clouds are more prevalent during the winter season. The lack of data of cloudiness in this area could be improved through the use of remote sensing analysis (MODIS satellite for instance).

The clear sky solar irradiation values show a strong north to south gradient and also the influences of the Coastal and Andes ranges. Maximum values of 30-34 [MJ m^{-2} day^{-1}] are more frequent in the north (summer). Minimum values of 4-6 [MJ $m^{-2}day^{-1}$] are common in the south during the winter season.

According to the Kc (clear-sky indices), we can see a relevant effect on the winter season and also with north-south and Pacific Ocean to Andes mountain effect. Maximum values of 34.3 [MJ m^{-2} day^{-1}] were obtained during the summer season (December). High elevations and north sides of the hills had high values of global solar irradiation. Southern exposures had lower values than northern ones.

The comparison of the measured and predicted values of daily global radiation shows that these values are aligned along the 1:1 line as shown in figures 6, 7 and 8.

Total annual measured global solar radiation has a mean value of 5862 [MJ m^{-2} yr^{-1}]. Talca has the highest value (6312 [MJ m^{-2} yr^{-1}]) and Puerto Montt, the most southern and coastal place, the lowest value (4231 [MJ m^{-2} yr^{-1}]). On monthly basis, total global radiation varied from about 26-30 [MJ m^{-2} day^{-1}] in December and January to minimum averages of around 4-6 [MJ m^{-2} day^{-1}] during mid-winter (June-July). This is coincident with the rainfall peak during the winter season (May to August). We presented this variation in Figure 9, where we included total irradiation estimated using ***r.sun*** model and the observed data as well.

As Bristow and Campbell model, the ***r.sun*** model performance presents overestimation of values for the study area (Figure 6). However, for monthly averages data, there was a strong relationship between observed and estimated values with ***r.sun***. During summer season (November – March) there was a minimized effect of cloudiness which probably was not considered in the model because of the lack of observations. In addition, a possible lack of accuracy in the observed data could affect these relationships. Further revision of calibration for solar irradiation sensors in the weather stations should be necessary to improve the accuracy of these measurements. Some stations presented monthly values over 32 [MJ m^{-2} day^{-1}] which probably are over standard values observed for similar conditions.

In the north of the gradient, the performance of the model was better than in the south. In the central area, the performance of the model was very good; however there was a little overestimation for summer season (highest values).

In the southern part of the study area, there was a very good correlation between observed and predicted values. However, we should expect a slight overestimation because of the greater effect of the clouds at these latitudes (> 40° S), which was probably underrepresented.

Linear regressions between predicted values for different models are shown in Table 2. This analysis was developed for representative locations in the gradient include in this study.
The Hargreaves-Samani model was corrected by the elevation for each specific location. The results presented in Figures 6 to 8 and Table 2 showed a good agreement between predicted and observed average monthly incoming solar radiation. The mean error for the three models used corresponds close to 1 [MJ m^{-2} day^{-1}].

4. Discussion

The ***r.sun*** model has been implemented in Europe and North Africa, and this analysis was explored for further applications in South America. A better estimation of the Clear-Sky index could improve the performance of the model for cloudy areas or during the winter season. This paper shows the application under horizontal conditions, however, it is possible to easily calculate the inclined solar radiation for steep terrains. The model can be used under any slope or aspect conditions. This makes the approach useful at individual sites as well as across broad landscapes.

The use of the ***r.sun*** model illustrates the possibility of obtaining realistic and spatially explicit data for different geographical locations. This characteristic is relevant for use in process-based models generally used in agriculture and forestry crops. On the other hand, the lack of the solar irradiation measurements from weather stations imposes a limitation for the use of mechanistic models. Due to the extreme variability of site conditions in the central-southern places of Chile, the use of temperature data (T_{max} and T_{min}) from the weather stations to estimate solar irradiation, do not provide good estimates for specific areas. The ***r.sun*** model gives us the necessary flexibility to estimate solar irradiation for any site condition and gives advantages in terms of flexibility, spatially explicit results, and no requirement for climatic data.

In general, for the whole area, the Hargreaves-Samani model showed very good performance in terms of standard errors. The next best estimations were with the ***r.sun*** model, especially in the central part of the research area. As noted previously, the transmittance in the south could be improved through a better estimation of cloudiness. We used the Bristow-Campbell model in the same way that Meza and Varas (2000), using the coefficients A=0.7; B=0.007 and C=2.4.

We also did not use the Bristow-Campbell approach used by Coops (2000), because it was fitted for special conditions in North America and not working well under Chilean conditions. Meza and Varas (2000) used the standard parameters of the model, and fit a model in order to get the optimum B coefficient for some specific places in Chile. For our comparison we decided to use one value for the coefficient B and the standard values for parameters A and C indicated in the literature.

Coops (2000) adjusted specific models for A and B and he suggested a C value of 1.5. Using the standard parameters of his adjustments did not improve the performance of the Bristow-Campbell model in our study.

In the ***r.sun*** model, the underlying equations for diffuse radiation were implemented to reflect European climate conditions and it should be a possible source of higher estimation errors for regions like Chile.

We calculated and built raster maps for monthly horizontal solar irradiation for the central-south regions of Chile. The model demonstrated very good performance for the site conditions.

The Bristow Campbell (1984) and Hargreaves-Samani (1992) methods provided very good estimations for specific locations (low standards errors), which represent advantages for

further uses in a specific location. Our estimations are closely related to previous estimations from Meza and Varas (2000).

There are several opportunities to improve the quality of our model, with the use of better information about clouds. The lack of cloudiness data for the study area was improved through linear regression adjusted for every month. Independent variables for oktas were rainfall, elevation, maximum and minimum temperatures.

Further improvements should be done through better measurements of cloudiness using satellite images, for instance MODIS. The results of this model could be easily connected to biological process models for further tree growth modeling.

Acknowledgements

We acknowledge with thanks permission given by Forestal Mininco and Modelo Nacional de Simulación de Pino Radiata to publish these data and the results of our analyses of them. The senior author acknowledges with thanks the support of the Forest Nutrition Cooperative, allowing him to pursue scientific objectives in his work and also thanks the Pontificia Universidad Católica de Chile (Marcelo Miranda and Catalina Gerstmann) for providing additional climatic data.

References

Almeida, A. and J.J. Landsberg. 2003. Evaluating methods of estimating global radiation and vapor pressure deficit using a dense network of automatic weather stations in coastal Brazil. Agric. For. Meteorol. 118: 237-250.

Almeida, A. C., J.J. Landsberg and P. J. Sands. 2004. Parameterisation of 3-PG for fast growing *Eucalyptus grandis* plantations. For. Ecol. Manage. 193: 179-295.

Annandale, J.G., N.Z. Jovanic, N. Benade, and R.G. Allen. 2002. Software for missing data error analysis of Penman-Monteith reference evapotranspiration. Irrig. Sci. 21: 57-67.

Ball, R. A., L. C. Purcell and S. K. Carey. 2004. Evaluation of Solar Radiation Prediction Models in North America. Agron. J. 96: 391-397.

Battaglia, M., P. Sands, D. White, and D. Mummery. 2004. CABALA: a linked carbon, water and nitrogen model of forest growth for silvicultural decision support. For. Ecol. Manage. 193: 251-282.

Beyer HG, Czeplak G, Terzenbach U, Wald L. 1997. Assessment of the method used to construct clearness index maps for the new European solar radiation atlas (ESRA). Sol. Energy 61:389-397.

Bindi, M. and P. Miglietta. 1991. Estimating daily global radiation from air temperature and rainfall measurements. Clim. Res. 1: 117-124.

Bristow, K.L., and G.S. Campbell, 1984. On the relationship between incoming solar radiation and daily maximum and minimum temperature. Agric. For. Meteorol. 31: 159-166.

Cano, D. J.M. Monget, M. Albuisson, H. Guillard, N. Regas and L. Wald. 1986. A method for the determination of the global solar radiation from meteorological satellite data. Sol. Energy. 37(1): 31-39.

Coops, N.C., R.H. Waring and J.J. Landsberg. 1998. Assessing forest productivity in Australia and New Zealand using a physiologically-based model driven with averaged monthly weather data and satellite-derived estimates of canopy photosynthetic capacity. For. Ecol. Manage. 104: 113–127.

Coops, N.C., R.H. Waring and J.B. Moncrieff. 2000. Estimating mean monthly incident solar radiation on horizontal and inclined slopes from mean monthly temperatures extremes. Int. J. Biometeorol. 44: 204-211.

Diabate, L., G. Moussu and L. Wald. 1989. Description of an operational tool for determining global solar radiation at ground using geostationary satellite images. Sol. Energy. 42(3): 201-207.

Diabate, L., J. Remund and L. Wald. 2003. Linke turbidity factors for several sites in Africa. Sol. Energy. 75: 111-119.

Duffie, J. A., and Beckman, W. A. 1980. Solar engineering of Thermal Processes. Wiley Inter-Science, New York. 762p.

Foyo-Moreno, I., I. Alados, F.J, Olmo, J. Vida and L. Alados-Arboledas. 2001. On the use of a cloud modification factor for solar UV (290-385 NM) spectral range. Theor. Appl. Climatol. 68: 41-50.

Garatuza-Payan, J., R. T. Pinker, W. J. Shuttleworth and C. J. Watts. 2001. Hydrological Sciences-Journal-des Sciences Hydrologiques. 46(3) : 465-478.

Hargreaves, G.H., and Z.A. Samani. 1982. Estimating potential evapotranspiration. J. Irrig. Drain. Eng. 108 : 225-230.

Hofierka, J. and M. Suri. 2002. The solar radiation model for Open Source GIS: implementation and applications. Proceedings of the Open Source GIS-GRASS users conference 2002 – Trento, Italy, 11-13 September 2002.

Kasten, F. and G. Czeplak. 1980. Solar and terrestrial radiation dependent on the amount and type of cloud. Sol. Energy. 24: 177-189.

Kermel, F. 1988. Estimating Hourly All-Sky Irradiation Components from Meteorological Data. J. Appl. Meteor. 27: 157-163.

Lefevre, M., L. Wald and L. Diabate. 2007. Using reduced data sets ISCCP-B2 from the Meteosat satellites to asses' surface solar irradiance. Sol. Energy. 81: 240-253.

Landsberg, J.J., and R.H. Waring. 1997. A generalized model of forest productivity using simplified concepts of radiation-use efficiency, carbon balance and partitioning. For. Ecol. Manage. 95: 209-228.

McMurtrie, R.E., D.A. Rock, and F.M. Kelliher. 1990. Modelling the Yield of *Pinus radiata* on a Site Limited by Water and Nitrogen. For. Ecol. Manage. 30: 381-413.

Meza, F., and E. Varas. 2000. Estimation of mean monthly solar global radiation as a function of temperature. Agric. For. Meteorol. 100: 231-241.

Mitasova, H., and L. Mitas. 1993. Interpolation by Regularized Spline with Tension: I. Theory and Implementation. Math. Geol. 25: 641-655.

Muneer, T., M.S. Gul and J. Kubie. 2000. Models for Estimating Solar Radiation and Illuminance from Meteorological Parameters. J. Sol. Energy Eng. 122: 146-153.

Neteler, M. and H. Mitasova. 2008. Open Source GIS: A GRASS GIS Approach. Third Edition. The International Series in Engineering and Computer Science: Volume 773, 406 pages, 80 illus., Springer, New York.

Remund, J., L. Wald, M. Lefevre, T. Ranchin and J. Page. 2003. Worlwide Linke turbidity information. Proceedings of ISES Solar World Congress, 16-19 June 2003, Goteborg, Sweden.

Romero, L.F., S. Tabik, J. M. Vias, and E. L. Zapata. 2008. Fast clear-sky solar irradiation computation for very large digital elevation models. Comp. Phys. Comm. 178: 800-808.

Sands, P.J. and J.J. Landsberg. 2002. Parameterisation of 3-PG for plantation grown *Eucalyptus globulus*. For. Ecol. Manage. 163: 273–292.

Santibáñez, F. 2003. Atlas Climático de Chile. Universidad de Chile. Santiago, Chile.

Suri, M. and Hofierka, J. 2004. A New GIS-based Solar Radiation Model and Its Application to Photovoltaic Assessments. Transactions in GIS, 8: 175-190.

Stape, J.L., M. G. Ryan, and D. Binkley. 2004. Testing the utility of the 3-PG model for growth of *Eucalyptus grandis x urophylla* with natural and manipulated supplies of water and nutrients. For. Ecol. Manage. 193: 219-234.

Wald L. 2000. SODA: a project for the integration and exploitation of networked solar radiation databases. European Geophysical Society Meeting, XXV General Assembly, Nice, France, 25-29 April 2000.

Wang, Y.P., and P.G. Jarvis. 1990. Description and validation of an array model-MAESTRO. Agric. For. Meteorol. 51: 257-280.

Tickle, P.K., N.C. Coops and S.D. Hafner. 2001. Assessing forest productivity at local scales across a native eucalypt forest using a process model, 3PG-SPATIAL. For. Ecol. Manage. 152: 275-291.

Thornton, P.E., and S.W. Running. 1999. An improved algorithm for estimating incident daily solar radiation from measurements of temperature, humidity, and precipitation. Agric. For. Meteorol. 93: 211-228.

Yilmaz, E., B. Cancino and E. Lopez. 2007. Construction of a Quadratic Model for Predicted and Measured Global Solar Radiation in Chile. Chin. Phys. Lett. 24(1) : 291-293.

Appendix

Appendix 1 - Steps for calculating global irradiation for horizontal surfaces using GRASS.

1.- Resampling DEM 30m.

From 30m to 500m spatial resolution

g.region res=500 –p

r.resamp.stats -w input=dem30m_Chile@Thesis output=dem500m_Chile method=median

2.- Aspect and slope map generation from dem 500m

g.region rast=dem500m_Chile –p

r.slope.aspect elevation=dem500m_Chile@Thesis slope=slope500m_Chile

aspect=aspect500m_Chile format=degrees prec=float zfactor=1.0 min_slp_allowed=0.0

3.- Generation of Linke map 3d. The same for Kc map.

g.region vect=LK_Chile1 align=dem30m_Chile –p

v.drape in=LK_Chile1 rast=dem30m_Chile method=bilinear out=LK_Chile1_3d

v.info LK_Chile1_3d

4.- Spatial interpolation for Linke turbidity (monthly).

g.region rast=dem500m_Chile –p

g.region t=2000 b=0 tbres=2000 res3=500 -p3

v.vol.rst input=LK_Chile1_3d@Thesis cellinp=dem500m_Chile@Thesis wcolumn=JAN

tension=40. smooth=0.1 segmax=700 npmin=200 dmin=249.848594 wmult=1.0 zmult=90

cellout=lkrst_Jan_500m –overwrite

d.rast map=lkrst_Jan_500m@Thesis –o

5.- Generation of Cloud map 3d.

g.region vect=Cloud align=dem30m_Chile –p

v.drape in=Cloud rast=dem30m_Chile method=bilinear out=Cloud_3d

v.info Cloud_3d

6.- Spatial interpolation for Kc index (monthly).

g.region rast=dem500m_Chile –p

g.region t=2000 b=0 tbres=2000 res3=500 -p3

v.info -c cloud3_3d

v.vol.rst input=cloud3_3d@Thesis cellinp=dem500m_Chile@Thesis wcolumn=JAN tension=10. smooth=0.1 segmax=700 npmin=25 dmin=249.848594 wmult=1.0 zmult=50 cellout=cloud_jan –overwrite

d.rast map=cloud_jan@Thesis –o # This is the Kc index for January

7.- Irradiation for horizontal surface: (Clear sky: 15 jan, 15 jul, 15……).

r.sun –s elevin=dem500m_Chile@Thesis aspin=aspect500m_Chile@Thesis slopein=slope500m_Chile@Thesis linkein=lkrst_Jan_500m@Thesis alb=0.2 beam_rad=15jan_b diff_rad=15jan_d day=15 step=0.5

r.mapcalc "15jan_g1 = 15jan_b + 15jan_d"

8.- Irradiation from Model for the weather stations:

statrad_new.shp weather stations in vector format

v.in.ogr -o {dsn=C:/statrad_new.shp} output=statrad_new min_area=0.0001 snap=-1

statrad_new.shp weather stations to raster format

v.to.rast input=statrad_new@Thesis output=statrad_new_r use=attr type=point,line,area layer=1 column=cat value=1 rows=4096

Determination of model pixel values for each met station

r.stats -a input=statrad_new_r,15jan_g out=jan.txt

9.- r.univar # generate data of raster map for the whole area.

r.univar cloud_jan

10.- Determination of overcast irradiation

Gh = Kc * 15jan_g

Gh = Global radiation under overcast condition

Kc = Clear-sky index

15jan_g1 = Monthy mean of Clear-sky radiation

Appendix 2 - List of parameters used in the ***r.sun*** model.

Parameter	Type	Description	Units	Specif value
elevin	raster	elevation	m	0 - 8900
aspin	raster	aspect (panel azimuth)	decimal degrees	0 - 360
slopein	raster	slope (panel inclination)	decimal degrees	0 - 90
linkein	raster	Linke atmosperic turbidity	dimensionless	0 - 7
latin	raster	Latitude	decimal degrees	-90 - 90
albedo	single value	Ground albedo	dimensionless	0.2
coef	raster	clear-sky index	dimensionless	0 - 1
day	single value	day number	dimensionless	15th of each month
declin	single value	solar declination	radians	-0.40928 - 0.40928
step	single value	time step	decimal hours	0.25

Table 1. Locations utilized in evaluation of solar irradiation models.

Station	Lat (º)	Lon (º)	Elev (m)
Curico	-35.0	-71.2	225
Talca	-35.4	-71.7	100
Cauquenes	-36.0	-72.4	140
Concepcion	-36.8	-73.1	12
Colicheu	-37.0	-72.4	130
Rucamanqui	-37.1	-71.8	356
Nacimiento	-37.3	-72.7	107
Los Angeles	-37.3	-72.4	147
Sta Barbara	-37.4	-72.0	410
Angol	-37.5	-71.4	75
Ercilla	-38.0	-72.4	250
Victoria	-38.1	-72.3	348
Temuco	-38.8	-72.6	114
Osorno	-40.6	-73.1	65
Puerto Montt	-41.4	-72.6	85

Table 2. Statistical performance of Hargreaves-Samani (HS), Bristow-Campbell (BC) and r.sun models for predicting irradiation at 15 sites in Chile. Monthly values of predicted irradiation were regressed against monthly average values of observed irradiation. In each model, the following information is included: number of observations (n), intercept (int.) of the regression, slope of the regression, coefficient of determination (R^2), and standard error (SE), for daily values or cumulative by month.

Site	Lat	Lon	Model	Elev (m)	Linear regression analysis						
					n	Mean obs (MJ m^{-2} day^{-1})	*Int.*	*Slope*	R^2	*SE* (MJ m^{-2} day^{-1})	*SE* (MJ m^{-2} $month^{-1}$)
					Base on monthly statistics						
Curico	-35.0	-71.2	HS	225	12	18.33	0.96	0.74	0.977	1.27	38.07
			BC		12	18.92	4.13	0.63	0.936	1.82	54.54
			r.sun		12	21.26	3.87	0.75	0.939	2.09	62.58
Talca	-35.4	-71.7	HS	129	12	18.69	1.65	0.86	0.989	0.91	27.30
			BC		12	18.91	4.63	0.72	0.965	1.34	40.11
			r.sun		12	20.23	2.81	0.88	0.980	1.24	37.08
Cauquenes	-36.0	-72.4	HS	145	12	18.50	1.50	0.99	0.996	0.51	15.36
			BC		12	18.79	4.40	0.84	0.985	0.88	26.49
			r.sun		12	20.54	2.88	1.03	0.981	1.23	36.90
Rucamanqui	-37.1	-71.8	HS	356	12	18.68	1.90	1.05	0.997	0.50	14.94
			BC		12	18.63	4.68	0.87	0.974	1.17	35.07
			r.sun		12	18.76	1.81	1.06	0.891	3.05	91.53
Colicheu	-37.0	-72.4	HS	147	12	18.57	2.54	1.05	0.989	0.93	27.93
			BC		12	18.59	5.22	0.87	0.969	1.30	38.85
			r.sun		12	19.46	3.11	1.07	0.979	1.30	38.88
Los Angeles	-37.5	-72.4	HS	130	12	18.53	2.76	0.93	0.976	1.36	40.71
			BC		12	18.53	5.40	0.78	0.952	1.63	48.84
			r.sun		12	19.21	3.09	0.95	0.969	1.60	47.97
Concepcion	-36.8	-73.1	HS	12	12	18.31	2.68	1.08	0.992	0.74	22.23
			BC		12	17.89	3.47	0.99	0.988	0.81	24.30
			r.sun		12	19.88	2.56	1.19	0.991	0.83	24.90
Sta Barbara	-37.7	-72.0	HS	410	12	15.45	0.36	0.94	0.996	0.51	15.15
			BC		12	17.32	1.51	0.98	0.983	1.06	31.77
			r.sun		12	19.64	2.60	1.06	0.984	1.10	33.03
Nacimiento	-37.5	-72.7	HS	107	12	13.68	0.24	0.79	0.989	0.74	22.14
			BC		12	15.85	-0.03	0.93	0.990	0.81	24.18
			r.sun		12	20.08	2.82	1.01	0.988	0.98	29.37
Angol	-37.8	-71.4	HS	75	12	16.51	0.23	1.15	0.992	0.71	21.30
			BC		12	18.00	2.31	1.11	0.975	1.26	37.92
			r.sun		12	19.04	1.39	1.25	0.988	0.97	29.07
Ercilla	-38.1	-72.4	HS	250	12	17.05	2.51	1.03	0.960	1.69	50.55
			BC		12	18.13	4.73	0.95	0.942	1.88	56.31
			r.sun		12	18.85	3.22	1.11	0.951	2.01	60.18
Victoria	-38.2	-72.3	HS	348	12	16.62	1.70	1.07	0.993	0.70	20.97
			BC		12	17.85	3.84	1.01	0.969	1.40	42.00
			r.sun		12	19.02	3.07	1.15	0.982	1.19	35.70
Temuco	-38.8	-72.6	HS	114	12	16.66	1.74	1.04	0.991	0.79	23.64
			BC		12	17.99	3.58	1.01	0.985	0.98	29.28
			r.sun		12	18.60	2.53	1.12	0.990	0.85	25.56
Osorno	-40.6	-73.1	HS	65	12	15.41	0.72	1.16	0.969	1.35	40.62
			BC		12	17.34	2.06	1.20	0.958	1.65	49.53
			r.sun		12	16.75	-1.17	1.41	0.960	1.89	56.64
Puerto Montt	-41.4	-72.6	HS	85	12	16.36	1.14	1.31	0.987	0.92	27.63
			BC		12	16.35	1.44	1.28	0.978	1.17	35.04
			r.sun		12	16.93	0.40	1.42	0.981	1.19	35.82

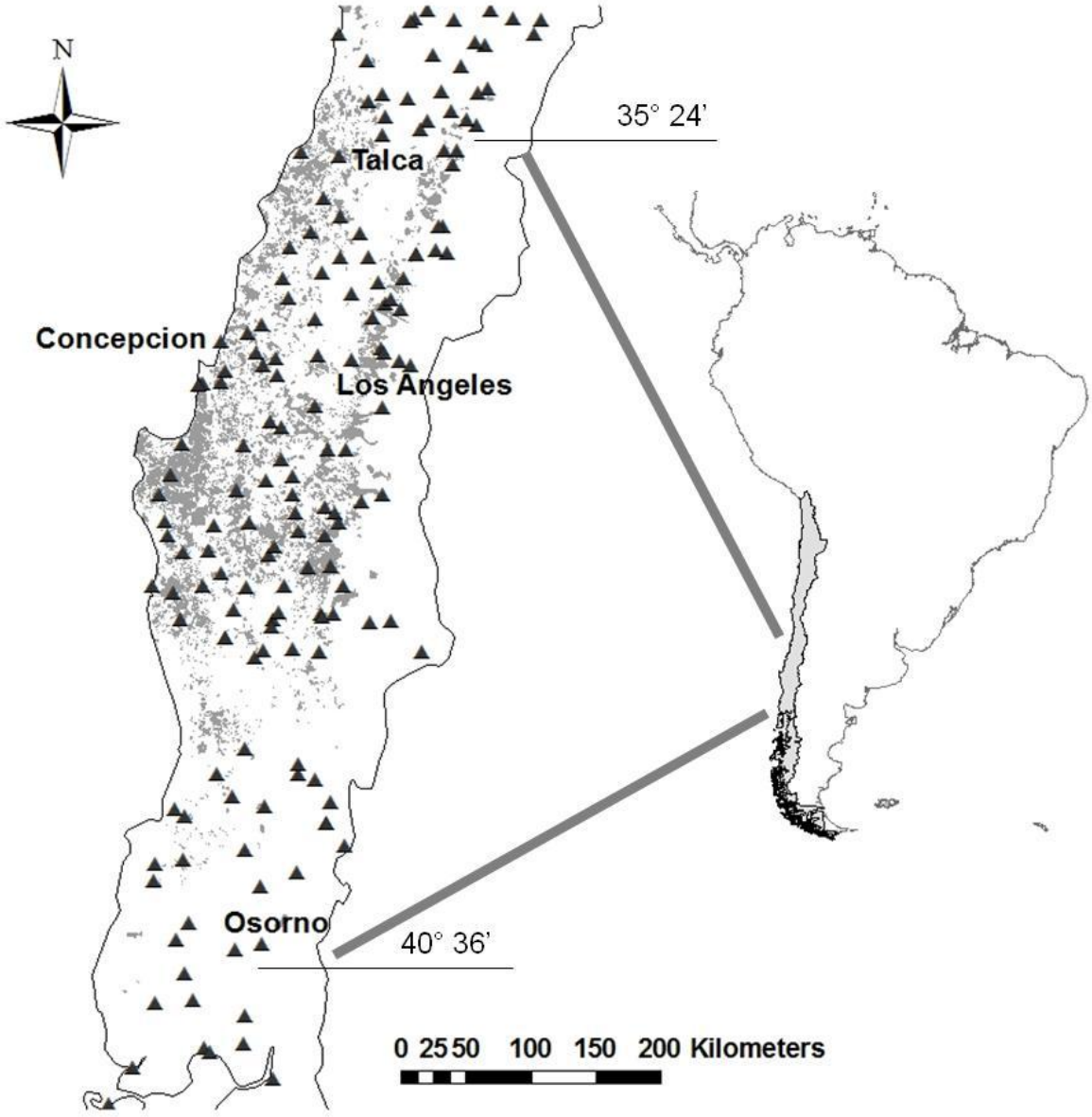

Figure 1. Research area in Chile, including forest plantations and weather stations network. (Plantations are in grey color).

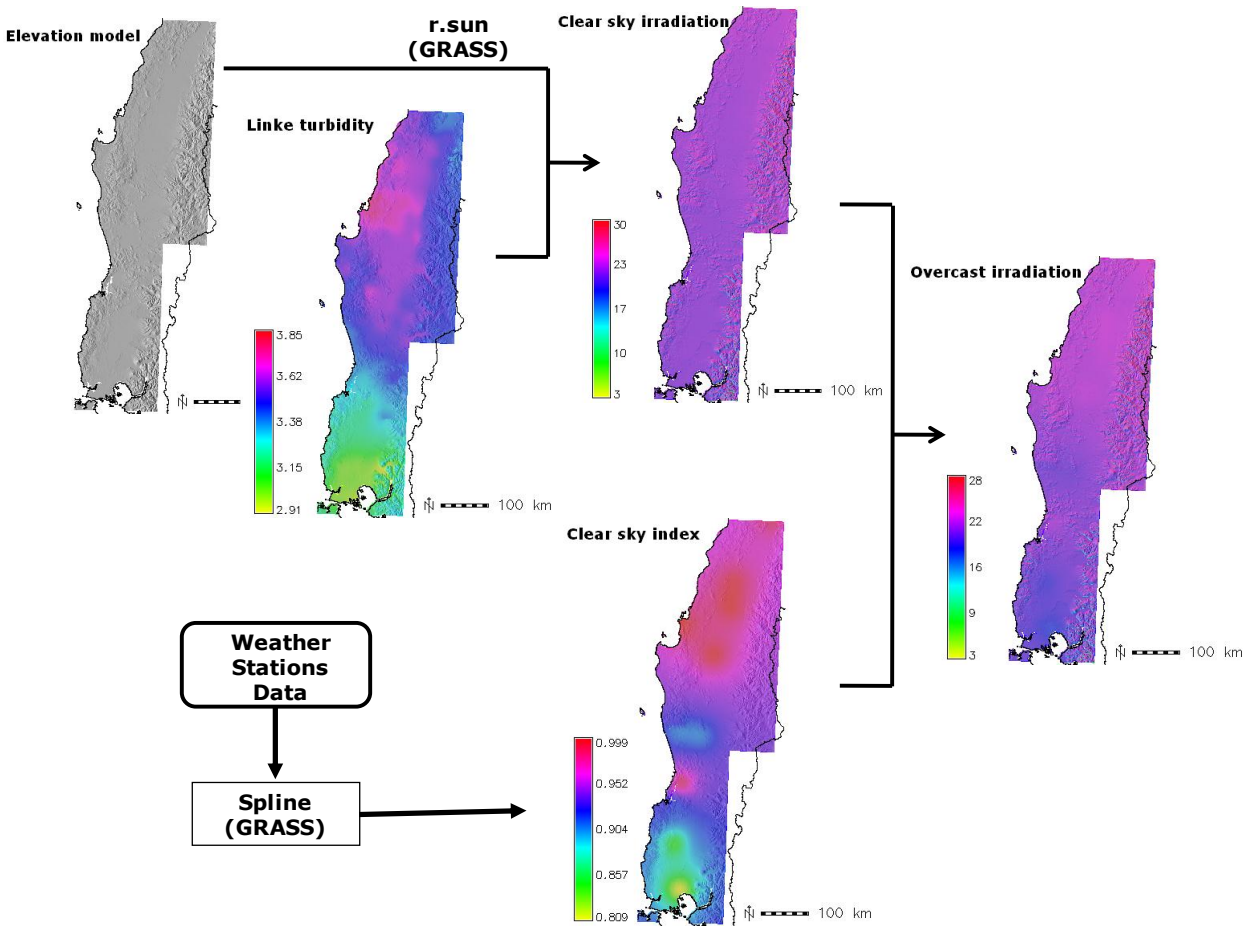

Figure 2. Diagram of sequence of activities for horizontal irradiation calculation.

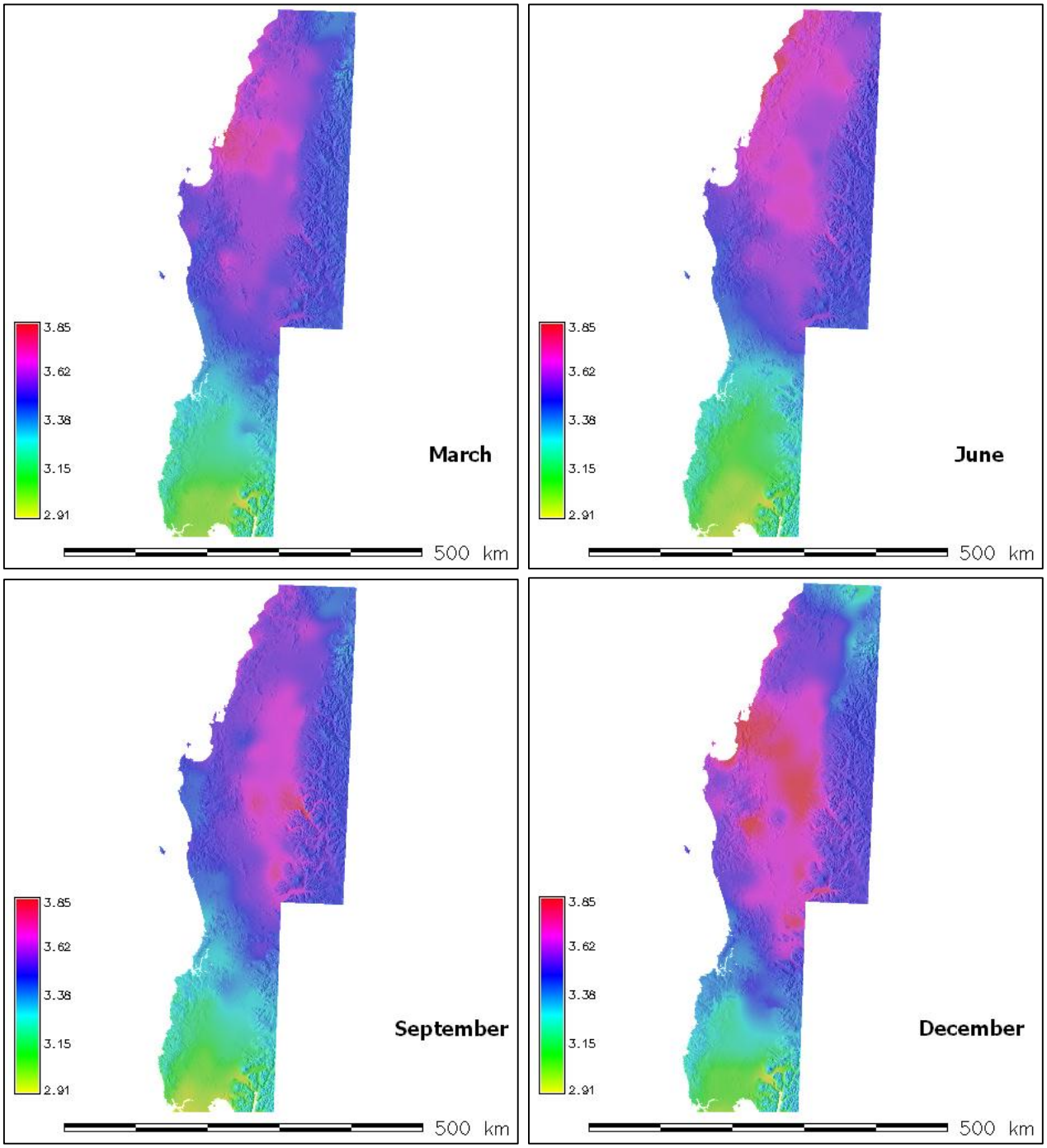

Figure 3. Linke turbidity maps for the study area for representative months in autumn (March), winter (June), spring (September), and summer (December) seasons.

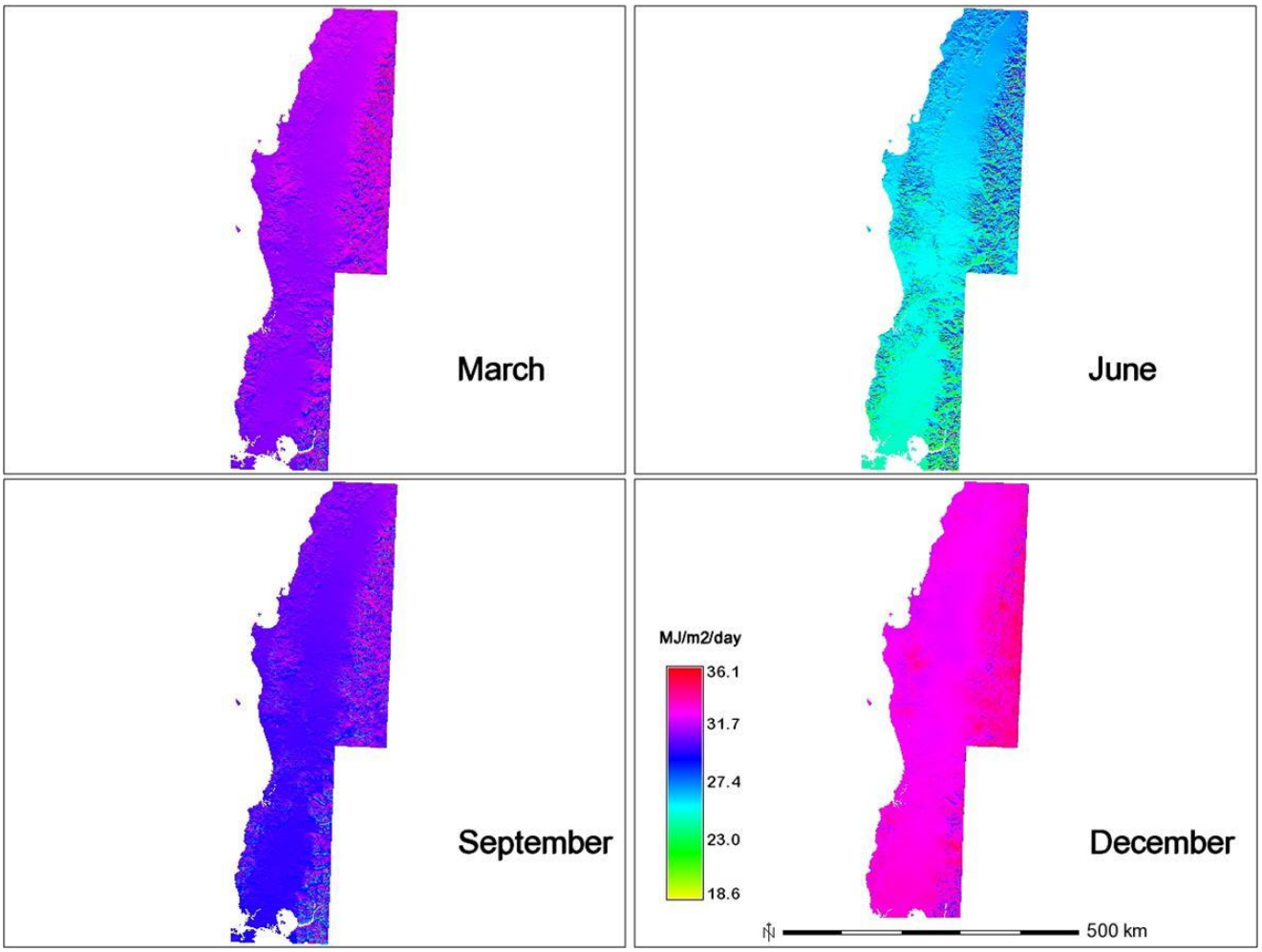

Figure 4. Monthly averages of clear-sky solar irradiation area for representative months in autumn (March), winter (June), spring (September), and summer (December) seasons.

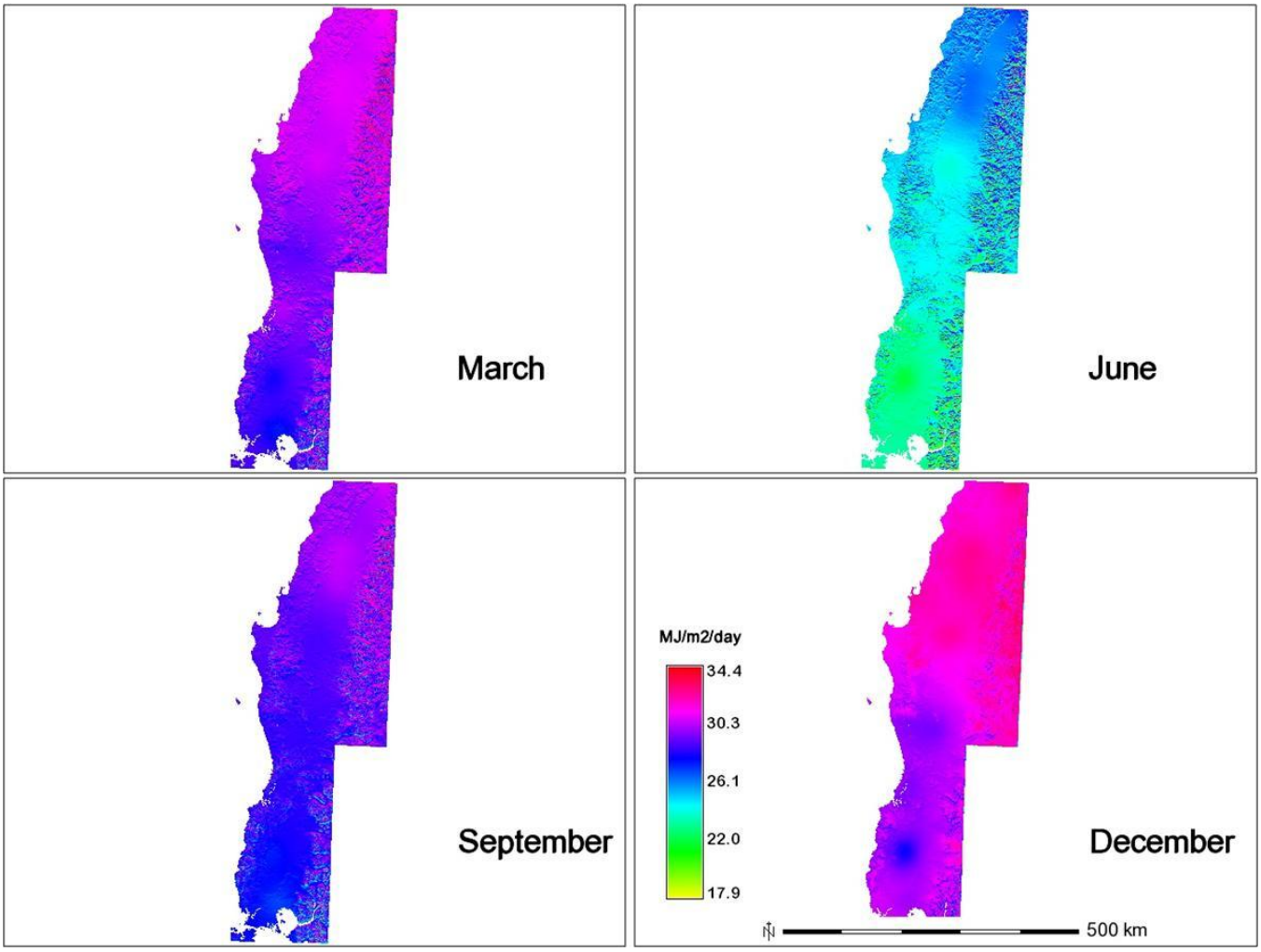

Figure 5. Monthly averages of overcast solar irradiation area for representative months in autumn (March), winter (June), spring (September), and summer (December) seasons.

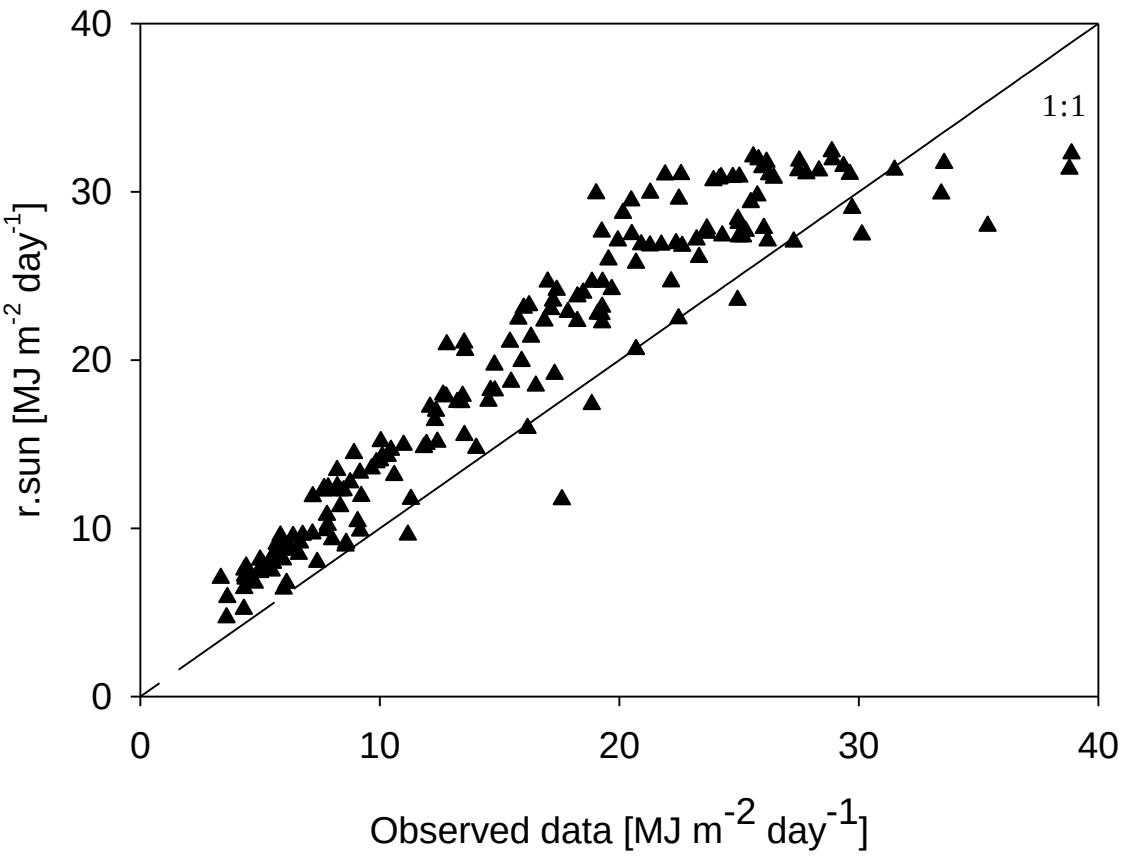

Figure 6. Observed and estimated average monthly global solar irradiation using the r.sun model. (Symbols represent data from 15 different weather stations).

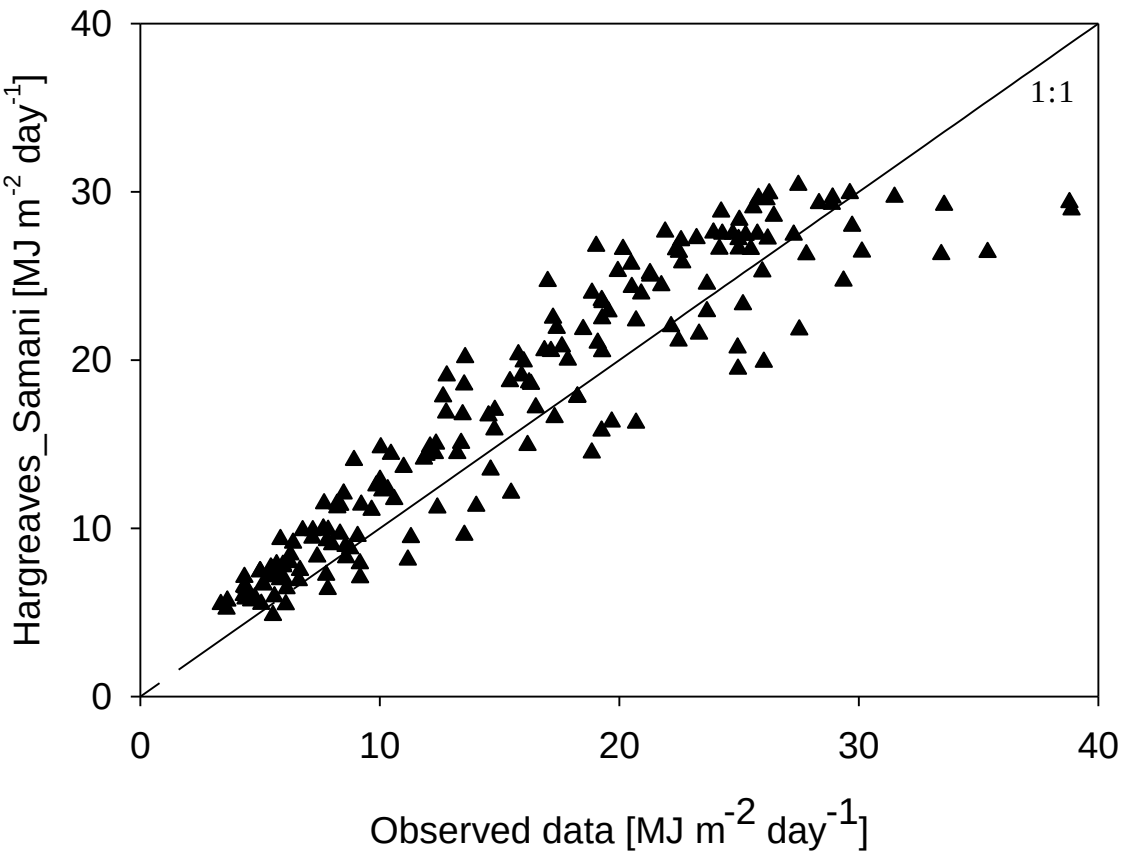

Figure 7. Observed and estimated average monthly global solar irradiation using Hargreaves and Samani model. (Symbols represent data from 15 different weather stations).

3.

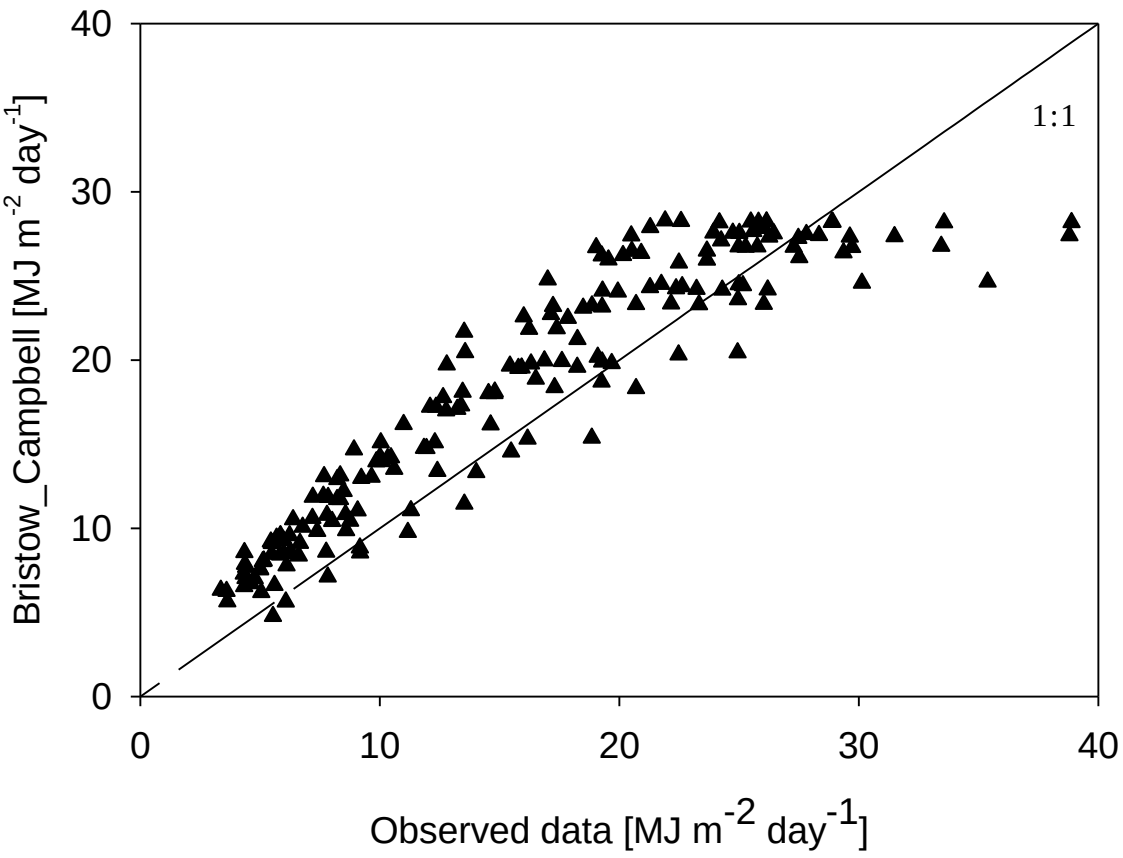

Figure 8. Observed and estimated average monthly global solar irradiation using Bristow and Campbell model. (Symbols represent data from 15 different weather stations).

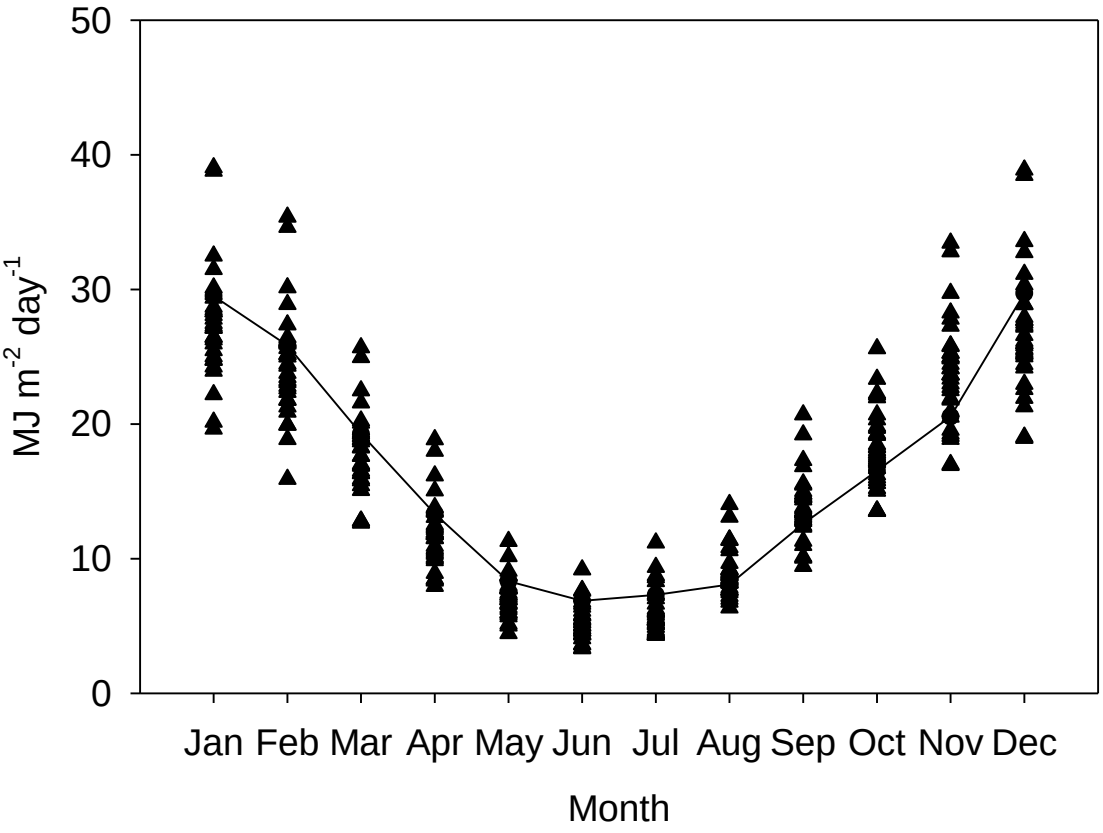

Figure 9. Global overcast sky solar irradiation on the study area. (Symbols represent observations from 15 locations and the solid line represents the average from the r.sun model).

CHAPTER 2

Estimating LAI in *Pinus radiata* Plantations in Chile Using Remote Sensing

Abstract

Previous research has shown strong relationships between leaf area index (LAI) and red and near infrared radiation measured with remote sensors. Remote sensing offers the best method of estimating LAI over large areas and through time. For forestry the operational use of remote sensors to estimate LAI has been limited because of the lack of ground data to calibrate regression models. We determined LAI using Landsat Thematic Mapper (TM) data covering a 5 year period (2005-2009) for a network of permanent sample plots in *Pinus radiata* plantations in Chile. In 2009, we calculated LAI from ground measurement using LI-COR LAI-2000 on each one hectare plot. These values of LAI were regressed against Simple Ratio (SR), Normalized Difference Vegetation Index (NDVI) and Reduced Simple Ratio (RSR), derived from the TM 2009 data. Linear relationships were strong with R^2 values of 0.65 for SR, 0.61 for NDVI and 0.67 for RSR. Using the RSR relationship, LAI values were estimated for the network of permanent sample plots of *Pinus radiata* plantations over the whole period.

1. Introduction

Wood production is strongly correlated with the amount of light interception (Jarvis and Leverenz 1983; Linder 1987; Cannell 1989; Sampson et al 1998). Light interception is a function of leaf area and its distribution. Leaf area index is a dimensionless variable (Zheng and Moskal 2009) generally defined as one-sided green leaf area per unit ground area in broadleaf canopies, and variously (projected or total) in needle canopies (Myneni et al. 1997). A strong correlation between stem wood production and leaf area has been demonstrated for *Pinus taeda* (Vose and Allen 1988; Dalla-Tea 1991 and Albaugh et al. 1998), *Eucalyptus* sp. (Coops 1997), *Pinus sylvestris* (Linder 1987), and *Pinus radiata* (Beets 1987).

Leaf area index is strongly related to many biological and physical processes, such as photosynthesis, respiration, transpiration, carbon and nutrient cycle, and rainfall interception (Zheng and Moskal 2009). Leaf area index is a key variable in process-based models (Landsberg et al. 1996; Landsberg and Gower 1997), and its accurate measurement is necessary to determine annual fluxes of energy and gas exchange, and the water balance of forests. Additionally, knowledge of the spatial and temporal variation of LAI is necessary for silvicultural management decisions, to optimize wood production from a sustainable point of view (Waring 2007). Due to its unique role in wood production, there have been several efforts to measure LAI over large areas using remote sensing technologies (Curran 1980, Chen and Cihlar 1996; Coops 1997, White et al. 1997; Stenberg et al. 2004; Flores et al. 2005, and Zheng and Moskal 2009).

Estimation of LAI is based on the selective absorption of radiation by vegetation canopies which results in distinctive patterns for the reflectance of shortwave radiation (Flores et al. 2005). Remote sensing of the near infrared (0.7-1.2 μm, *NIR*) and red (0.6-0.7 μm, *R*) wavelengths of the electromagnetic spectrum is commonly used for LAI estimation (Running et al. 1986). In the *NIR* region, within leaf scattering is high and the radiation from the

canopy is therefore generally high (Coops 1997). In the *R* spectrum, high absorption by pigment results in low radiation reflection.

Following these patterns, LAI is usually positively related to an increase in the difference between *NIR* and *R* radiation. This relationship generally holds for different ecosystems; however, the canopy density, understory vegetation, and phenology and environmental factors such as terrain, solar angle, and atmospheric conditions all have been shown to influence this relationship (Curran 1980; Coops 1997). The effects of these factors are critical when LAI is calculated with remotely sensed data over time, when using different scenes (Chavez 1996; Song et al. 2001; and Riaño et al. 2003).

Several indices have been developed using relationships between NIR and R bands. The normalized difference vegetation index (NDVI= (R-NIR)/(R+NIR)), the simple ratio (SR= R/NIR), and the reduced simple ratio (RSR) (Stenberg 1996) are three common indices. Strong site and time specific relationships have been developed (Stenberg et al. 2004, Flores et al. 2005); however, few studies have assessed LAI using multi-temporal remote sensing images. This is not surprising because calibrating remotely sensed data and ground measurements is time consuming and when multiple images are used through time additional atmospheric and topographic corrections are required.

Our main objective was to quantify spatial and temporal variations in LAI in *Pinus radiata* plantations in central Chile. Specific objectives were: (a) to analyze the effects of atmospheric and topographic corrections on remotely sensed LAI estimates, (b) calibrate a relationship between remotely sensed LAI and ground based estimates of LAI made using a LI-COR LAI2000, and (c) to estimate LAI for 2005 to 2009 using remotely sensed data.

2. Methods

Study location

The study area was located in central Chile (34°43' S and 40°36' S). About 90% of the commercial *Pinus radiata* (63%) and *Eucalyptus spp*. (28%) plantations of Chile are located in this area (Figure 1).

This area includes different soils (volcanic ashes, granitic, metamorphic, red clay and sands) and annual precipitation varies between 640 mm (30 yr average) in the north to 2200 mm in the southern extreme of the study area. Due to the Mediterranean climate, most of this precipitation is concentrated during the winter season so extended droughts are frequent during the growing season (September to April) (Santibañez 1993).

Ground measurement of LAI

We selected permanent sample plots (PSP) from the database of the Insigne model (Modelo Nacional de Simulación de Pino radiata, Chile). We selected a subset of 37 (Tables 1 and 4) that contained the most complete growth data, precise geographical location and covered the North-South, West-East gradient of the research area. For these 37 PSPs, we measured LAI with LI-COR LAI-2000. Each plot was geographically located using a global positioning system with an average error of less than 10 m. For each plot, 30 LAI measurements were made along several transects on the east-north side of the plot at a height of 60 cm between 0700 and 1000 EST or between 1600 and 1800 EST using a 45° view cap (Figure 2). We used two sensors, one below (in the plot) and the second above, in an open field adjacent to the plot area where the light sensor had an unobstructed view of the sky. The above sensor recorded data every 15 seconds. The below sensor was maintained around 60 cm above the ground, with the sun behind the person measuring. Both, below and above sensors were

oriented in the same direction. The 30 measurements were averaged to estimate the plot LAI for each individual plot.

The LAI-2000 data were post-processed using the manufacturer-provided software (FV2000, LI-COR, Inc., Lincoln, NE) based on (i) nearness in time of above and below canopy readings and (ii) elimination of values where transmittance was less than zero. Because the homogeneity of the stands, the time of day for our measurements, and the lack of external influences on the above canopy sensor, we used all 5 rings to calculated LAI.

We also obtained measurements with the TRAC instrument (Chen and Cihlar 1996; Liames et al. 2008) under clear sky conditions.

The conditions of optimal solar zenith angle (close to 57°) on a transect perpendicular to sunbeams were not covered because the field work team prioritized the measurement with LI-COR LAI2000. Furthermore, for all the analysis in this research we only used LAI obtained with LI-COR LAI2000.

Satellite image processing

Twenty three scenes of Landsat TM were utilized for the period 2005 to 2009 (Table 2). Images for path/row 233-85 (central north of the area) and 1-85 (coast north) were not available for 2006. All images were cloud free. For 2009 we acquired images in similar dates according the field campaign to measure LAI using Licor LAI-2000. For other years we acquired TM scenes for the same date (March). It was necessary to geometrically correct images using 15 control points (road intersections and/or curves of rivers spreading in all the image, especially in corners associated with georeferenced maps provided by private companies in Chile), with a RMSE of the control points of about 0.5 pixels, or around 15 m. Absolute atmospheric correction of the images was done using the DOS3 method (Song et al. 2001) and the original pixel size (30m x 30 m) was maintained. The digital numbers from the

Landsat TM scenes were first converted to radiance using the gains and offset values from the images header files. Then, the radiance values were converted to exo-atmospheric reflectance (reflectance at the top of atmosphere) (Chander 2009). We calculated the downwelling diffuse radiation of the surface using the public version of **6s** (Second Simulation of Satellite Signal in the Solar Spectrum) model (Vermote et al. 1997). We used the public version which comprises over 100 Fortran subroutines designed to compile in Unix, and processing every single image with time (Universal Time, expressed as decimal hours: hh.ddd), and location (Mid latitude summer).

The sequence of activities for geometric, atmospheric and topographic correction developed for each individual image is presented in figure 3.These data were geo-registered to the Universal Transverse Mercator (UTM) Zone 18-S coordinated using land use maps. The raw digital count values were converted to equivalent radiance values using the gain and offset values of the sensor calibration data included in the TM header metadata file.

A Digital Elevation Model (DEM) was used to generate the slope, aspect and illumination for each scene. The slope computed at each pixel is the plane formed by the vector connecting the left and right neighbors versus the vector connecting the upper and lower neighbors of the pixel. The illumination of each pixel was computed considering the solar zenith and azimuth angles when the Landsat TM image was acquired as well as the slope and the aspect of each pixel. To apply these procedures for each band, we built a model using Erdas Imagine 9.2 (Erdas Inc., Atlanta, GA). Due to the characteristics of the topography in Chile, we assumed non-Lambertian behavior and based on Riaño et al. (2003) we chose the C-correction method.

Analysis of ground and satellite measurements

A 100x100 m window of satellite data was extracted for each field plot to assess index responses to plot vegetation characteristics, including LAI. We selected at least a square of

3x3 pixels in each image. The adjustment between the plot position (georeferenced from Global Positioning System) and each scene was obtained through the use of aerial photography of the area.

Spectral vegetation indices

We used ground measurements of LAI (LAI-2000) collected between March 9, 2009 and April 29, 2009, and compared these data to three different Spectral Vegetation Indices (SVI) calculated from Landsat TM scenes: Normalized Difference Vegetation Index (NDVI), Simple Ratio (SR), and Reduced Simple Ratio (RSR). They were calculated from the atmospherically reflectance values of Landsat TM spectral channels 3 (red: 630-690 nm), 4 (NIR: 750-900 nm), and 5 (MIR: 1550-1750 nm) as:

$$SR = \frac{\rho_{TM4}}{\rho_{TM3}}$$

$$NDVI = \frac{\rho_{TM4} - \rho_{TM3}}{\rho_{TM4} + \rho_{TM3}}$$

$$RSR = \frac{\rho_{TM4}}{\rho_{TM3}} * \frac{\rho_{TM5max} - \rho_{TM5}}{\rho_{TM5max} - \rho_{TM5min}}$$

Where ρ_{TMmax} and ρ_{TMmin} were represented by the largest and smallest reflectance values in channel 5 for the Landsat TM pixels covering the 1 ha plot area.

For the inter-annual analysis, we lacked the complete sequence of images for the whole area; however we worked with the same set of 37 representative plots located within the research

area for this analysis. We analyzed the relationship between the ground-based measurements and each of the three spectral indices using a least squares regression.

Statistical analysis

We analyzed the relationship between the ground-based LAI measurements and each of the three spectral indices using least squares regression within the Proc Reg Procedure of SAS (v. 9.3, SAS Inst., Cary, NC). The dependent variable was LAI for year 2009 and independent variables were NDVI, SR or RSR for images of 2009. Significant terms were obtained with $P < 0.05$. We used linear and exponential models. We compared our estimated values for fall 2009 with observed data from LAI-2000.

3. Results

The LAI estimated by LAI-2000 ranged from 1.52 to 4.71. The LAI distribution was close to normal and was centered on 2.53. The highest LAI values were found in the coastal range and on recent volcanic ash soils) and lowest values in the north.

Vegetation indices NDVI, SR and RSR were increased with atmospheric correction of Landsat TM images (Figure 4, 5 and 6). A mean difference of 18 % for NDVI was obtained before and after atmospheric correction. For SR and RSR indices, the differences were 78% and 68% respectively.

NDVI, SR and RSR (after atmospheric correction) showed strong positive correlations with LAI from 2009 measurement but differed with their predictive power as indicated by the sensitivity to changes in LAI (Figures 7, 8 and 9). NDVI presents saturation above LAI 2.5. RSR correlated slightly better with LAI ($r^2 = 0.67$), than SR ($r^2 = 0.65$) or NDVI ($r^2 = 0.61$). In term of LAI estimation, RSR had a lower standard error (0.268) than NDVI (0.292) and SR (0.276).

Non-linear models presented similar regression coefficients. Therefore, a regression with RSR to estimate of LAI for years 2005 to 2009 was developed:

$$LAI = 0.385 + 0.324RSR$$

The estimated values of this model were well fitted with observed data (p=0.04) (Figure 10). Using the relationship LAI between RSR, we calculated LAI for each site for each year. Estimations for 2005 to 2009 ranged from 1.2 to 4.2 m^2m^{-2} (Table 4). Sites with high growth rates in volume show higher peak values of LAI, especially those located in volcanic ash soils. Some wet sandy soils also presented high values. Sites with water limitations (chapter 3) had low maximum estimated LAI. The gradient (research area) usually has some years with high water deficit and it is common for the presence of several months without rain (Santibáñez 1993).

4. Discussion

LAI estimates made with a LI-COR LAI-2000 in central Chile allowed us to estimate LAI from previous years using the vegetation index RSR (Reduced Simple Ratio).

The RSR index was better correlated with LAI2000 than the other indices tested SR (Simple Ratio) and NDVI (Normalized Difference Vegetation Index). Linear models fitted very well for our data set. NDVI showed saturation as LAI increased over 2.5 m^2 m^{-2}. SR and RSR are less sensible to this phenomenon. The suitability of the RSR index for LAI estimation was supported by results of Stenberg et al. (2004) in coniferous stands. The RSR index takes into account the largest and smallest reflectance values covered in band 5 for Landsat TM pixels RSR over SR has the advantage to reduce the background reflectance, such as understory, litter, and soil (Chen 1996, Pavlic et al. 2002).

We did not obtain reference measurements through destructive sampling methods and no previous estimates have been reported for *Pinus radiata* in Chile; therefore, our study could not evaluate the accuracy of the LAI measurements using the LI-COR LAI-2000 or TRAC. Further analysis should be done in order to obtain more precise measurements of clumping effect using the TRAC instrument.

Our calculations provide the first opportunity to use historical Landsat TM data to generate LAI estimations in a time series for tree growth analysis and modeling in Chile. Additionally, this information can be used as input for ecosystem and hydrological models.

In term of applicability, the LI-COR LAI-2000 has a couple of advantages over TRAC including: 1) previous experience with other *Pinus* species which allows us to calibrate and to use the equipment, 2) data processing is easy to do using the software obtained from the manufacturer. Some disadvantages of LI-COR LAI-2000 are the price of the equipment and the restriction to capture only diffuse irradiation, which is only possible early in the morning, late in the afternoon, or on cloudy days.

We developed an atmospheric correction for each individual band for the set of 23 Landsat TM scenes for our study. As indicated by Song et al. (2001), we found strong differences between corrected and uncorrected images indicating the need to make atmospheric corrections if a project requires the use of images from multiple dates.

Values following topographic correction were correlated with the values that had received atmospheric correction. Probably the position of the plots according the sun angle in summer in Chile reduced dramatically this effect. Further analysis should be developed in order to evaluate the usefulness of topographic corrections during seasons with lower sun angles. This is important as Monthly estimates of LAI are needed for process-based productivity models. Landsat TM data is a promising tool to monitor plantation LAI on a large scale of space and

time where there is an extensive area cover by forest plantations, with heterogeneous landscape and steep topography, like Chile.

Acknowledgements

We acknowledge the work team led by Andrea Avaria, who collaborated in the field campaign in order to measure LAI and other variables from the plots. The senior author acknowledges with thanks the support of the Forest Nutrition Cooperative, allowing him to pursue scientific objectives in his work.

References

Albaugh, T.J., H.L. Allen, P.M. Dougherty, L.W. Kress, and J.S. King. 1998. Leaf Area and Above-and Belowground Growth Responses of Loblolly Pine to Nutrient and Water Additions. For. Sci. 44(2), pp. 317-328.

Beets, P.N. and R.K. Brownlie. 1987. Puruki experimental catchment: site, climate, forest management, and research. N.Z. J. For. Sci. 17:137-160.

Bréda, N.J.J., 2003. Ground-based measurements of leaf area index: a review of methods, instruments and current controversies. J. Exp. Bot. 54, 2403-2417.

Cannell, M.G.R. 1989. Physiological basis of wood *production*: a review, Scand. J. For. Res. 4, pp. 459-490.

Chander, G., B.L. Markham, and D. Helder. 2009. Summary of current radiometric calibration coefficients for Landsat MSS, TM, ETM+, and EO-1 ALI sensors. Remote Sens. Environ. 113 (2009) 893-903.

Chang, J., C., D.E., Leigh, L., Aaron, D., Dalsted, K. and Volz, M. 2008. Evaluating Modified Atmospheric Correction Methods for Landsat Imagery: Image-Based and Model-Based Calibration Methods. Comm. Soil Sci. Plant Anal. 39: 9, 1532-1545.

Chavez, P.S. 1996. Image-Based Atmospheric Corrections – Revisited and Improved. Photogramm. Eng. Rem. S. Vol. 62, No. 9, pp. 1025-1036.

Chen, J.M., Cihlar, J. 1996. Retrieving Leaf Area Index of Boreal Conifers Forests Using Landsat TM Images. Remote Sens. Environ. 55: 153-162.

Chen, J. M., 1996. Optically-based methods for measuring seasonal variation of leaf area index in boreal conifer stands. Agric. Forest Meteorol. 80: 135-163.

Chen, J.M., A. Govind, O. Sonnentag, Y. Zhang, A. Barr, and B. Amiro. 2006. Leaf area index measurements at Fluxnet-Canada forest sites. Agric. Forest Meteorol. 140: 257-268.

Chen, J. M., G. Pavlic, et al. 2002. Derivation and validation of Canada-wide coarse-resolution leaf area index maps using high-resolution satellite imagery and ground measurements, Remote Sens. Environ. 80: 165-184.

Coops, N., A. Delahaye, and E. Pook. 1997. Estimation of Eucalypt Forest Leaf Area Index on the South Coast of New South Wales using Landsat MSS Data. Aust. J. Bot. 45: 757-769.

Curran, P. 1980. Multispectral remote sensing of vegetation amount. Prog. Phys. Geog. 4; 315-341.

Dalla-Tea, F. and E.J. Jokela. 1991. Needlefall, canopy light interception, and productivity of young intensively managed slash and loblolly pine stands. For. Sci. 37:1298-1313.

Flores, F.J., H.L. Allen, H.M. Cheshire, J.M. Davis, M. Fuentes, and D. Kelting. 2005. Using multispectral satellite imagery to estimate leaf area and response to silvicultural treatments in loblolly pine stands. Can. J. For. Res. 36: 1587-1596.

Gower, ST, C.J. Kucharik, and J.M. Norman. 1999. Direct and indirect estimation of leaf area index, fAPAR and net primary production of terrestrial ecosystems. Remote Sens. Environ. 70, 29-51.

Hadjimitsis, D.G., G. Papadavid, A. Agapiou, K. Themistocleous, M.G. Hadjimitsis, A. Retalis, S. Michaelides, N. Chrysoulakis, L. Toulios, and C.R.I. Clayton. 2010. Atmospheric correction for satellite remotely sensed data intended for agricultural applications: impact on vegetation indices. Nat. Hazards Earth Syst. Sci. 10, 89-95.

Hirose. T. 2005. Development of the Monsi–Saeki Theory on Canopy Structure and Function. Ann. Bot. 95: 483-494.

Jarvis, P.G. and J.W. Leverenz. 1983. Productivity of temperate, deciduous, and evergreen forests. *In* Encyclopaedia of Plant Physiology New Series, Vol. 12D, Physiological Plant Ecology IV. Eds. O.L. Lange, P.S. Nobel, C.B. Osmond and H. Zeiger. Springer-Verlag, Berlin, pp 233-280.

Jonckheere, I.S., K. Fleck, B. Nackaerts, P. Muys, P. Coppin, M. Weiss, and F. Baret. 2004. Review of methods for in situ leaf area index determination: Part I. Theories, sensors and hemispherical photography. Agric. Forest Meteorol. Volume 121, Issues 1-2, 2, Pages 19-35.

Landsberg, J.J. and S.T. Gower. 1997. Applications of physiological ecology to forest management. Academic Press, San Diego.

Landsberg, J.J., S.D. Prince, P.G. Jarvis, R.E. McMurtrie, R. Luxmoore and B.E. Medlyn. 1996. Energy conversion and use in forests: the analysis of forest production in terms of radiation utilisation efficiency (e). *In* The Use of Remote Sensing in the Modeling of Forest Productivity. Eds. H.L. Gholz, K. Nakane and H. Shimoda. Kluwer Academic Press, Dordrecht, The Netherlands, pp 273-298.

Leblanc, S.G., J.M. Chen, and M. Kwong. 2002. Tracing Radiation and Architecture of Canopies. TRAC Manual Version 2.1. Canada Centre for Remote Sensing.

Leblanc, S.G. and J.M. Chen, 2005. Tracing Radiation and Architecture of Canopies Manual, Saint-Hubert, Quebec, Canada.

Le Dantec, V., E. Dufrêne, and B. Saugier. 2000. Interannual and spatial variation in maximum leaf area index of temperate deciduos stands. Forest Ecol. Manag. 134:71-81.

LI-COR, LAI-2000 Plant Canopy Analyzer, Lincoln, Nebraska.

Liames, J.S., R. Congalton, A. Pilant, and T. Lewis. 2008. Validation of and Integrated Estimation of Loblolly Pine (*Pinus taeda* L.) Leaf Area Index (LAI) Using Two Indirect Optical Methods in the Southeastern United States. South. J. Appl. For. 32(3): 101-110.

Linder, S. 1987. Responses to water and nutrition in coniferous ecosystems. Ecol. Stud. 61: 180-202.

Mahiny, A.S., and B.J. Turner. 2007. A Comparison of Four Common Atmospheric Correction Methods. *Photogramm. Eng. Rem. S.* Vol. 73, No. 4, pp. 361-368.

Minnaert, M. 1941. The reciprocity principle in lunar photometry. Astrophysics Journal 93**,** 403-410

Monsi, M, and T.Saeki. 1953. U¨ ber den Lichtfaktor in den Pflanzengesellschaften und seine Bedeutung f€ur die Stoffproduktion. Japanese Journal of Botany 14: 22–52.

Moran, M.S., Jackson, R.D., Slater, P.N., and Teillet, P.M. 1992. Evaluation of simplified procedures for retrieval of land surface reflectance factors from satellite sensor output. Remote Sens. Environ. 41:169–184.

Myneni, R.B., R.R. Nenami, and S.W. Running. 1997. Estimation of Global Leaf Area Index and Absorbed Par Using Radiative Transfer Models. IEEE Trans. Geosci. Remote Sensing 35: 1380-1393.

Nilson, T. 1971. A theoretical analysis of the frequency gaps in plant stands. Agric. For. Meteorol., 8: 25-28.

Riaño, D., E. Chuvieco, J. Salas, and I. Aguado. 2003. Assessment of Different Topographic Corrections in Landsat-TM Data for Mapping Vegetation Types (2003). IEEE T. Geosci. Remote Vol. 41, No. 5, pp. 1056-1061.

Richter, R., T. Kellenberger, and H. Kaufmann. 2009. Comparison of Topographic Correction Methods. Remote Sens. Vol 1, pp. 184-196.

Richter, R. 1997. Correction of atmospheric and topographic effect for high spatial resolution satellite imagery. Int. J. Remote Sensing, Vol. 18, No. 5, pp. 1099±1111.

Running, S.W., D.L. Peterson, M.A. Spanner, and K.B. Teuber. 1986. Remote sensing of coniferous forest leaf area. Ecology 67: 273-276.

Santibáñez, F.,and J. Uribe. 1993. Atlas Agroclimático de Chile: regiones sexta, séptima y octava. Ministerio de Agricultura. Santiago, Chile, p. 18.

Sampson, D.A., and H.L. Allen. 1995. Direct and indirect estimates of Leaf Area Index (LAI) for lodgepole and loblolly pine stands. Trees 9: 119-122.

Sampson, D.A., J.M. Vose, and H.L. Allen. 1998. A conceptual approach to stand management using leaf area index as the integral of site structure, physiological function, and structure supply. In Waldrop, T.A., ed. Proceedings of the ninth biennal southern silvicultural research conference; 1997 February 25-27; Clemson, SC. Gen. Tech. Rep. SRS-20. Asheville, NC. U.S. Department of Agriculture, Forest Service, Southern Research Station. 628 p.

Stenberg, P., 1996. Correcting LAI-2000 estimates for the clumping of needles in shoots of conifers. Agric. Forest Meteorol. 79, 1-8.

Stenberg, P., Rautiainen, M., Manninen, T., Voipio, P. & Smolander, H. 2004. Reduced simple ratio better than NDVI for estimating LAI in Finnish pine and spruce stands. Silva Fennica 38(1): 3-14.

Song, C., C.E. Woodcock, K.C. Seto, M.P. Lenney, and S.A. Macomber. 2001. Classification and Change Detection Using Landsat TM Data: When and How to Correct Atmospheric Effects?. Remote Sens. Environ. 75:230-244.

Teillet, P.M., B. Guindon, and D.G. Goodeonugh, 1982. On the slope-aspect correction of multispectral scanner data. Can. J. Remote Sens., vol. 8, pp. 84-106.

Teillet, P. M., and Fedosejevs, G. 1995. On the dark target approach to atmospheric correction of remotely sensed data. Can. J. Remote Sens. 21:373-387.

Vermote, E.F., D. Tanre, J.L. Deuze, M. Herman, and J.J. Morcrette. 1997. Second Simulation of the Satellite Signal in the Solar Spectrum, 6S: An Overview. IEEE T. Geosci. Remote S. 35(3): 675-686.

Vose, J.M., and H.L. Allen. 1988. Leaf Area, Stemwood Growth, and Nutrition Relationships in Loblolly Pine. For. Sci. Vol. 34, No. 3, pp. 547-563.

Waring, R.H. and S.W. Running. 2007. Forest Ecosystems: Analysis at Multiple Scales. 3rd ed. Elsevier Academic Press. London.

Welles, J.M., 1990. Some indirect methods of estimating canopy structure. Rem. Sens. Reviews 5: 31-43.

Welles, J.M., Norman, J.M., 1991. Instrument for Indirect Measurement of Canopy Architecture. Agr. J. 83: 818-825.

White, J.D., S.W. Running, R. Nemani, R.E. Keane, and K.C. Ryan. 1997. Measurement and remote sensing of LAI in Rocky Mountain montane ecosystems. Can. J. For. Res., Vol. 27, pp. 1714-1727.

Zhang, Y., J.M. Chen and J.R. Miller. 2005. Determining digital hemispherical photograph exposure for leaf area index estimation. Agric. Forest Meteorol. 133: 166-181.

Zheng, G., and LM. Moskal. 2009. Retrieving Leaf Area Index (LAI) Using Remote Sensing: Theories, Methods and Sensors. Sensors, Vol. 9, pp. 2719-2745.

Appendix

Appendix 1 - Indirect methods for LAI estimation on the ground

There are several indirect methods based to measure the light transmission through canopies. The greatest advantage of these methods is the capacity to obtain data without foliage collections or any other destructive method (Bréda, 2003). However, the direct methods are more precise and are used for calibration of indirect methods. Unfortunately, the direct methods require higher investments in resources (Sampson and Allen 1995; Sampson et al. 1998).

According to Monsi and Saeki (1953) and Hirose (2005), the total amount of radiation intercepted by the canopy layer depends on incident irradiance, canopy structure and optical properties. All these concepts are integrated in the Beer-Lambert law.

During the last decades, there has been a strong development of instruments oriented to indirectly measure the LAI of forest canopies. Some instruments are based on gap fraction analysis, while others on gap size distribution. The LI-COR LAI-2000 (LAI-2000) is an optical instrument which calculates LAI by comparing differential light measurements above and below canopy. This instrument measures gap fraction and reaches an asymptotic saturation level at a value of about 5 (Gower et al. 1999).

Gap fraction can be defined as the fraction of sky seen from underneath the canopy. It changes with the zenith view angle. It equals minus one of crown closure at the zenith and always zero in the horizontal direction. Gap size is defined as the physical dimension of a gap through the canopy.

Gaps result from tree crown, branch, shoots and leaves which have different sizes and the size distribution carries the information on the canopy architecture. For the same gap fraction, there can be different gap size distributions.

Two canopy attributes affect radiation penetration and indirect LAI measurements. First is the leaf angular distribution affecting radiation transmission through the canopy at different angles and the second is leaf spatial distribution (Jonckheere et al. 2004).

The principle for optical measurements of LAI comes from Beer's law (Nilson 1971):

$$P(\theta) = e^{-G(\theta)\Omega L/\cos\theta}$$

Where P is the gap fraction

θ is the zenith angle,

Ω is the clumping index (leaf spatial distribution, random=1)

G(θ) is the projection coefficient (leaf angular distribution)

L is the leaf area index

Then the effective LAI will be obtained by:

$$L_e = \Omega L$$

Where L_e is the effective LAI (as measured by LI-COR LAI-2000) and LAI (L) can be calculated as follow (Chen et al 2006):

$$L = (1 - \alpha)L_e/\Omega$$

Where α is the woody-to-total area ratio and Ω is the clumping index obtained from the TRAC (Tracing Radiation and Architecture of Canopies) instrument.

The LAI-2000 estimates LAI based on the amount of canopy radiation transmittance measured across a hemispherical field by five concentrically nested sensors (Welles 1990; Welles and Norman 1991).). An "effective" LAI (*Le*) is calculated from this measurement using:

$$L_e = 2\int_0^{x/2} -\ln\big(T(\theta)\big)\cos\theta\sin\theta\ d\theta$$

Where:

T is the canopy transmittance measured across the zenith angle, θ.

The measure of effective LAI (L_e) has been termed effective because of the noise of this measure by self-shading at the needle-to-shoot level (Stenberg et al. 1996), branch and canopy levels (White et al. 1997)., and stand level (Chen and Cihlar 1996).

Leaf spatial distribution refers to the natural arrangements of leaves in the tree canopy (Chen and Cihlar 1996).

a. Random distribution: For each layer of leaves, there is 37% overlapping. Clumping index =1. True for some crops.
b. Clumped distribution: For each layer of leaves, there is more than 37% overlapping. Clumping index <1. True for almost all natural canopies.
c. Regular distribution: For each layer of leaves, there is less than 37% overlapping. Clumping index >1. True for few crops.

Among the instruments oriented to measure gap size distribution, TRAC (Tracing Radiation and Architecture of Canopies) and hemispherical photography (DHP) have provided efficient and reliable estimations (Zhang et al. 2005). For coniferous stands if these methods are combined with clumping analysis, there is a high potential to provide more accurate estimates of LAI than destructive measurements, because they quantify the effect of non-random distribution of foliage (Chen 1996; Leblanc et al. 2005).

Appendix 2 - Atmospheric correction of Landsat TM images

Atmospheric correction is arguably the most important part of the pre-processing of satellite remotely sensed data (Le Dantec et al 2000; Song et al. 2001; Mahiny 2007; Chang 2008). Such a correction is especially important in cases where multi-temporal images are compared and analyzed. For agricultural applications, in which several vegetation indices are applied for monitoring purposes, multi-temporal images are used (Hadjimitsis et al. 2010).The same author found a mean difference of 18% for the NDVI between before and after the atmospheric correction.

Among several image-based calibration models, Song et al. (2001) recommended an approach called DOS3, which was based on the previous DOS model of Chavez (1996).

This method is based in the relationship between the at-satellite radiance and the surface reflectance for a uniform Lambertian surface and a cloudless atmosphere and can be written as:

$$L_{sat} = L_p + \frac{\rho F_d T_v}{\pi\,(1 - s\rho)}$$

where L_{sat} is at-satellite radiance, L_p is the path radiance, F_d is the irradiance received at the surface, T_v is the atmospheric transmittance from the target toward the sensor, s is the fraction of the upward radiation backscattered by the atmosphere to the surface, and ρ is the surface reflectance. The incoming irradiance at the Earth surface . $F_d = E_b + E_{down}$, where E_{down} is the downwelling diffuse irradiance and E_b is the beam irradiance. $E_b = E_0 \cos(\theta_z)\, T_z$, where E0 is the exoatmospheric transmittance in the illumination direction, and Θ_z the solar zenith angle. Since s is small, it can be neglected, and solving for ρ, we have

$$\rho = \frac{\pi\,(L_{sat} - L_p)}{T_v(E_0 \cos(\theta_z)\, T_z + E_{down})}$$

$$T_v = e^{-\tau/\cos(\theta_v)}$$

$$T_z = e^{-\tau/\cos(\theta_z)}$$

where θ_z is the solar zenith angle. For Landsat satellite, the sensor viewing zenith (θ_v) is 0 so finally $T_v = e^{-\tau}$.

In this research, atmospheric correction was based on the method suggested by Song et al. (2001), assuming losses by atmospheric transmittance (T_v and T_z) and diffuse downward radiation at the surface (E_{down}). In this case we assumed Rayleigh scattering only, which means, no aerosols.

The optical thickness for Rayleigh scattering (τ) is estimated as follow:

$$\tau = 0.008569\,\lambda^{-4}\,(1 + 0.0113\,\lambda^{-2} + 0.00013\,\lambda^{-4})$$

where λ is wavelength in μm. E_{down} for a Rayleigh atmosphere was estimated using an atmospheric radiative transfer code. We used the 6S model (Vermote et al. 1997) for a Rayleigh atmosphere, that is, zero aerosol optical depth at 550 m.

Due to the atmospheric scattering effects, the dark object is not absolutely dark (Chavez 1996). Assuming 1% surface reflectance for the dark objects (Chavez 1996; Moran et al. 1992), the path radiance is estimated as

$$L_p = G * DN_{min} + B - 0.01\,[E_0 \cos(\theta_0)\,T_z + E_{down}]\,T_v/\pi$$

where G is the sensor gain and B the bias used for converting the sensor signals (DN) to at-satellite radiance. The minimum DN value, DN_{min} was selected as the darkest DN with at least a thousand pixels for the entire image (Teillet and Fedosejevs 1995).

Appendix 3 - Topographic correction

The effects of the topography, coupled with a low sun angle at the time of satellite overpass can create significant shadowing effects in the data. These effects constrain the application of image classification techniques to further analysis of the data and their applications (Richter 1997, 2009).

The correction of illumination variations is referred to as topographic normalization or topographic correction.

Methods for correcting the topographic effect may be grouped into two categories: those based on band ratios, and those requiring digital elevation models (DEMs). The former are much simpler and do not require additional input data. The reflectance is assumed to increase or decrease proportionally in band ratios (Riaño et al. 2003). Therefore, the ratio between them will compensate for topographic effects. This assumption is valid for the incident angles, which are wavelength independent, but not for the diffuse irradiance, which changes in each spectral band (Riaño et al. 2003). An additional problem is the loss of spectral resolution when ratios are used, which is a drawback in multispectral classification.

The second group of topographic correction methods based on modeling illumination (*IL*) conditions and requires a DEM of the same resolution as the image to be corrected. The DEM is required to compute the incident angle, defined as the angle between the normal to the ground and the sun rays. The *IL* parameter varies from -1 (minimum) to +1 (maximum illumination) and may be computed as follows:

$$IL = \cos(\gamma) = \cos(\theta_p)\cos(\theta_z) + \sin(\theta_p)\sin(\theta_z)\cos(\phi_a - \phi_0)$$

where γ is the incident angle, θ_p is the slope angle; θ_z is the solar zenith angle; ϕ_a is the solar azimuth angle; and ϕ_0 is the aspect angle (all in radians). Once *IL* is computed for the whole image, the flat-normalized reflectance of each pixel is estimated using different methods. They can be grouped into two categories: Lambertian and non-Lambertian, depending on

whether they assume that reflectance is independent of observation and incident angles or not.

The Lambertian assumption is very convenient to simplify procedures but is unrealistic, because most terrains are rugged, having a non-Lambertian behavior (Riaño et al. 2003). The bidirectional reflectance distribution function (BRDF) describes how reflectance varies in each cover considering the angles of incidence and observation. The determination of BRDF is rather complex, since it describes the reflectance behavior at all possible angles of reflection. Therefore, sometimes it is more convenient to assume a Lambertian surface rather than introducing a model that does not comply with the non-Lambertian properties of the surface.

Lambertian techniques assume that the surface reflects energy equally in all directions. The following are Lambertian techniques:

Cosine correction

$$L_H = L_T \frac{\cos(\theta_z)}{IL}$$

where L_H is radiance of horizontal surface, and L_T is radiance of inclined surface. This method is known for resulting in overcorrection of weakly illuminated areas as it does not take into account sources of illumination other than the direct irradiance (e.g. diffuse skylight or light reflected from surrounding pixels).

Modified cosine correction

This method seeks to improve the above equation by taking into account average illumination conditions, and reducing the overcorrection effect. It is computed as:

$$L_H = L_T + \left[\frac{(IL_m - IL)}{IL_m}\right]$$

where IL_m is the average *IL* value for the study area.

Non-Lambertian techniques try to model the roughness of the surface, or the degree to which it is Lambertian. Usually, they require the calculation of correction coefficients which are wavelength dependent. Therefore, each band is processed separately.

The computation of the correction factors will be done using a subset of pixels from the same land cover class. First, we will extract the pixel values from the image bands and illumination layers, and then, we will compute the correction factors.

Among the non-Lambertian techniques are:

Minnaert correction

This method was proposed by Minnaert (1941), who modified the cosine correction by including a factor which measures the extent to which a surface is Lambertian. This method is computed as:

$$L_H = L_T + \left[\frac{\cos(\theta_z)}{IL}\right]^{K_k}$$

where K_k is the Minnaert constant for band *k*. *K* ranges between 0 and 1. If *K*=1, then the equation becomes the same as the cosine correction, meaning that the surface behaves as a perfect Lambertian reflector.

The value of *K* is computed by linearization of the above equation:

$$\ln(L_H) = \ln(L_T) + K_k ln\left[\frac{\cos(\theta_z)}{IL}\right]$$

where $ln(L_H)$ is the intercept of the regression, and K_k is the slope of the regression for band *k*.

C-correction

This technique was introduced by Teillet et al. (1982) and includes the calculation of the parameter "*C*", as follows:

$$L_H = L_T + \left[\frac{\cos(\theta_z) + C_k}{IL + C_k}\right]$$

where

$$C_k = \frac{b_k}{m_k}$$

where b_k and m_k are the regression coefficients (for band k) of:

$$L_T = b_K + m_K IL$$

Modified C-correction

This technique was proposed by Riaño et al. (2003). The assumption is that most methods produce and overcorrection in those pixels were *IL* is low. Therefore, a variation in the calculation of the *IL* is developed in order to smooth the original slope.

Originally, the slope is calculated as:

$$\theta_p = \arctan\left(\frac{\mathrm{b}}{\mathrm{a}}\right)$$

which was transformed into

$$\theta_p^{'} = \arctan\left(\frac{\mathrm{b}}{\mathrm{X} * \mathrm{a}}\right)$$

where *X* could be for instance 3,5 or 7.

Table 1. Structural characteristics plots selected for ground measurement of LAI during 2009 (dbh: diameter at breast height, i.e. 130 cm).

	LAI	Height [m]	DBH [cm]	Density [trees ha^{-1}]	Basal Area [m^2 ha^{-1}]
Min	1.5	9.7	12.2	590	11.5
Max	4.0	22.4	26.3	1,360	46.2
Mean	2.4	15.5	18.8	945	26.2

Table 2. Landsat 5 TM satellite images used in the study.

Site	Scene	Date	Sun elevation angle (°)	Sun Azimuth angle (°)
Coast VII Region	1_85	February 24, 2005	45	63
	1_85	January 29, 2007	54	76
	1_85	January 16, 2008	54	76
	1_85	March 7, 2009	43	59
Coast VIII Region	1_86	January 7, 2005	54	77
	1_86	January 13, 2007	54	75
	1_86	February 17, 2008	47	64
	1_86	March 7, 2009	42	58
VII Region	233_85	April 6, 2005	35	47
	233_85	February 7, 2007	47	69
	233_85	February 1, 2008	49	68
	233_85	February 12, 2009	48	68
VIII Region	233_86	February 1, 2005	49	71
	233_86	February 20, 2006	46	63
	233_86	February 23, 2007	46	61
	233_86	February 10, 2008	49	67
	233_86	February 12, 2009	47	67
IX Region	233_87	February 1, 2005	49	70
	233_87	February 4, 2006	49	68
	233_87	February 23, 2007	43	66
	233_87	February 26, 2008	44	60
	233_87	February 12, 2009	46	66

Table 3. Predictive regression relationships of the LAI against NDVI, SR, and RSR for *Pinus radiata* in Chile.

Model	R^2	SE of estimate LAI	Parameter	Estimate	95% confidence interval Lower	Upper	*p-value*
LAI = *a* + *b* NDVI	0.61	0.29	Intercept (*a*)	-2.62	-4.41	-0.82	0.0066
			Slope (*b*)	6.72	4.24	9.20	< 0.001
LAI = *a* + *b* SR	0.65	0.28	Intercept (*a*)	0.27	-0.41	0.95	0.4170
			Slope (*b*)	0.30	0.20	0.40	< 0.001
LAI = *a* + *b* RSR	0.67	0.27	Intercept (*a*)	0.39	-0.23	1.00	0.2039
			Slope (*b*)	0.32	0.22	0.43	< 0.001
LAI = $a * \exp^{b*NDVI}$	0.65	0.28	Intercept (*a*)	0.18	0.12	0.25	0.0358
			Slope (*b*)	3.44	3.23	3.64	<0.0001
LAI = $a * \exp^{b*SR}$	0.65	0.28	Intercept (*a*)	0.92	0.87	0.97	<0.0001
			Slope (*b*)	0.13	0.12	0.14	<0.0001
LAI = $a * \exp^{b*RSR}$	0.67	0.27	Intercept (*a*)	0.14	0.09	0.18	<0.001
			Slope (*b*)	0.02	0.01	0.03	<0.001

Note: LAI was measured with LI-COR LAI 2000 during late summer 2009. NDVI, SR and RSR were calculated for the corresponding Landsat 5TM images.

Table 4. Annual LAI (maximum) obtained from linear regression between RSR and LAI, for selected plots from 2005 to 2009 (blank spaces correspond to lack of Landsat TM scenes for 2006; plot# ordered from minimum to maximum LAI observed for 2009)

Plot #	2005	2006	2007	2008	2009	2009_obs
1	1.47	1.28	1.23	1.76	1.48	1.52
2	1.46	1.58	2.21	1.76	1.69	1.55
3	1.47		1.74	1.48	1.76	1.60
4	1.30	1.38	1.73	1.15	1.49	1.61
5	1.23		1.09	1.09	1.25	1.63
6	1.65	1.36	1.86	1.87	2.02	1.69
7	1.55	1.88	2.54	2.03	2.14	1.83
8	2.54	2.78	3.08	2.06	2.35	1.98
9	1.67	1.72	2.18	1.85	1.97	2.05
10	1.87	1.93	2.35	1.97	1.56	2.05
11	1.95		2.01	2.12	1.95	2.10
12	1.65		1.84	1.58	1.60	2.17
13	1.82		1.81	1.71	1.76	2.18
14	2.51	2.61	3.09	2.88	2.68	2.18
15	1.92	1.99	2.64	2.40	2.51	2.19
16	1.48	1.72	2.31	1.92	1.94	2.23
17	1.27		1.10	1.07	2.25	2.29
18	2.73	2.83	3.24	2.77	2.57	2.34
19	2.86	2.27	2.76	2.35	2.57	2.35
20	1.51	1.96	2.76	2.21	2.33	2.36
21	2.45	2.40	2.61	2.57	2.60	2.40
22	1.41	1.96	2.53	1.91	2.21	2.42
23	3.05	3.21	3.57	2.74	1.79	2.49
24	2.07	2.00	2.21	2.03	2.11	2.52
25	1.66	1.72	2.27	1.94	1.95	2.55
26	3.17	2.73	3.04	1.97	2.13	2.57
27	2.34	2.01	2.62	1.59	2.23	2.58
28	2.03	2.30	3.11	2.62	2.39	2.63
29	2.81	2.93	3.41	3.07	2.99	2.74
30	2.99	2.56	2.90	2.88	2.70	2.75
31	2.83	2.79	3.59	2.76	2.67	2.78
32	2.46		2.93	2.40	2.75	2.79
33	2.56	2.02	2.90	2.77	2.84	2.95
34	2.43	2.14	2.53	2.33	3.15	3.18
35	1.89	2.15	2.76	2.51	2.97	3.38
36	2.44		2.26	2.02	3.28	3.49
37	3.75	3.58	4.24	3.44	3.60	3.95
Max	1.2	1.3	1.1	1.1	1.3	1.5
Min	3.8	3.6	4.2	3.4	3.6	4.0
Mean	2.1	2.2	2.5	2.2	2.3	2.4

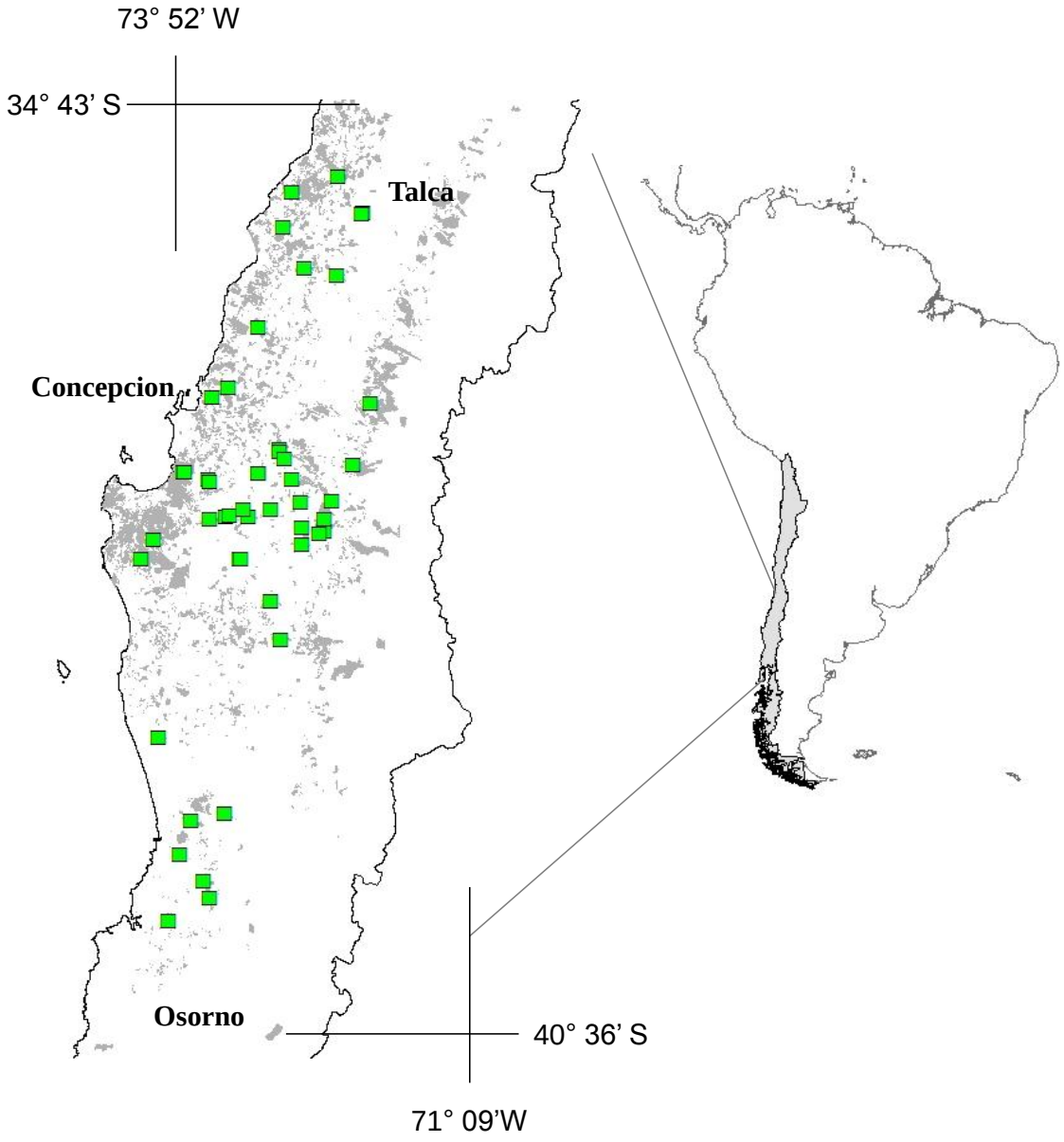

Figure 1. Research area for remote sensing LAI estimations in Chile and plots selected for ground measurements using LI-COR LAI-2000 (boxes, and grey color represent forest plantations).

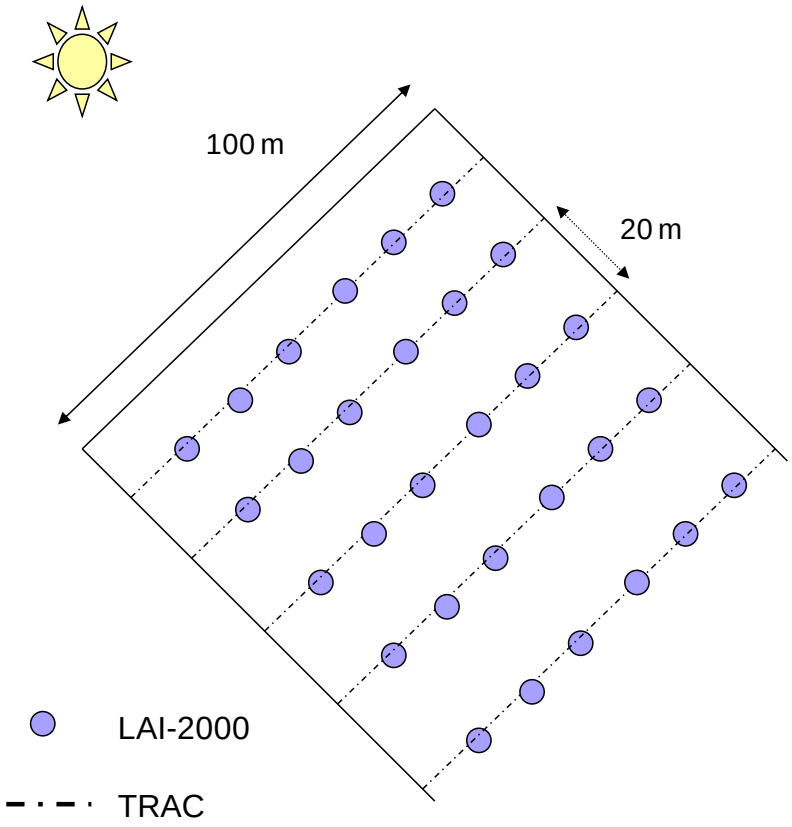

Figure 2. Sampling scheme in 1 ha plot where TRAC, LAI-2000 and forestry measurements were collected. (Based in Leblanc et al., 2002, adapted for southern hemisphere).

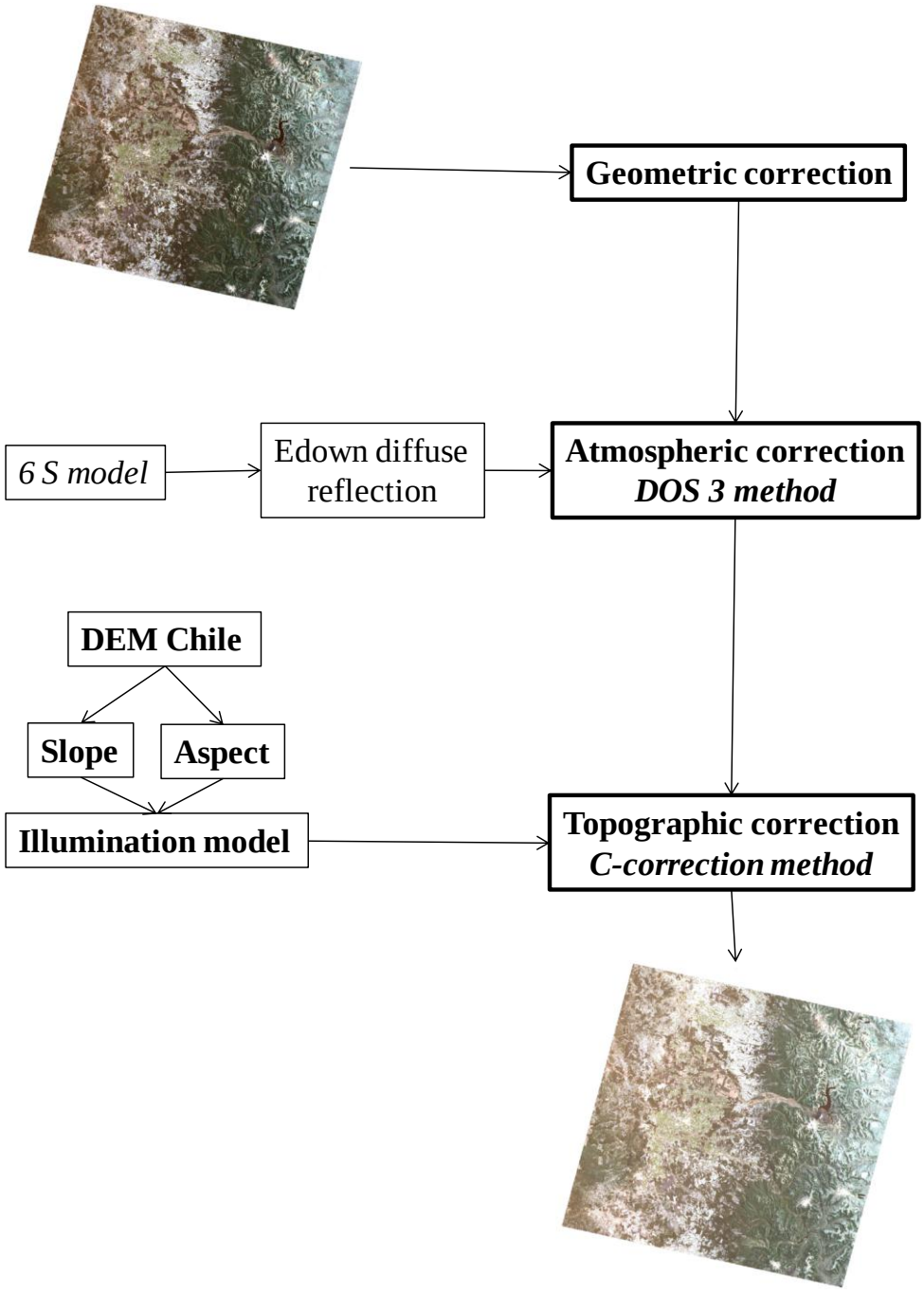

Figure 3. Diagram of main processing steps for geometric, atmospheric and topographic correction of Landsat TM images.

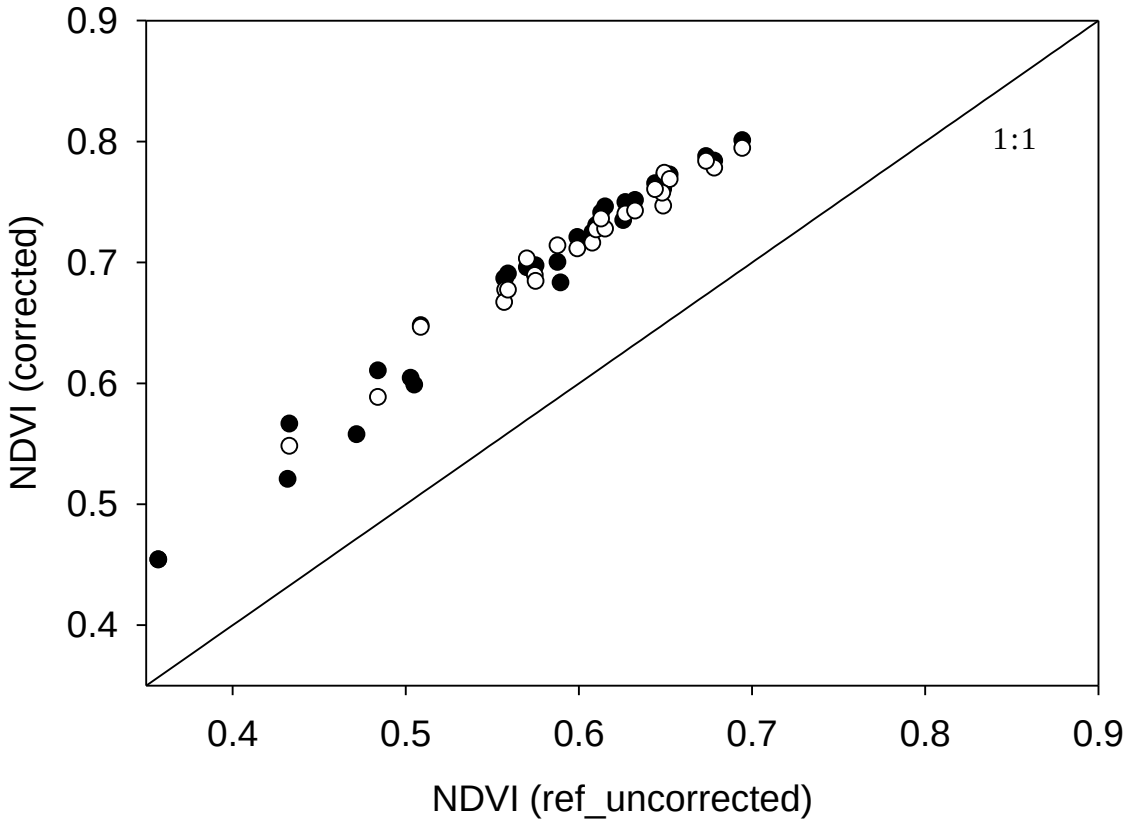

Figure 4. Normalized Difference Vegetation Index (NDVI) indice obtained before (ref_uncorrected) and after (corrected), atmospheric (●) and atmospheric and topographic correction (○).

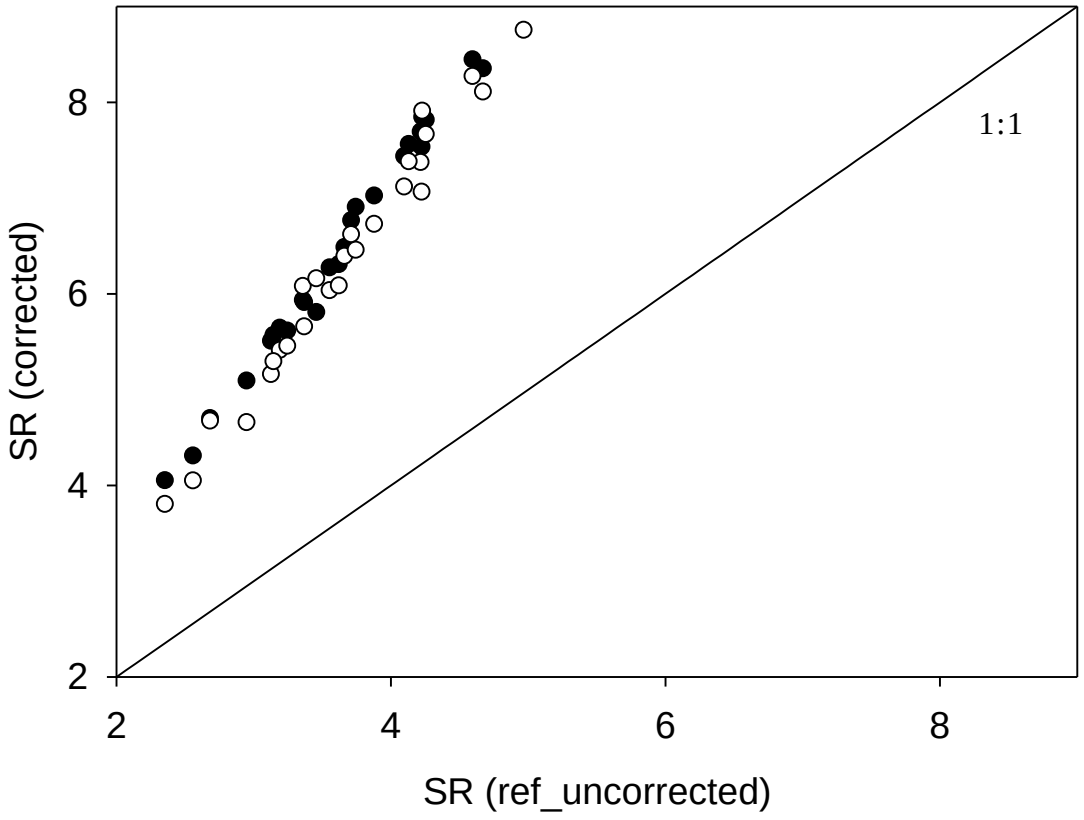

Figure 5. Simple Ratio (SR) indices obtained before (ref_uncorrected) and after (corrected), atmospheric (●) and atmospheric and topographic correction (○).

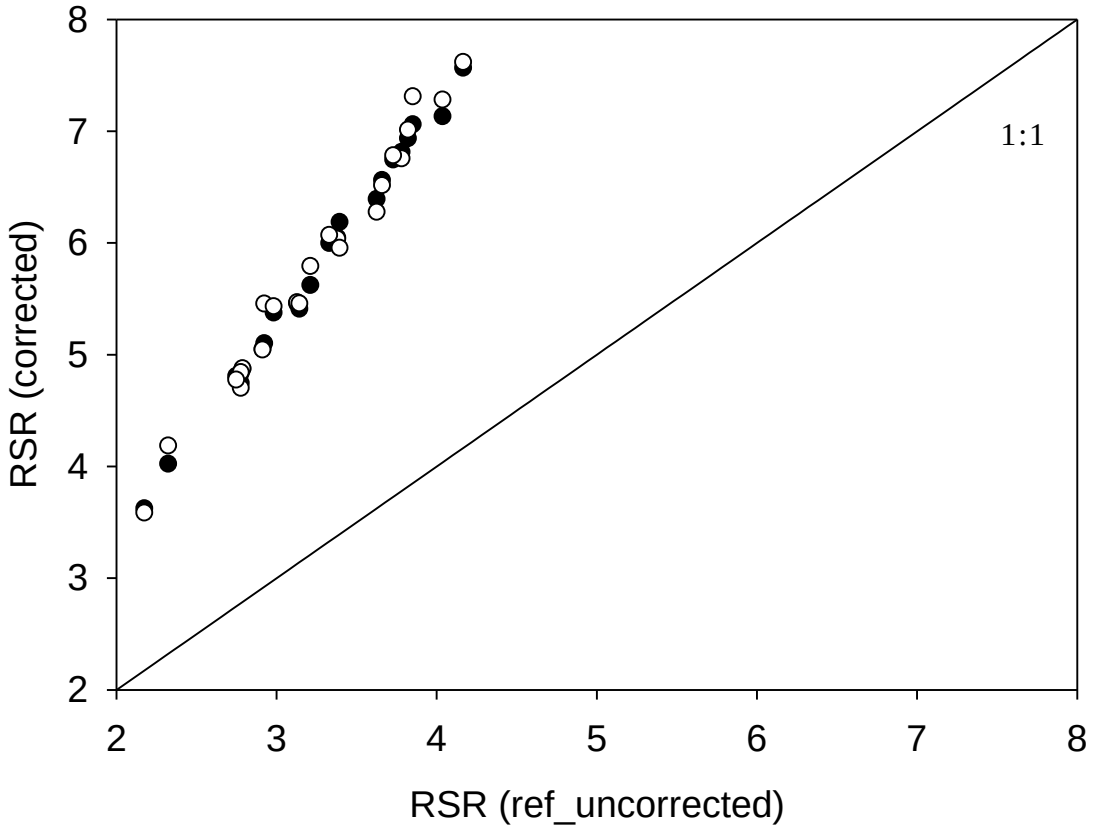

Figure 6. Reduced Simple Ratio (RSR) indice obtained before (ref_uncorrected) and after (corrected), atmospheric (●) and atmospheric and topographic correction (○).

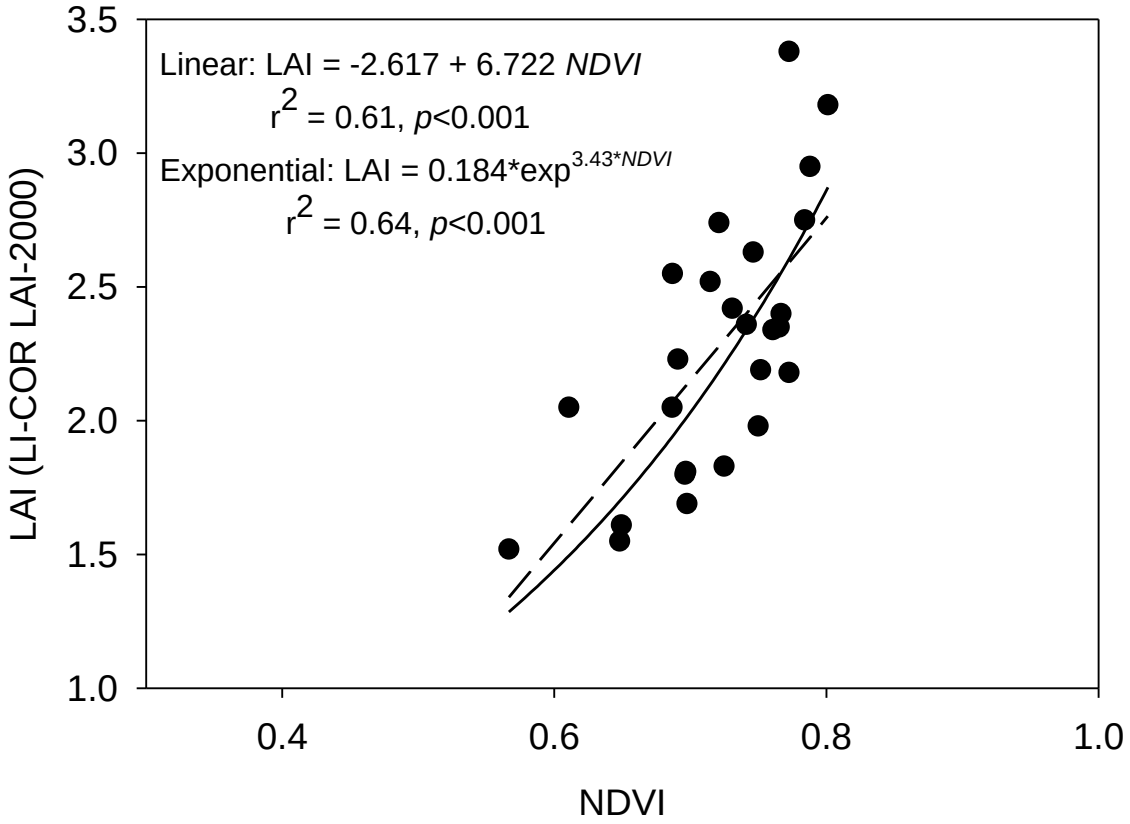

Figure 7. Relationship between LAI and NDVI for plots measured with LI-COR LAI-2000.

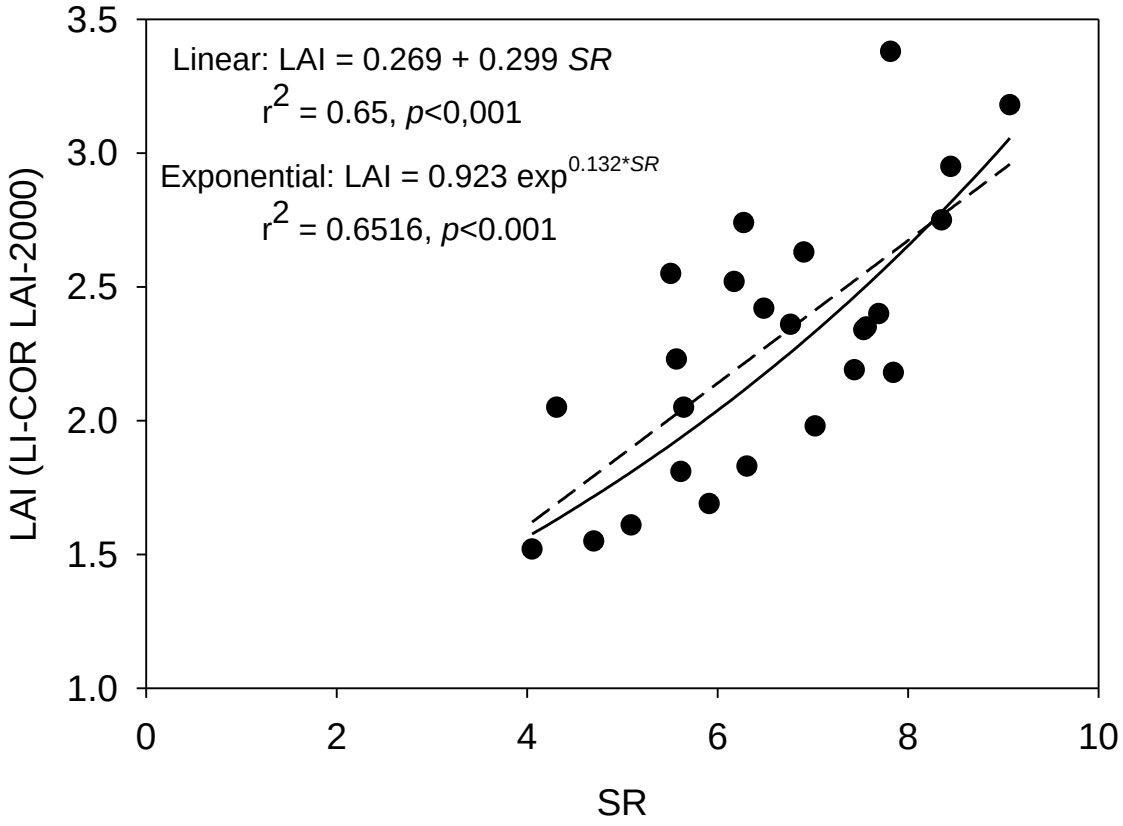

Figure 8. Relationship between LAI and SR for plots measured with LI-COR LAI-2000.

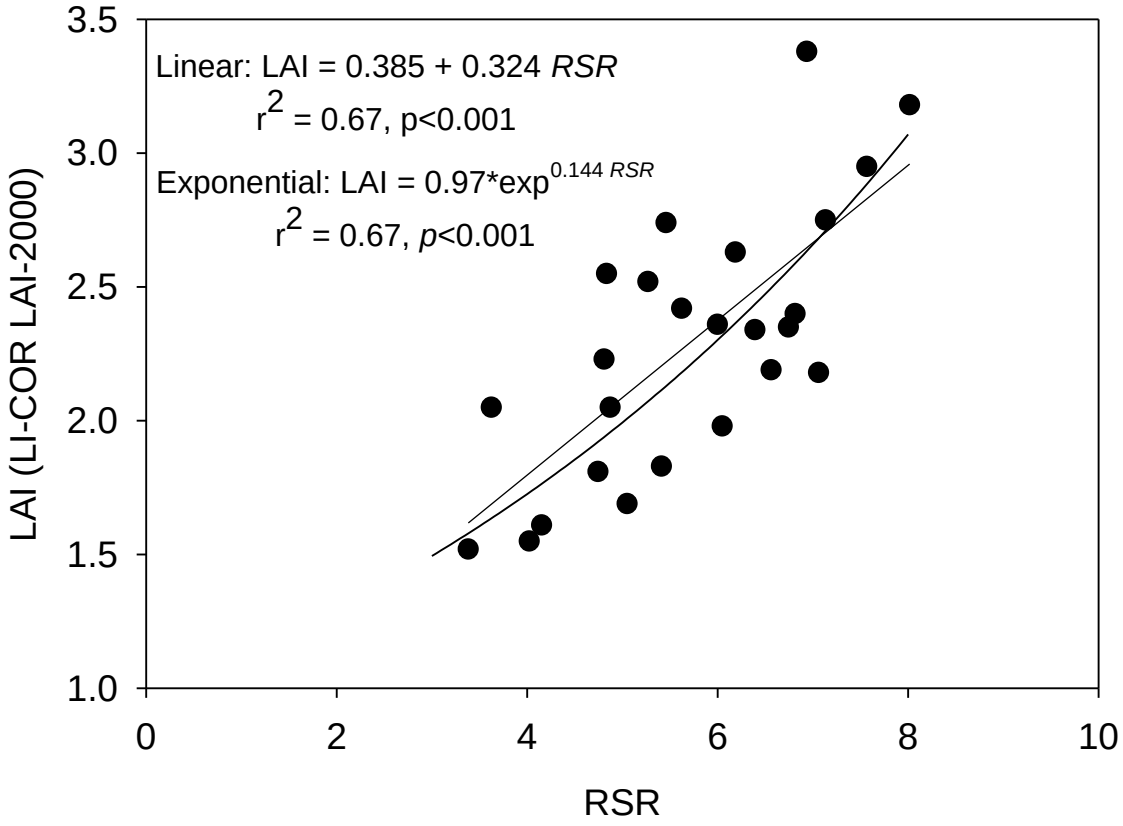

Figure 9. Relationship between LAI and RSR for plots measured with LI-COR LAI-2000.

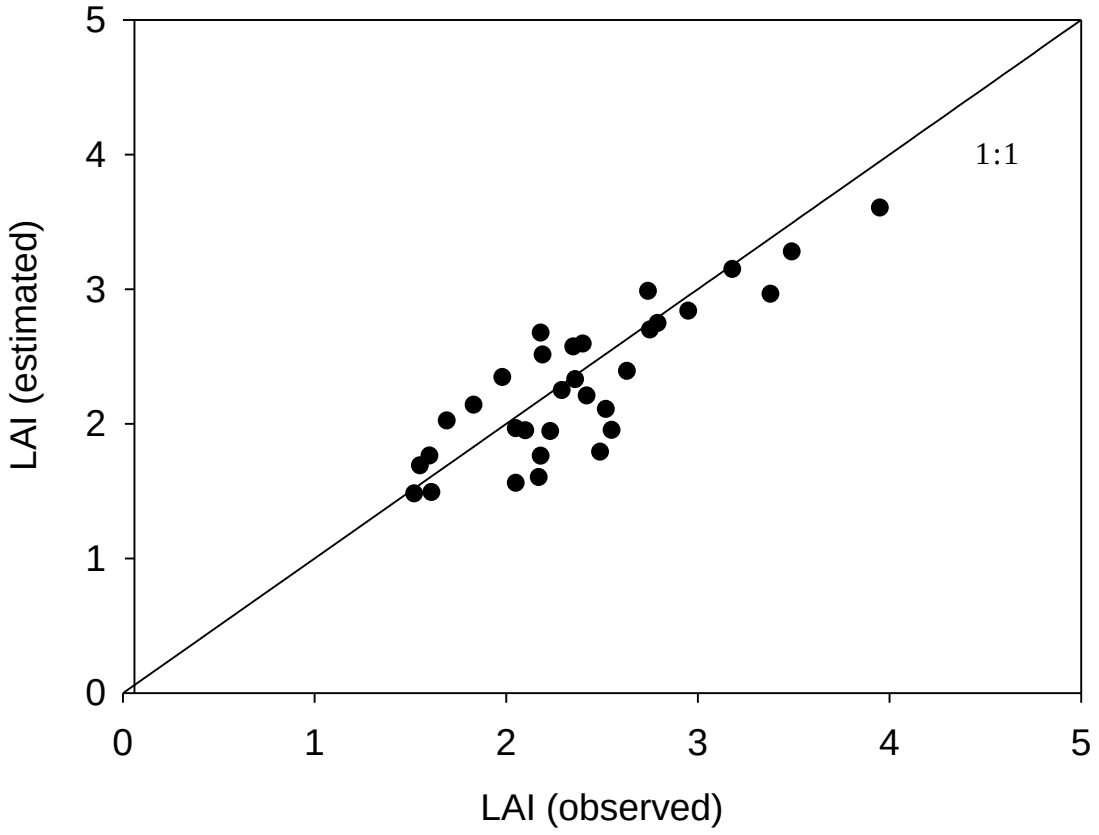

Figure 10. Comparison between observed and estimated LAI for 2009, using the RSR model.

CHAPTER 3

Factors Influencing the Growth of Radiata Pine Plantations in Chile

Abstract

We examined environmental factors affecting growth rates of *Pinus radiata* in Chile. The relationships between annual volume growth and soil, climate, canopy and stand factors were examined using data from 48 permanent sample plots in *Pinus radiata* plantations in central Chile. Water availability (as affected by precipitation, soil water holding capacity, and PET) appeared to be the factor most limiting to leaf area and growth. Maximum growing season temperature also negatively affected growth. Sites with highest productivities had the lowest annual water deficits. The most productive sites used water and light more efficiently. Good sites produced 1.6 as compared to 0.49 kg of wood per m^3 of potentially evapotranspired water on less productive sites. In addition, productive stands produced 0.5 as compared to 0.31 g of wood per MJ on less productive sites. The inclusion of simple climatic variables such as maximum temperature and precipitation into Chilean *Pinus radiata* growth and yield models should improve their performance as yield models.

1. Introduction

Commercial plantations of *Pinus radiata* D. Don are the basis for forest industry in Chile. This species was introduced circa 1881 near Concepcion city (Contesse 1986). *Pinus radiata* planting were first used to stabilize dunes in the Chanco area. With the first government promotion in 1931, *Pinus radiata* was established across several site types and climate conditions. By 1973, the area occupied by this species was only 158,800 hectares (INFOR 1974); however with the new government Ordinance Law 701 of 1974[1], there was a large increase in *Pinus radiata* planting. During a 20 year period, the Chilean government invested about 120 million US$. These investments in pine plantations were augmented by public investments in roads and ports and private industry investments. By 2009, Chile had a 2.3 million ha of plantations, with 63% represented by *Pinus radiata* (INFOR 2010).

Thousands of hectares of *Pinus radiata* plantations were established on highly eroded soils (Hartwig 1994), with primitive soil preparation practices such as burning, tillage in the slope direction, and no fertilization. More intensive practices including improved genetics, weed control, boron application, and subsoiling were initiated in the early 1990s. These practices improved survival and also individual tree growth; however, there is still much variability in diameter, height, and volume growth across sites. Climatic variation is assumed to be more important in causing this variation than variation in genetics, seedling establishment practices, and operations quality. However, this hypothesis has not been tested.

Pinus radiata plantations exhibit growth rates that vary within and between years on the same site. This variation results from environmental conditions that affect canopy development, canopy function, and partitioning of assimilate. Cannel (1989) reviewed the physiological basis for wood production and recommended that growth be analyzed in terms of light use. This concept implies that wood production is determined by the amount of light

[1] This law provided funds to pay 75% of the cost of plantation establishment and also lowered the Complementary Global Tax (Cerda 1998).

intercepted, its efficiency of use, and the proportion of photosynthate partitioned to wood. Environmental factors other than light, such as nutrient supply, low or high temperatures, and water stress can have large effects on leaf area production and retention, and therefore dry matter production through their effect on the amount of light intercepted (Waring 1983). Extreme temperatures and severe drought may reduce light use efficiency, or increase respiration or foliage loss, while water and nutrient availability may also influence partitioning (Cannell 1989).

The effects of moisture and nutrient availability on the growth of *Pinus radiata* have been studied under conditions of natural rainfall, induced drought, and irrigation for more than 60 years. Turner and Lambert (1986) reported on nutritional relationships. Linder et al. (1987) and Snowdon and Benson (1992) identified water and nutrients as key factors limiting growth of *Pinus radiata* at the Biology of Forest Growth (BFG) study near Canberra, Australia. The importance and complexity of the interactions between moisture and nutrients and their effects on the physiological processes involved in tree growth have been reported by many authors (Linder and Rook 1984) and have been the basis for much modeling work (e.g. McMurtrie et al. 1990). Most relevant field experiments with *Pinus radiata* involve either addition of nutrients, manipulation of stocking or removal of weeds as a means of lowering moisture stress. The BFG experiment (Benson et al. 1992) provided a unique opportunity to examine tree growth over a wide range of growing conditions on the same site where both moisture and nutrients were manipulated and quantified. Linder et al. (1987) reported the effect of irrigation and fertilization on canopy dynamics and growth in that experiment during a severe drought.

Most of the research on *Pinus radiata* has been undertaken in Australia and New Zealand. Little systematic analyses have been undertaken in Chile. Good growth rates may have limited interest and government funding for more detailed analysis of the ecophysiological basis for wood production.

In this study we examined growth in *Pinus radiata* plantations in 48 locations spanning 650 km along a gradient in central Chile. Objectives were: (1) to examine year to year variability in stand growth; (2) to identify the soil, climatic, canopy and stand factors that contribute to the variability in growth; and (3) to quantify relationships between stand growth in relation to the supply, use and efficiency of water and light.

2. Material and Methods

Study area

Sample plots were located in *Pinus radiata* plantations throughout South-central Chile in an area ranging from 34°43' to 40°36' S latitude (north to south) and 71°09' to 73°52' W longitude (west to east) (Figure 1). Long-term mean annual precipitation ranged from 500 mm in the north to greater than 2,000 mm in the southwest.

Permanent sample plots data

The plots used for this study were selected from a larger set of plantations where permanent sample plots were installed in 1997 or 1998 to provide data for the Modelo Nacional de Simulación de Pino radiata de Chile (Real 2006). Plots were 11 or 12 years old in 2009. All plots were installed using a standard protocol. Most plots were installed by the two largest forestry companies in Chile (Arauco and CMPC). Based on the 2008 measurements, plots were classified by geographic location; mean annual volume increment, soil texture, elevation and distance from the Pacific Ocean. A subsample of 48 plots was selected to represent the range of conditions (Tables 1, 2, 3 and Figure 1). Another critical component in the selection process was the availability of annual tree measurements during the period 2004 to 2008. All plots were located on moderate micro relief slopes (< 3%), especially in the flat central valley. On steep terrain, such as coastal range, most plots were installed in soils with slopes greater than 20%.

The operational establishment activities for the plantations included: slash management and/or subsoiling. The stands were planted in either July 1997 or July 1998, by hand, at different spacing ranging between 3 x 2 (meters, between and within plantation rows) to 3 x 3. All plots received an operational fertilizer treatment of boron (3 g/tree). Weed control was applied in 2 m bands at least 2 times, first immediately after planting and the second at the beginning of the second growth season. Plants (seedlings and cuttings) were provided from the operational programs of each company and had high levels of genetic gain in both volume and stem straightness.

In each stand, a circular inventory plot of 1,000 m^2 was established at year 0. To calculate elevation, a digital elevation model (DEM) was generated with a cell size of 30 m and simplified to 400 m for further analysis.

Volume and site index calculations

Plots were measured during the winter season of every year (May-August) starting with the year of planting (1997 or 1998). Total height (ht) and diameter at breast height (dbh, since age 4 was measured on all trees of each individual plot of 1,000 m^2). Individual tree volume (m^3 ha^{-1}) was calculated using the following equation (Mininco 1995):

$$\text{Volume} = 0.00214 + 0.0000295\,(\text{dbh})^2 + 0.001349\,(\text{ht}) + 0.00002486\,(\text{dbh})^2\ (\text{ht})$$

Where:

dbh = diameter at breast height [cm]

ht = total height [m]

Individual volumes were summed to obtain volume per plot and per hectare. For our study, we used year 2004 through 2009 measurements to calculate current annual increments (CAI, volume growth). We converted volume growth to biomass growth using site-specific values of wood density according Peredo and Mora (2004). We estimated site index using the following equation (Mininco 1995):

$$SI = 10^{(LOG(hdom) - 0.3455 + \frac{6.91}{age})}$$

Where:

SI	=	Site index at 20 years old (m). Average of 100 highest trees per hectare [m]
hdom	=	Dominant height [m]
Age	=	Stand age [years]

Soil data

Soil samples were obtained to a depth of 20 cm at five locations inside each plot providing a composite sample of approximately 1 kg per plot. This soil was dried at 65° C to a constant weight. Soil pH was obtained with both water and $CaCl_2$.Total organic carbon and organic matter was obtained by wet combustion and titration (Walkley and Black 1934). Total soil nitrogen using Kjeldahl (Page 1982). P was measured using a 0.5 mol/L solution of sodium bicarbonate at pH 8.5 (Olsen et al. 1954) and Bray and Kurtz-2 (Bray and Kurtz 1945) methodologies. Ca, Mg, K and Na were obtained using a 1 mol/L ammonia acetate (NH_4Ac) at pH 7.0 extraction (Page 1982). Extractable aluminum was obtained using ammonia acetate pH 4.8 and spectrophotometry (Sadzawka et al. 2004). Boron was measured using extraction with $CaCl_2$ and colorimetric determination (McGeehan et al 1989). Soil texture was determined by the hydrometer method (Miller et al. 1997). Due to budget constraints, we were only able to obtain soil samples from 37 plots.

Soil moisture holding capacity estimates (millimeters of water per meter of soil) were obtained for each plot using tabular values based upon soil texture and measured horizon depths to a total depth of 1 m (Modelo Nacional de Simulación de Pino Radiata).

Climate data

Daily precipitation and temperature data were available from 224 weather stations in the study region (Figure 1). This data set comes from a network of weather stations belonging to Chilean agencies and a private forestry company. All data were integrated into a spatial database. The climate database prepared for the analysis included location of meteorological stations (latitude, longitude), altitude (in meters) and monthly rainfall and temperatures (maximum and minimum) values. Monthly air temperature and precipitation values for each plot were obtained using a distance-weighted average from the nearest stations (30 km radius) using ArcGis 9.3 (ESRI 2009).

In total, 50 of 224 weather stations were used. The number of weather stations assigned to each site varied from 1 to 7, depending on the density and location of weather stations. Values of climatic variables were obtained by averaging across all weather stations. For each climatic variable, we calculated whole year averages and growing season (September to April) averages. Using maximum and minimum temperature we calculated vapor pressure deficit (VPD, in mBar) through the following equation (Sands 2002):

$$VPD = \left[\frac{6.1078 * e^{(17.269 * T\max/(237.3 + T\max))} - 6.1078 * e^{(17.269 * T\min/(237.3 + T\min))}}{2} \right]$$

Where:

VPD = Vapor pressure deficit [mBar]

Tmax = maximum temperature [°C]

Tmin = minimum temperature [°C]

Potential evapotranspiration was calculated using the Penman-Monteith equation following the procedures of Allen et al. (1998), ASCE-EWRI (2004) and Snyder and Eching (2006).

Water index

We defined water index (WI) as follow:

$$WI = Pp - PET + SWC$$

Where:

WI = Water deficit index during the year [mm $year^{-1}$]

Pp = Precipitation during the year [mm $year^{-1}$]

PET = Potential Evapotranspiration during the year, calculated as Penman-Monteith [mm $year^{-1}$]

SWC = Soil Water Holding Capacity at 1 m soil depth [mm]

We considered the year starting in August until July of the following year. The Penman-Monteith equation was used to calculate a water balance for each plot (Allen et al. 1989, 1998; ASCE-EWRI 2004; Snyder and Eching 2006). We used annual values of potential evapotranspiration (PET) and moisture deficit calculated by the site water balance model. In order to compute moisture deficit using the Penman-Monteith model, the following information was used: historical maximum and minimum monthly air temperature, historical mean monthly precipitation, averaged wind speed and the soil moisture holding capacity of the soil to a predetermined depth (1 m in our study). We estimated monthly solar irradiation using the Bristow-Campbell model (Thornton and Running 1999) to include annual variation in our estimates of PET. All values were calculated for every plot using climate data from neighbor weather stations (30 km radius).

Canopy data

Stand LAI (projected $m^2\ m^{-2}$) was measured once in fall 2009 (end of growing season 2008-2009) in each of 48 PSP using a LI-COR LAI-2000. For each plot, 30 LAI measurements along several transects on the east-north side of the plot were made at a height of 60 cm

between 0700 and 1000 EST or between 1600 to 18000 EST using a 45° view cap. Simultaneously, above canopy light measurements were collected in an open field adjacent to the study site where the light sensor had an unobstructed view of the sky. The above sensor took data every 15 seconds, while we were measuring inside each plot. The below sensor was maintained around 1 m above the ground, with the sun in the back of the measure. Both, below and above sensors were maintained in the same direction. To avoid the influence of direct irradiation in the above sensor, we installed a board cup to protect the lens. The 30 measurements were averaged to estimate the plot LAI.

To account for variation between years, we used estimations from remote sensing calculations (see chapter 2). With the georeferenced plot and a sequence of Landsat TM scenes, we estimated LAI using following equation (from chapter 2):

$$LAI = 0.39 + 0.32 * RSR$$

Where:

LAI = Leaf Area Index [m^2 m^{-2}]

RSR = Reduced Simple Ratio (vegetation index)

In order to estimate annual light interception, we estimated monthly values of LAI using the proportional adjustment of Whitehead et al. (1994) and assumed the behavior of LAI was the same for each site. With these data we estimated monthly intercepted solar irradiation (APAR) using the Beer-Lambert law and an extinction coefficient of 0.45 (Landsberg and Waring 1997). Photosynthetically active radiation (PAR) was calculated as 50% of incoming radiation (Landsberg and Gower 1997).

APAR

We calculated intercepted radiation using the Beer's law:

$$APAR = (1 - e^{-kL}) * PAR$$

Where:

APAR = Intercepted (actual) Photosynthetically Active Radiation (daily-monthly [MJ m^{-2} day^{-1}] or yearly [TJ ha^{-1} yr^{-1}])

K = Extinction coefficient (0.5 according Landsberg 1997)

L = Leaf Area Index [m^{-2} m^{-2}]

PAR = Photosynthetically active radiation (daily-monthly [MJ m^{-2} day^{-1}] or yearly [TJ ha^{-1} yr^{-1}]).This value was determined by 50% of solar incoming radiation (Landsberg 1997).

Data modeling

We developed our analysis in two steps:

- Explanatory using data from 2009 measurements
- Explanatory using the whole data set from 2005 to 2009

Explanatory and prediction model using 2009 data set

We developed this analysis using only LAI estimates from the LI-COR LAI-2000 obtained during the fall season of 2009. With these data we examined the factors that affected growth across sites during the 2008-2009 growing season. This analysis was oriented to provide information about one specific year and further comparison with a longer period of time.

Explanatory using 2005 - 2009 data set

In this analysis, we included all growth measurements and also remote sensing estimates of annual peak LAI for the period 2005-2009 in order to examine both within site (across year) and between site variations in growth. The information from this analysis will provide

information about spatial and temporal changes for the plots. In addition, we can compare these results, including variation in environmental conditions, with the 2009 year.

Statistical analysis

Correlation analyses were developed between all variables. After this procedure, we selected variables of interest (high r^2 and significant p-values, i.e. less than 0.05) and included them in regression analysis. We grouped of the independent variables (31) into soil, climatic, canopy, and stand attribute groups (following procedures of Stape et al. 2004b and Rojas 2005) (Table 4). We selected the most relevant variables from the correlation analysis and regressed volume growth against these variables.

For the 2009 measurement where LAI was obtained with the LI-COR LAI-2000, we developed least squares multiple regression analysis (SAS 2009) in order to determine the relationship between stem growth (annual increment) and variables of soil, climate, canopy, stand, and their combinations. The null hypothesis was tested at $\alpha = 0.05$ level.

For the whole data set (2005-2009), we used LAI estimated from remote sensing data. We analyzed linear model against variables of soil, climatic, canopy, stand and combinations of these variables.

We developed a repeated measures analysis with Proc Mixed (SAS 2009) in order to determine temporal and space variations in productivity.

3. Results

Site and stand characteristics

The 48 plots covered an extensive range of soil and climate conditions where *Pinus radiata* is growing in Chile. Clay content varied between 8 to 64% at 0.3 m depth. 46 plots had less than 50% of clay content. Total C organic varied between 0.28 to 12.6% (with higher values in volcanic ash soils). P values for Olsen and Bray and Kurtz-2 extractions varied between 3-18 and 0.32 – 111 ppm respectively. Lowest content were found in volcanic soils and highest in sandy soils. Exchangeable K, Ca and Mg varied between 0.05-1.7, 0.16-9.9 and 0-4.3%, respectively. Volcanic ash soils also had the highest content of extractable Al. Water holding capacity (1 m depth) varied from 44 to 480 mm. Averaged rainfall ranged from 540 to 2300 mm per year (23 sites with rainfall less than 1000 per year). The annual rainfall differed across sites and years (Figure 2). Several sites located in the central valley or northern limit have frequently summer seasons with little or zero rainfall, which means around 5-6 months with high water deficit. Mean annual temperatures ranged from 14 to 18° C and PET ranged from 670 mm to 1050 mm with differences between sites (coefficient of variation of 17%). Total annual PAR (photosynthetically active radiation) ranged between 22 to 36 TJ per hectare per year.

Leaf Area Index estimated with LI-COR LAI-2000 ranged 1.3 to 4.5; while values estimated using remote sensing ranged 1.2 to 3.7. Total intercepted Photosynthetically active radiation (APAR) ranged between 10 to 27 TJ per hectare per year. Value estimates of LAI from the LAI-2000 were within the expected range for *Pinus radiata* (Raison et al. 1992).

Current annual volume increment at age 11 to 12 years ranged from 8 to 58 m^3 ha^{-1} per year. Volume growth varied across years and sites and followed the expected trajectory when graphed against age (Figure 3). Between years, volume growth varied widely suggesting a strong effect of soil and climate conditions on the productivity. Stocking ranged from 560 to

1560 trees/ha (Table 2), indicating that several stands had been thinned. Site index varied from 18 to 36 m, with highest values concentrated on volcanic ash soils.

Relationships between volume increment and environmental and stand factors

We calculated Pearson correlations among environmental and stand variables and selected the most important relationships according to the strength of the correlation coefficient (r) and *P*-values < 0.05 (Tables 5 and 6). Among soil variables, soil water content, latitude, and elevation showed a significant effect on stand growth. Soil phosphorus was also significantly correlated with growth but only for 2009. Schlatter and Gerding (1999) found strong relationship between *Pinus radiata* growth versus soil texture (poor results in sands and good in clay loamy soils), depth (good results in recent volcanic ash), soil water content (poor in sands and good in marine sediments and recent volcanic ash), phosphorus (limiting productivity in recent volcanic ash and marine sediments) and boron (critical especially in the dry central valley). Volume growth showed significant positive relationships with rainfall (annual and growing season) and water deficit index and negative relationships with VPD, maximum temperature, potential evapotranspiration and water deficit index. Leaf area index and APAR were also positively correlated with stand growth.

Volume growth against environmental and stand factors for 2009 measurement

Among climatic variables, maximum temperature and annual rainfall explained 58% of variation in volume growth (Table 7). Volume growth was positively affected by annual rainfall (r^2=0.44, *P*<0.001) (Figure 6) and water deficit index (r^2=0.4, *P*<0.001) (Figure 7). Water index alone explained 40% of variation in volume growth but also was highly correlated with rainfall.

LAI explained 19% of variation in volume growth. Site index explained 60% of variation. The inclusion of maximum temperature, LAI and annual rainfall in a multiple linear

regression increased model predictability (r^2= 0.73, P<0.001). LAI affected volume growth; however the magnitude of this effect was related with maximum temperature. High maximum temperatures limited LAI while moderate temperatures positively affected LAI and growth. In addition, LAI was also limited by water availability. Lowest values for the water deficit index (e.g. near 0) produced a positive effect on LAI and volume growth. The opposite effect was observed with the reduction in the amount of water (e.g. -400 or -800 mm yr^{-1}). Water index was negatively correlated with maximum temperature (r^2 = - 0.70, Table 5) and maximum temperature was also negatively correlated with annual and growing season rainfall (r^2 = -0.64 and -0.61, respectively (Table 5).

Among the canopy factors, volume growth was positively correlated with LAI and annual APAR (r^2 = 0.46 and 0.33, respectively). Finally, volume growth was positively correlated with site Index (r^2 = 0.78)

Volume growth against environmental and stand factors for period 2005-2009

With a linear model, LAI, maximum temperature, and annual rainfall explained 48% of variation in volume growth. Volume growth was explained by 20% by soil factors (latitude and soil water content); 36% by climate factors (maximum temperature and water deficit index); 18% by canopy factors (LAI) and 25% by Site Index (Table 8).

Maximum temperatures and water index exerts a strong control in LAI. Stand located in areas with temperatures above 28˚C and with high water stress (W_{-400} or less) have maximum LAI of 2.5 (Figures 8 and 9).

The performance of the linear model is limited by the annual variation in rainfall and temperatures, however is highly relevant the tremendous participation of two basic variables (maximum temperature and precipitation).

Volume growth was positively affected by annual precipitation (Figure 10), water index (Figure 11) and negatively affected by increases of temperatures and vapor pressure deficit (Figures 12 and 13). These variables have year by year variability.

We found a positive effect on volume growth when we considered PAR and APAR (Figures 14 and 15).

Relationships between stand growth in relation to the supply, use and efficiency of water and light

Among sites with low, medium and high water deficit index, water supply varied by 2.6-fold (656-1720 mm per year), water used by potential evapotranspiration by 3.95-fold (682-1036 mm per year), and water use efficiency by 3.3-fold (m^3 of wood per m^3 of potential evapotranspiration). Water use efficiency decreased as water use increased and increased as water supply (rainfall) increased (Table 9).

The annual volume growth of the high productivity site (low water deficit index) was 2.2-fold more than low productivity sites. Light supply (PAR) was similar across sites (32 TJ ha^{-1} per year); however, light-capture efficiency varied by 1.4-fold (22-16 TJ ha^{-1} per year), and light-use efficiency by 1.6-fold (0.31-0.50 g wood per MJ^{-1}). Volume growth did not correlate well with annual PAR (Figure 14).

Repeated measures analysis showed a high variability of sites (permanent sample plots), years and sites within years as we expected. Annual variation in rainfall, maximum temperatures and water deficit during each year explained the variation in productivity.

4. Discussion

Spatial and temporal variability of *Pinus radiata* growth in Chile

At the middle of the rotation (age 11-12 years), volume growth ranged between 9 to 58 m^3 ha yr^{-1} (3.3-19.4 Mg ha^{-1}). Highest values were found in the south, the piedmont of the Andes Mountains, and on the western side of the coastal range (Figure 1). This spatial pattern indicated a strong effect of rainfall and also mild temperatures during the growing season.

The distribution of sites with high productivity follows a similar pattern as determined by Flores and Allen (2004), with areas of high productivity in the south, coastal range and piedmont of Andes Mountains. Seasonal variation in climatic variables is influencing the amount and rate of volume growth. Years with high rainfall concentrated in the growing season are correlated with increases in LAI and volume growth.

Factors contributing to the growth of *Pinus radiata* in Chile

Volume growth was most strongly correlated with rainfall and maximum temperature (Tables 7 and 8). Due to the Mediterranean climate, the rainfall is mostly concentrated in winter months, while strong water deficits develop during the growing season (spring, summer and fall). Additionally, high temperatures during the growing season increase the vapor pressure deficit, limiting tree growth even more. Similar conditions exist in Australia (Raison 1992). Less productivity in Chile as compared with New Zealand is perhaps explained by lower amounts of summer rainfall. Gerding and Schlatter (1995) found that annual rainfall was highly correlated with volume growth ($r = 0.48$) for sites with similar conditions as our study, and also found an important effect of latitude with the increase of productivity in the south.

Using only data from 2009 resulted in stronger relationships between volume growth and maximum temperature, precipitation, and soil water deficit than when all data (2005-2009) were used (Table 7). Annual changes in rainfall are strongly correlated with productivity, for 2009 this variable explained 44% of variation in volume growth.

A linear model possibly is not capturing the temporal changes in these climatic variables for the whole period while the 2009 measurement is only indicating a short term result.

Highest maximum temperatures occurred in the northern part of the *Pinus radiata* range and also in the central valley of the study area. Among soil factors, soil water holding capacity contributed positively to volume growth (r^2= 0.33). Gerding (1995) also found a correlation between soil water capacity and site index of 0.47. Additionally, soil carbon, organic matter, and latitude influenced site productivity. These variables are related with geology and land use. Highest amount of soil carbon are frequently found in recent volcanic ash soils (Tosso 1994) and also in the southern coastal range, where marine sediments are present. Gerding (1995) separated soils and found positive correlations between site index and soil carbon concentrations for sandy soils at 45 cm depth (r = 0.69) and metamorphic at 17 cm of depth (r = 0.55). We did not find significant correlations between soil texture and volume growth. Gerding (1995) also found a strong negative effects between superficial coarse sand (size > 2 mm) content and site index (r = -0.63).

Under water stress and high temperatures in the environment, there was an evidence of reductions in LAI. Similar effects were found for *Eucalyptus globulus* by Battaglia et al. (1998). The same conditions could have affected the phenology patterns of *Pinus radiata* (Dougherty et al. 1994) and the LAI (Hebert and Jack 1998; Vose et al. 1994).

Total PAR was almost the same across the whole gradient (Table 3), however APAR differed depending on stand LAI. LAI was highly correlated with soil organic matter and water deficit index (Table 5). Linder (1987) found a strong positive correlation between volume

growth and APAR of *Pinus radiata* in Australia, however, in our conditions, this relationship was not evident. Possible reasons include: 1) overriding effects of water limitations (soil water deficits, high vapor pressures) , 2) high respiration (high maximum temperatures), 3)lack of seasonal data for LAI, which could change the amount of energy captured, especially during spring and fall 4) nutrient limitations, and 5) differences in above and belowground partitioning depending the water limitation.

Overall, peak LAI was good predictor of volume growth (Tables 7 and 8). Little information is available concerning the seasonal variation in LAI of *Pinus radiata* in Chile although we expect that there may be strong seasonal differences in LAI and therefore APAR given the importance of water availability for leaf production and senescence (Rubilar 2005).

Based on our results, the inclusion of simple climatic variables such as maximum temperature and precipitation into Chilean *Pinus radiata* growth and yield models should improve their performance as yield models as found by Snowdon et al. (1998) for Australian *Pinus radiata* models. Their performance as growth models (used to update inventories) should be dramatically improved when annual variations in maximum temperature and precipitation can be incorporated.

Models using basic variables such as temperature and rainfall were useful to estimate volume growth, however, for temporal and spatial analyses, the use of process-based models are more flexible to capture the variation in the environment (Coops 1998).

Site resources supply and efficiency of use of water and light

Annual rainfall differed across sites with low water deficit and high water deficit ranging by 2.6-fold (Table 9). The water use for our plantations was extremely different accounting for 40% to 100% of the annual rainfall. Sites located in areas with high water deficits could be demanding additional water from groundwater. The highest productivity was in areas with

high rainfall and high soil water holding capacity. Water use efficiency ranged 1.6 to 0.5 [kg m^{-3} of water] with dry sites (north) being less efficient than the wettest sites (south and south-western side of the Coastal range) (Figure 16). These values are lower than estimations from Binkley et al. (2004) when it showed a range between 6.9 to 9.0 kg m^{-3} for irrigated stands of *Eucalyptus grandis*. We estimated water use efficiency as the relationship between stem volume wood and amount of water used while Binkley et al. (2004) indicated a relationship between Gross Primary Productivity (GPP) and water use. Trees growing with less constraint in water supply can fix more CO_2 per unit of light intercepted (Binkley et al. 2004).

In Chile, we found an inverse relationship between water use (potential evapotranspiration calculated by Penman-Monteith equation) and water use efficiency. Huber and Trecaman (2004) in Chile and Sheriff et al. (1996) in Australia found similar patterns of water use efficiency. In our sites, *Pinus radiata* needed between 230 to 770 m^3 of water (evapotranspired) in order to produce 1 m^3 of annual wood. Similar values were found in Chile by Huber and Trecaman (2004). The combination between high temperatures and drought conditions could reduce photosynthesis, because the trees may be unable to use water from evapotranspiration to cool leaves (Battaglia et al. 2009). For *E. globulus* growing in Australian conditions, the amount of water evapotranspired required to produce 1 m^3 of wood varied between 150 m^3 (in environment with low pressure deficit), to 1,000 m^3 (in regions with high vapor pressure deficit) (Battaglia el at. 2009).

Plantations growing in less restrictive sites were more light use efficient, with around 0.5 g MJ^{-1}, which should be a conservative value in comparison with other *Pinus* species growing in USA (0.63 g MJ^{-1} for *Pinus strobus*, Pangle et al. 2009). However, in our case the calculation was done only for the stemwood, while Pangle et al. (2009) divided the Annual Net Primary Productivity (ANPP) by APAR. Doing some corrections using allometric relationship, we expected to find higher values of light-use efficiency. Under similar conditions (ideally without stress), light-use efficiency should decrease with the increase of incident PAR (Medlyn 1998). The strong effects of environmental stresses in Chile limit the

possibility to compare between different locations. Sites with high incoming solar radiation can have low values of LUE due to the limitation of water and differences in above and below ground partitioning between sites (Medlyn 1998). Under Chilean condition, new evaluations should be developed in order to precise the degree in which LUE is reduced by environmental stress according previous experiences of Runyon et al. (1994).

Plantations located in more favorable conditions (high annual rainfall, mild temperatures and lower VPDs) captured more solar irradiation than those located in the central valley and north (approx. latitude 35˚S) (Figure 17). Highly productive sites with average LAI of 3.1 are capturing on an annual basis about 70% of PAR, while less productive sites with LAI of 1.3 are capturing only 47% of PAR.

LAI was strongly associated with organic matter and soil water deficit index. Even though the sites located in the north have generally more light resources (more less cloudy days per year), trees possibly are not capturing this resource due to the limitations in water (Figures 16 and 17). Linear and positive relationships between LAI and volume growth under no limitation of water has been reported by Snowdon and Benson (1992), Albaugh et al. (1998) and Stape (2004). In our study, we found this relationship where growing season temperatures were mild. Changes in resource use efficiency (water, light and nutrients) can be explained by the duration of the appropriate conditions for photosynthesis (Cannell 1989; Landsberg and Gower, 1997; Stape 2004). Light use efficiency has a slightly different pattern than water use efficiency, especially in the southern and northern limit of the gradient (Figures 18 and 19). Possibly our estimations of LAI using remote sensor did not work very well in the extremes of the gradient (or probably underrepresented in the database for LAI regressions). Further improvements should be done in order to increase the number of observations of LAI in the gradient, including seasonal measurements.

Our results indicate that the recommendation to increase plantation area on dry sites should be critically reviewed, because plantations on these sites have low productivity and low

resource use efficiency. Even though these plantations are recovering highly eroded soils, the extremely high demand for water and the chronic water stress dramatically increase the probability of risks, such as drought, fires, pest and diseases. This stress in these locations should be increased if we consider the effects of the global warming (Battaglia et al. 2009; Neuenschwander 2010). A more integrated (private, social and environmental) strategy should be developed in order to increase the use of technology on highly productive sites, in order to obtain more volume per unit of water, light and nutrients.

Additional studies such as the FNC Regionwide 13 studies in Chile will provide information to understand the relationships between soil nutrient supply, nutrient capture by the trees, and nutrient use efficiency and their relationships with water.

Due to the growing competition for land in Chile, the incorporation of resource use efficiency concepts into land acquisition analyses could improve the outcomes of these analyses for both for existing or new investors. The same amount of stem biomass can be produced with different amounts of resources. Specifically thinking of water, if we need to produce 10^6 m^3 of stemwood in 20 year old rotation and we considered mean annual growth of 30 m^3 ha^{-1} yr^{-1} for highly productive sites and 13 m^3 ha^{-1} yr^{-1} for poor sites, we will need 1,667 and 3,846 ha, respectively of plantations. On a good site, the water use will be 234 x 10^6 m^3 compared to 783 x 10^6 m^3 of water on the poor site for the same amount of wood produced.

Acknowledgments

We acknowledge with thanks permission given by Modelo Nacional de Simulación de Pino radiata to publish these data and the results of our analyses. The senior author acknowledges with thanks the support of the Forest Nutrition Cooperative allowing him to pursue scientific objectives in his work.

References

Albaugh, T.J., H.L. Allen, P.M. Dougherty, L.W. Kress, and J.S. King. 1998. Leaf Area and Above and Belowground Growth Responses of Loblolly Pine to Nutrient and Water Additions. For. Sci. 44(2): 317-328.

Allen, R.G., L.S. Pereira, D. Raes, and M. Smith. 1998. Crop evapotranspiration: Guidelines for computing crop water requirements. FAO Irrig. And Drainage Paper 56. FAO, Rome.

Allen, R.G., M.E. Jensen, J.L., and R.D. Burman. 1989. Operational Estimates of Reference Evapotranspiration. Agron. J. 81(4): 650-662.

Almeida, A., J.J. Landsberg, P.J. Sands, M.S. Ambrogi, S. Fonseca, S.M. Barddal, and F.M. Bertolucci. 2004a. Needs and opportunities for using a process-based productivity model as a practical tool in Eucalyptus plantations. For. Ecol Manage. 193: 167-177.

Almeida, A. C., J.J. Landsberg and P. J. Sands. 2004b. Parameterisation of 3-PG for fast growing *Eucalyptus grandis* plantations For. Ecol Manage. 193: 179-295.

ASCE-EWRI. 2004. The ASCE Standardized Reference Evapotranspiration Equation. Technical Committee report to the Environmental and Water Resources Institute of the American Society of Civil Engineers from the Task Committee on Standardization of Reference Evapotranspiration. 173 p.

Battaglia, M., M.L. Cherry, C.L. Beadle, P.J. Sands and A. Hingston. 1998. Prediction of leaf area index in eucalypt plantations: effect of water stress and temperature. Tree Phys. 18: 521-528.

Battaglia, M., J. Bruce, C. Brack, and T. Baker. 2009. Climate Change and Australia's plantation estate: Analysis of vulnerability and preliminary investigation of adaptation options. Forest&Wood Products Australia. Melbourne, Victoria, Australia.

Benson, M.L., B.J. Myers and R.J. Raison. 1992. Dynamics of stem growth of *Pinus radiata* as affected by water and nitrogen supply. For. Ecol Manage. 52: 117-137.

Binkley, D., J.L. Stape and M.G. Ryan. 2004. Thinking about efficiency of resource use in forests. For. Ecol Manage.193: 5-16.

Bray, R.H., and L.T. Kurtz. 1945. Determination of total, organic, and available forms of phosphorus in soils. Soil Sci. 59: 39-45.

Cannell, M.G.R. 1989. Physiological Basis of Wood Production: a Review. Scand. J. For. Res. 4: 459-490.

Cerda V., I., and R.Nuñez S. 1998. Appreciation of the Chilean Forest Resource: Plantations of *Pinus radiata* and *Eucalyptus sp*. 1985-1996. FAO document.

Coops, N.C., R.H. Waring and J.J. Landsberg. 1998. Assessing forest productivity in Australia and New Zealand using a physiologically-based model driven with averaged monthly weather data and satellite-derived estimates of canopy photosynthetic capacity. For. Ecol Manage. 104: 113–127.

Coops, N.C., Waring, R.H., 2001a. Estimating forest productivity in the eastern Siskiyou Mountains of southwestern Oregon using a satellite driven process model, 3-PGS. Can. J. For. Res. 31, 143–154.

Contesse, D. 1986. Apuntes y consideraciones para la historia del pino radiata en Chile. Boletin de la Academia Chilena de la Historia, 97: 351-373.

Dougherty, P.M., D. Whitehead, and J.M. Vose. 1994. Environmental influences on the phenology of pine. Ecol. Bull. 43: 64-75.

Dye, P.J., S. Jacobs and D. Drew. 2004. Verification of 3-PG growth and water-use predictions in twelve Eucalyptus plantation stands in Zululand, South Africa. For. Ecol. Mana. 193: 197-218.

ESRI. 2009. ArcMap 9.2, Redlands, CA.

Flores, F. & Allen H. 2004. Efectos del clima y capacidad de almacenamiento de agua del suelo en la productividad de rodales de pino radiata en Chile: Un análisis utilizando el modelo 3-PG. Bosque, 25(3): 11-24.

Gerding, V. and J.E. Schlatter. 1995. Important site variables and factors for *Pinus radiata* D. Don productivity in Chile. Bosque 16(2): 39-56.

Hartwig C., F. 1994. La Tierra que Recuperamos. Santiago, Chile, Editorial Los Andes.

Hebert, M.T., and S.B. Jack. 1998. Leaf area index and site water balance of loblolly pine (*Pinus taeda* L.) across a precipitation gradient in East Texas. For. Ecol. Mana. 105: 273-282.

Huber, A., and R.Trecaman. 2004. Water-use efficiency for *Pinus radiata* stands in Chile. Bosque 25(3): 33-43.

INFOR. 1974. Estadísticas forestales. Serie informativa N° 23. Santiago, Chile.

INFOR. 2010 Estadísticas forestales chilenas 2008. Instituto Forestal (INFOR), Ministerio de Agricultura. Santiago, Chile. www.infor.cl

Landsberg, J.J., and R.H. Waring. 1997. A generalized model of forest productivity using simplified concepts of radiation-use efficiency, carbon balance and partitioning. For. Ecol Manage. 95: 209-228.

Landsberg, J.J. and S.T. Gower. 1997. Applications of physiological ecology to forest management. Academic Press, San Diego, USA.

Linder,S. 1987. Responses to water and nutrients in coniferous ecosystems. In: E.-D. Schulze and H. Zwölfer, Editors, Potentials and Limitations of Ecosystem Analysis, Ecol. Stud. **61**: 180–202.

Linder, M.L. Benson, B.J. Myers and R.J. Raison. 1987. Canopy dynamics and growth of *Pinus radiata*. I. Effects of irrigation and fertilization during a drought, Can. J. For. Res. **17:** 1157–1165.

Linder and D.A. Rook. 1984. Effects of mineral nutrition on carbon dioxide exchange and partitioning in trees. In: G.D. Bowen and E.K.S. Nambiar, Editors, Nutrition of Plantation Forests, Academic Press, London, pp. 211–236.

Neuenschwander, A. 2010. El Cambio Climático en el Sector Silvoagropecuario de Chile. FUNDACIÓN PARA LA INNOVACIÓN AGRARIA. Gobierno de Chile. Santiago, Chile. 126p.

McMurtrie, R.E., D.A. Rock, and F.M. Kelliher. 1990. Modelling the Yield of *Pinus radiata* on a Site Limited by Water and Nitrogen. For. Ecol Manage. 30: 381-413.

Medlyn, B.E. 1998. Physiological basis of the light use efficiency model. Tree Phys. 18: 167-176.

McGeehan, S.L., K. Topper, and D.V. Naylor. 1989. Sources of variation in hot water extraction and colorimetric determination of soil boron. Commun. Soil Sci. Plant Analysis 20: 1777-1786.

Miller, R.O., J. Kotuby-Amacher, Rodriguez, J.B. 1997. Particle Size Analysis (Hydrometer). p. 96-99. Western States Laboratory Proficiency Testing Program Soil and Plant Analytical Methods. Version. 4.00.

Mininco. 1995. Compendio de funciones para especies de interés de Forestal Mininco S.A. Concepción, Chile.

Nightindale, J.M., M.J. Hill, S.R. Phinn, I.D. Davies, A.A. Held, and P.D. Erskine. 2008. Use of 3-PG and 3-PGS to simulate forest growth dynamics of Australian tropical rainforests. 1. Parameterisation and calibration for old-growth, regenerating and plantation forests. For. Ecol Manage. 254: 107-121.

Olsen, S.R., C.V. Cole, F.S. Watanabe, and L.A. Dean. 1954. Estimation of available phosphorus in soils by extraction with sodium bicarbonate. U.S. Dep. of Agric. Circ. 939.

Pangle L., J.M. Vose and R.O. Teskey. 2009. Radiation use efficiency in adjacent hardwoods and pine forests in the southern Appalachians. For. Ecol. Manage. 257: 1034-1042.

Page, A. L. 1982. Methods of soil analysis: chemical and microbiological properties. 2nd ed. Madison: American Society of Agronomy/Soil Science Society of America, pt. 2. (Agronomy Series).

Peredo, M.L. and C.Mora. 2004. Technological characterization of Arauco's forest resource. Bioforest S.A. Concepción, Chile.

Raison., R.J., Khanna, P.K., Benson, M.L., Myers, B.J., McMurtrie, R.E. and Lang, A.R.G. 1992. Dynamics of *Pinus radiata* foliage in relation to water and nitrogen stress: II. Needle loss and temporal changes in total foliage mass. For. Ecol. Manage. 52: 159-178.

Real, P. 2006. National Growth and Yield Simulation Project: example of cooperation among private sector and research institutes. The Second International Symposium on Plant Growth Modeling, Simulation, Visualization and Applications. November 13-17, 2006, Beijing, P.R. China.

Rojas, J.C. 2005. Factors influencing responses of loblolly pine stands to fertilization. PhD thesis. North Carolina State University. 162p.

Rubilar, R. 2005. Environmental constraints on growth phenology, leaf area display, and above and belowground biomass accumulation of *Pinus radiata* (D. Don) in Chile. PhD thesis. North Carolina State University. 208p.

Runyon, J., R.H. Waring, S.N. Goward and J.M. Welles. 1994. Environmental limits on net primary production and light use efficiency across the Oregon Transect. Ecol. Appl. 4: 226-237.

Sadzawka R., A., M.Carrasco, R,Grezm and M.Mora. 2004. Métodos de análisis recomendados para los suelos chilenos. Comisión de normalización y acreditación. Sociedad chilena de la ciencia del suelo. Santiago, Chile.

Sands, P.J. and J.J. Landsberg. 2002. Parameterisation of 3-PG for plantation grown *Eucalyptus globulus.* For. Ecol Manage. 163: 273–292.

SAS Institute, Inc. 2009. SAS/STAT user's guide. Release 9.1.3 SAS Institute, Cary, North Carolina, USA.

Schlatter, J., and V. Gerding. 1999. Productivity in an example of six characteristic sites of the VIII Region with *Pinus radiata* D. Don. Bosque 20(1): 65-77.

Sheriff, D.W., J.P. Mattay and R.E. McMurtrie. 1996. Modeling productivity and transpiration of *Pinus radiata*: climatic effects. Tree Phys. 16: 183-186.

Snowdon, P. and Benson, M.L., 1992. Effects of combinations of irrigation and fertilisation on the growth and above-ground biomass production of *Pinus radiata*. For. Ecol Manage. 52, pp. 87–116.

Snowdon, P., R.C. Wollons and M.L. Benson. 1998. Incorporation of climatic indices into models of growth of *Pinus radiata* in a spacing experiment. New Forests 16: 102-123.

Snyder, R.L. and S.Eching. 2006. Penman-Monteith daily (24-hour) and Hargreaves-Samani Equations for Estimating Reference Evapotranspiration from Monthly Data. University of California-Davis (http://biomet.ucdavis.edu/Evapotranspiration).

Stape, J.L., M. G. Ryan, and D. Binkley. 2004a. Testing the utility of the 3-PG model for growth of *Eucalyptus grandis x urophylla* with natural and manipulated supplies of water and nutrients. For. Ecol Manage. 193: 219-234.

Stape, J.L., D. Binkley, and M.G. Ryan. 2004b. *Eucalyptus* production and the supply, use and efficiency of use of water, light and nutrients across a geographic gradient in Brazil. For. Ecol Manage. 193: 17-31.

Vose, J.M., P.M. Dougherty, J.N. Long, F.W. Smith, H.L. Gholz and P.J. Curran. 1994. Factors influencing the amount and distribution of leaf area of pine stands. Ecol. Bull. 43: 102-114.

Tickle, P.K., N.C. Coops and S.D. Hafner. 2001. Assessing forest productivity at local scales across a native eucalypt forest using a process model, 3PG-SPATIAL. For. Ecol Manage. 152: 275-291.

Thornton, P.E., and S.W. Running. 1999. An improved algorithm for estimating incident daily solar radiation from measurements of temperature, humidity, and precipitation. Agric. For. Meteor. 93: 211-228.

Tosso T., J. 1985. Suelos volcánicos de Chile. Instituto de Investigaciones Agropecuarias. Santiago, Chile. 723p.

Waring, R.H. 1983. Estimating forest growth and efficiency in relation to canopy leaf area. Adv. Ecol. Res. 13:327-354.

Waring, R.H. 2000. A process model analysis of environmental limitations on the growth of Sitka spruce plantations in Great Britain. Forestry 75, 65-79

Walkley, A. and I. A. Black. 1934. An examination of Degtjareff method for determining soil organic matter and a proposed modification of the chromic acid titration method. Soil Sci. 37:29-37.

Whitehead, D., F.M.Kelliher, C.M.Frampton, and M.J.S.Godfrey. 1994. Seasonal development of leaf area in a Young, widely spaced *Pinus radiata* D. Don stand. Tree Phys. 14: 1019-1038.

Appendix

Appendix 1 - Adjustment of 3-PG model

In order to analyze the observed data from plots, we used the process based model 3-PG (Physiological Processes Production Growth) which was previously calibrated, parameterized and validated (Alvarez 2010 not published).

The model called 3-PG (Physiological Principles Predicting Growth), developed by Landsberg and Waring (1997), is a simple process-based, stand-level model of forest growth. It requires few parameter values and only readily available site and climatic data as inputs. The 3-PG model predicts the time course of stand development, water use, and available soil water. Its primary output variables are net primary production, the standing biomass in foliage, stem (i.e. all above-ground woody tissue) and roots, stem number, available soil water, and transpiration. However, it also infers variables familiar to the forest manager or of use as inputs into management programs, e.g. leaf area index, average stem diameter at breast height, main stem volume, and mean annual increment.

The model has found numerous applications for various species (Coops et al. 1998; Waring 2000; Sands and Lansberg 2002; Almeida et al. 2004a, 2004b; Dye et al. 2004; Stape et al. 2004a). A modified version, 3-PG Spatial (Coops et al. 1998; Tickle et al. 2001; Nightindale et al. 2008), has been applied to study forest productivity across landscape areas (Coops et al. 1998; Coops and Waring 2001a).

A full description of the original 3-PG is provided by Landsberg and Waring (1997). The 3-PG model consists of five simple sub-models: the assimilation of carbohydrates, the distribution of biomass between foliage, roots and stems, the determination of stem number, soil water balance, and conversion of biomass values into variables of interest to forest managers. The state of the stand is updated each month.

The 3-PG model requires as climatic inputs monthly average values of solar radiation (Q (MJ m^{-2} d^{-1})), mean air temperature (Ta (°C)), atmospheric vapor pressure deficit (D (mbar)), rainfall (R (mm per month)), and frost days (dF (days per month)).

If mean maximum and minimum air temperatures (Tx and Tn (°C)) are known, Vapor pressure deficit can also be estimated from Tx and Tn, e.g. as half the difference between the saturated vapor pressure at Tx and Tn. The 3-PG model can be run for any number of years, using either actual monthly weather data or long-term monthly averages. Using averages is the normal procedure unless there is particular interest in specific events, such as droughts.

Other inputs are factors describing the physical properties of the site: latitude, a site fertility rating (FR), maximum available soil water (mm), and a general descriptor of soil texture. Outputs from 3-PG can be either monthly or annual values. They include stem, root and foliage biomass (WS, WR andWF (t ha^{-1})), available soil water (mm), and stand transpiration (ET (mm)). Stand-level outputs include canopy leaf area index (L), main-stem volume (V (m^3 ha^{-1})), average stem diameter at breast height (B (cm)), mean annual stem-volume increment (MAI (m^3 ha^{-1} per year)), and stem number (N (trees ha^{-1})).

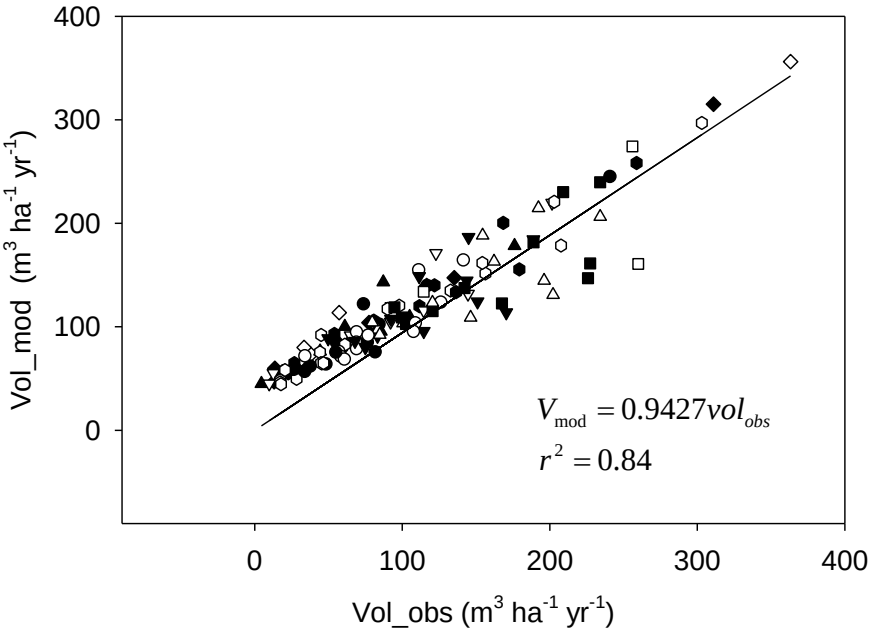

Appendix 2 - Observed and estimated stand growth using 3-PG process- based model.

Table 1. Location, soil taxonomy, soil type, superficial texture, distance from the Ocean Pacific and soil water holding capacity for the 48 plots selected.

Plot #	Lat	Lon	Elev [m]	Soil Order	Soil Type	Sand [%]	Clay [%]	Dist. [km]	SWHC [mm/1m]
1	-35.3	-72.0	141	Ultisol	Metamorphic	51	22	23	160
2	-35.4	-72.3	88	Alfisol	Metamorphic	54	27	11	121
3	-35.4	-72.3	88	Alfisol	Metamorphic	77	8	11	121
4	-35.4	-72.3	88	Alfisol	Metamorphic	39	40	11	121
5	-35.5	-71.8	100	Alfisol	Metamorphic	29	22	55	121
6	-35.5	-71.9	100	Alfisol	Metamorphic	28	31	55	121
7	-35.5	-71.8	89	Alfisol	Metamorphic	28	31	56	135
8	-35.6	-72.4	475	Alfisol	Metamorphic	25	30	17	112
9	-35.8	-72.2	181	Inceptisol	Aluvial	22	28	32	163
10	-35.9	-72.0	158	Alfisol	Granitic	36	41	55	113
11	-36.0	-72.3	374	Andisol	Volcanic ash	27	30	81	271
12	-36.2	-72.6	278	Alfisol	Granitic	17	64	23	142
13	-36.6	-72.8	213	Inceptisol	Metamorphic	55	22	16	149
14	-36.7	-72.9	290	Inceptisol	Metamorphic	84	9	8	195
15	-36.7	-71.7	588	Andisol	Volcanic ash	14	14	108	340
16	-36.7	-71.7	588	Andisol	Volcanic ash	14	14	108	340
17	-37.0	-72.3	122	Andisol	Dry sand	45	29	62	130
18	-37.0	-72.4	122	Andisol	Dry sand	40	25	62	130
19	-37.0	-71.1	623	Andisol	Volcanic ash	16	26	110	287
20	-37.1	-72.5	97	Mollisol	Wet sand	19	46	54	63
21	-37.1	-72.5	97	Mollisol	Wet sand	51	12	54	63
22	-37.1	-73.1	626	Ultisol	Metamorphic	83	9	7	195
23	-37.1	-72.3	168	Mollisol	Wet sand	83	10	78	44
24	-37.1	-72.3	168	Mollisol	Wet sand	88	9	78	44
25	-37.2	-73.0	165	Alfisol	Granitic	87	8	24	193
26	-37.2	-72.9	165	Alfisol	Granitic	82	9	24	193
27	-37.3	-72.0	213	Andisol	Volcanic ash	30	23	107	66
28	-37.3	-72.2	223	Andisol	Dry sand	55	10	88	53
29	-37.3	-72.6	94	Entisol	Aluvial	89	8	53	110
30	-37.4	-73.3	428	Ultisol	Metamorphic	45	12	28	149
31	-37.4	-72.8	181	Alfisol	Granitic	77	8	47	92
32	-37.4	-72.6	76	Andisol	Aluvial	29	22	59	103
33	-37.4	-72.1	297	Andisol	Dry sand	95	1	105	68
34	-37.4	-72.7	179	Alfisol	Granitic	87	10	48	198
35	-37.4	-72.9	194	Ultisol	Metamorphic	89	8	39	193
36	-37.4	-72.2	626	Andisol	Volcanic ash	11	47	94	51
37	-37.5	-72.0	293	Andisol	Dry sand	31	46	106	76
38	-37.5	-72.1	293	Andisol	Dry sand	57	32	106	76
39	-37.5	-72.2	200	Andisol	Dry sand	95	1	99	105
40	-37.6	-72.6	93	Inceptisol	Aluvial	41	20	72	192
41	-37.9	-72.4	255	Alfisol	Red clay	16	45	95	481
42	-38.8	-73.2	85	Inceptisol	Aluvial	11	44	16	193
43	-39.2	-73.0	290	Ultisol	Volcanic ash	85	8	17	216
44	-39.5	-73.0	41	Ultisol	Volcanic ash	29	23	16	209
45	-39.6	-72.8	197	Ultisol	Volcanic ash	39	44	37	334
46	-39.7	-72.1	171	Ultisol	Volcanic ash	29	22	45	373
47	-39.9	-73.1	231	Ultisol	Red clay	29	56	19	239
48	-40.1	-73.0	130	Ultisol	Volcanic ash	29	22	23	217
	Min		41			11	1	7	44
	Max		626			95	64	110	481
	Mean		229			48	24	53	164

Table 2. Stand characteristics of 48 plots selected including LAI estimation from LAI-2000.

Plot #	Age [years]	DBH [cm]	Site Index [m, 20 yr]	Leaf Area Index [m^2 m^{-2}]	Basal Area [m^2/ha]	Trees/ha	Stem volume [m^3/ha]	MAI [m^3/ha/year]	Height [m]
1	11	17.8	30.1	1.6	25.9	1,040	158.7	14.4	15.3
2	11	15.9	34.1	1.9	19.7	990	137.2	12.5	16.9
3	11	19.3	37.2	2.3	24.6	840	178.6	16.2	18.8
4	11	20.0	35.5	2.1	25.4	810	176.9	16.1	18.1
5	12	13.5	19.9	2.2	15.1	1,050	76.7	6.4	11.1
6	11	14.4	24.5	2.6	15.2	930	78.5	7.1	11.7
7	12	14.7	18.9	2.2	18.7	1,110	85.2	7.1	10.2
8	11	20.1	34.7	2.8	28.6	900	191.1	17.4	17.4
9	11	14.6	26.3	2.3	17.7	1,060	95.6	8.7	12.3
10	12	21.1	30.8	3.5	25.9	740	173.0	14.4	17.6
11	11	23.2	29.0	1.6	29.2	690	149.6	13.6	13.5
12	11	15.1	27.0	1.6	21.0	1,170	114.6	10.4	12.7
13	11	19.6	37.8	2.5	28.7	950	202.3	18.4	18.3
14	11	23.9	37.0	3.1	36.3	810	253.4	23.0	18.9
15	12	18.7	35.2	2.6	26.7	970	190.9	15.9	18.3
16	11	20.2	39.5	3.0	31.1	970	237.8	21.6	20.1
17	11	12.2	25.5	1.5	11.5	980	62.6	5.7	11.4
18	11	14.1	26.5	2.6	14.2	910	93.1	8.5	12.8
19	12	20.0	32.1	2.0	32.5	1,040	223.9	18.7	17.9
20	11	18.7	29.3	2.4	21.1	770	113.2	10.3	13.4
21	11	18.9	30.9	1.8	20.8	740	122.2	11.1	14.9
22	11	17.9	32.8	4.5	38.0	1,510	249.6	22.7	16.5
23	11	15.0	29.0	2.1	13.9	790	80.1	7.3	13.4
24	11	18.5	34.1	2.4	26.3	980	165.6	15.1	15.9
25	12	15.0	25.2	1.7	14.6	830	82.7	6.9	13.1
26	12	16.7	29.6	2.4	20.6	940	129.6	10.8	15.4
27	11	19.1	31.3	2.1	39.0	1,360	227.2	20.7	14.8
28	11	15.5	26.6	2.2	19.0	1,010	100.1	9.1	12.3
29	12	20.7	27.5	3.2	39.7	1,180	239.8	20.0	15.7
30	12	20.6	34.3	2.2	41.0	1,230	287.3	23.9	18.4
31	12	20.5	31.1	3.4	26.4	800	180.6	15.0	17.9
32	12	18.6	27.0	2.7	30.6	1,130	177.8	14.8	14.6
33	11	15.1	25.1	2.2	22.2	1,240	117.1	10.6	12.2
34	12	19.7	30.4	2.2	24.4	800	155.3	12.9	16.4
35	11	19.5	33.9	2.8	23.0	770	155.0	14.1	17.4
36	11	11.4	23.8	1.6	16.0	1,560	86.7	7.9	10.8
37	11	16.1	27.2	2.6	21.6	1,070	118.3	10.8	13.0
38	11	13.0	21.9	1.6	15.3	1,150	70.1	6.4	9.7
39	11	15.3	26.5	2.4	24.1	1,310	134.9	12.3	13.1
40	11	23.9	37.2	3.0	26.5	590	179.1	16.3	18.3
41	12	21.2	29.2	2.4	30.8	870	194.3	16.2	16.6
42	11	26.4	44.3	2.5	46.5	850	376.5	34.2	22.5
43	12	23.9	33.8	2.8	39.9	890	264.5	22.0	19.1
44	11	23.6	37.4	2.6	34.0	780	240.1	21.8	19.1
45	11	23.8	33.9	2.3	36.9	830	235.9	21.4	17.2
46	11	24.3	35.1	3.4	33.7	730	221.7	20.2	17.8
47	11	23.9	31.6	2.0	25.1	560	150.6	13.7	16.1
48	12	25.8	34.8	4.0	45.0	860	329.6	27.5	20.2
Min	11	11	19	2	11	560	63	6	10
Max	12	26	44	4	47	1,560	376	34	23
Mean	11	19	31	2	26	960	168	15	16

Table 3. Climatic characteristics of plot locations.

Plot #	Lat	PPGS [mm yr^{-1}]	PPT [mm yr^{-1}]	VPD [bar]	TMAX [°C]	TMIN [°C]	Trans [mm yr^{-1}]	PET [mm yr^{-1}]	TPAR [TJ ha^{-1} yr^{-1}]
1	-35.3	120.4	742.3	15.2	30.8	5.8	372.5	945.3	30.0
2	-35.4	171.8	954.1	6.9	28.8	4.8	312.4	800.4	34.1
3	-35.4	171.8	954.1	6.9	28.8	4.8	312.4	800.4	33.5
4	-35.4	171.8	954.1	6.9	28.8	4.8	312.4	800.4	34.1
5	-35.5	108.1	656.1	14.9	30.1	3.8	410.2	1036.5	21.8
6	-35.5	108.1	656.1	14.9	30.1	3.8	410.2	1036.5	35.8
7	-35.5	108.1	656.1	14.9	30.1	3.8	410.2	1036.5	35.8
8	-35.6	171.8	954.1	6.9	28.8	4.8	312.4	800.4	34.1
9	-35.8	108.1	656.1	14.9	30.1	3.8	410.2	1036.5	35.4
10	-35.9	106.8	540.9	16.7	32.0	4.7	363.2	961.3	34.1
11	-36.0	513.6	1237.0	5.5	27.3	2.1	257.3	672.0	35.4
12	-36.2	135.2	666.7	15.6	30.7	3.8	370.1	935.7	24.9
13	-36.6	201.1	1061.0	7.0	22.0	5.1	277.1	706.1	35.3
14	-36.7	269.5	1087.1	7.0	26.1	5.1	280.7	714.4	34.1
15	-36.7	364.1	1260.3	16.2	29.4	3.8	354.2	893.6	35.3
16	-36.7	364.1	1260.3	16.2	29.4	3.8	354.2	893.6	34.2
17	-37.0	216.5	840.3	15.7	31.1	3.8	356.6	898.3	34.1
18	-37.0	216.5	840.3	15.7	31.1	3.8	356.6	898.3	34.1
19	-37.0	470.8	1403.7	14.9	30.0	3.4	343.0	863.4	28.0
20	-37.1	216.5	840.3	15.7	31.1	3.8	356.6	898.3	33.2
21	-37.1	216.5	840.3	15.7	31.1	3.8	356.6	898.3	33.5
22	-37.1	269.5	1087.1	7.0	26.1	5.1	280.7	714.4	35.4
23	-37.1	210.2	779.0	15.5	30.9	4.9	270.5	683.0	34.0
24	-37.1	210.2	779.0	15.5	30.9	4.9	270.5	683.0	35.4
25	-37.2	256.6	1112.8	15.5	30.9	4.9	270.5	683.2	34.0
26	-37.2	256.6	1112.8	15.5	30.9	4.9	270.5	683.2	34.5
27	-37.3	470.8	1403.7	14.9	30.0	3.4	343.0	863.4	28.0
28	-37.3	256.6	1112.8	15.5	30.9	4.9	270.5	683.2	34.0
29	-37.3	243.3	910.4	15.5	30.9	4.9	270.1	681.6	34.0
30	-37.4	360.5	1136.8	7.1	23.9	7.3	289.9	733.3	30.6
31	-37.4	256.6	1112.8	15.5	30.9	4.9	270.5	683.2	34.0
32	-37.4	243.3	910.4	15.5	30.9	4.9	270.1	681.6	35.2
33	-37.4	243.3	910.4	15.5	30.9	4.9	270.1	681.6	31.0
34	-37.4	256.6	1112.8	15.5	30.9	4.9	270.5	683.2	35.4
35	-37.4	256.6	1112.8	15.5	30.9	4.9	270.5	683.2	34.0
36	-37.4	470.8	1403.7	14.9	30.0	3.4	343.0	863.4	33.2
37	-37.5	243.3	910.4	15.5	30.9	4.9	270.1	681.6	24.9
38	-37.5	243.3	910.4	15.5	30.9	4.9	270.1	681.6	31.0
39	-37.5	243.3	910.4	15.5	30.9	4.9	270.1	681.6	31.1
40	-37.6	245.4	1119.7	13.2	29.9	5.5	308.5	777.9	30.6
41	-37.9	369.4	1208.0	12.6	28.9	4.3	314.9	791.4	35.4
42	-38.8	560.6	1639.0	9.4	24.4	4.7	276.4	699.7	31.1
43	-39.2	871.1	2288.3	9.4	24.4	4.9	273.1	686.9	34.0
44	-39.5	698.9	1663.3	9.4	24.4	4.9	267.9	674.2	35.4
45	-39.6	698.9	1663.3	9.4	24.4	4.9	267.9	674.2	30.0
46	-39.7	698.9	1663.3	9.4	24.4	4.9	267.9	674.2	35.2
47	-39.9	698.9	1663.3	9.4	24.4	4.9	267.9	674.2	30.0
48	-40.1	871.1	2288.3	9.4	24.4	4.9	273.1	686.9	35.2
	Min	107	541	6	22	2	257	672	22
	Max	871	2,288	17	32	7	410	1,036	36
	Mean	317	1,104	13	29	5	309	783	33

Table 4. List of variables used on statistical analysis with volume growth as dependent variable and the independent variables structured by soil, climatic, canopy and stand.

Category	Variables
Soil	Soil C, Soil N, P (Bray-2 and Olsen), K, Ca, Mg, Al-extractable, Sand, Silt, Clay, pH, Soil water holding capacity, elevation, distance from the ocean, latitud, longitude
Climatic	Rainfall (annual and growing season), transpiration, potential evaoptranspiration, water deficit index, vapor pressure deficit, max and min temperature, total PAR
Canopy	LAI, APAR
Stand	Stocking, age, site index

Table 5. Coefficients of correlation for environmental and stand variables for stand growth (top right are results for 2009 measurement and bottom left results for period 2005 to 2009). Bold values are significant with $\alpha = 0.05$.

	CAI	C	OM	SWC	Elev	Lat	Ppgs	Ppt	VPD	Tmax	WI	PET	Trans	LAI	T_APAR	SI
CAI	**1**	0.19	0.19	**0.39**	**0.30**	**-0.37**	**0.65**	**0.68**	**-0.70**	**-0.73**	**0.65**	**-0.38**	**-0.40**	**0.46**	**0.33**	**0.78**
C	**0.20**	**1**	**0.99**	-0.02	-0.01	-0.16	0.15	0.08	-0.06	-0.16	-0.06	0.13	0.13	0.26	0.01	-0.09
OM	**0.20**	**0.99**	**1**	0.14	-0.22	0.07	-0.27	-0.10	-0.04	0.11	**0.49**	**-0.55**	**-0.55**	**0.65**	**0.70**	0.36
SWC	**0.33**	-0.07	0.11	**1**	**0.29**	-0.27	**0.42**	**0.42**	-0.19	**-0.29**	**0.59**	0.04	0.04	0.18	**0.30**	**0.36**
Elev	**0.14**	**-0.30**	**0.37**	**0.31**	**1**	-0.04	**0.33**	**0.36**	-0.08	-0.12	0.22	-0.01	-0.01	-0.07	-0.07	0.19
Lat	**-0.42**	-0.12	**-0.33**	**-0.35**	0.1	**1**	**-0.67**	**-0.53**	**0.30**	**0.53**	**-0.77**	**0.63**	**0.61**	**-0.34**	-0.20	-0.24
Ppgs	**0.48**	0.14	-0.01	**0.36**	0.07	**-0.72**	**1**	**0.94**	**-0.41**	**-0.61**	**0.71**	-0.26	-0.26	**0.35**	0.26	**0.47**
Ppt	**0.50**	0.11	0.11	**0.32**	0.07	**-0.66**	**0.82**	**1**	**-0.52**	**-0.64**	**0.71**	**-0.29**	**-0.30**	**0.39**	**0.35**	**0.52**
VPD	**-0.53**	-0.09	**0.20**	**-0.25**	-0.02	**0.23**	**-0.39**	**-0.48**	**1**	**0.93**	**-0.59**	**0.53**	**0.56**	**-0.33**	-0.24	**-0.73**
Tmax	**-0.57**	-0.16	0.13	**-0.35**	0.01	**0.47**	**-0.55**	**-0.58**	**0.89**	**1**	**-0.70**	**0.54**	**0.56**	**-0.36**	-0.26	**-0.74**
WI	**0.50**	-0.04	**0.42**	**0.59**	**0.19**	**-0.80**	**0.79**	**0.72**	**-0.43**	**-0.57**	**1**	**-0.73**	**-0.72**	**0.44**	**0.43**	**0.60**
PET	**-0.22**	0.19	**-0.63**	-0.02	0.00	**0.61**	**-0.30**	**-0.36**	**0.22**	**0.27**	**-0.66**	**1**	**-0.62**	**0.33**	**-0.29**	**-0.40**
Trans	**-0.22**	**0.20**	**-0.63**	-0.01	0.00	**0.59**	**-0.30**	**-0.36**	**0.23**	**0.27**	**-0.66**	**1.00**	**1**	**-0.36**	**-0.30**	**-0.42**
LAI	**0.43**	**0.36**	**0.31**	**0.31**	0.10	**-0.60**	**0.58**	**0.45**	**-0.30**	**-0.36**	**0.66**	**-0.51**	**-0.51**	**1**	**0.82**	**0.41**
T_APAR	**0.34**	0.11	**0.39**	**0.30**	-0.03	**-0.52**	**0.46**	**0.40**	**-0.29**	**-0.32**	**0.60**	**-0.52**	**-0.52**	**0.85**	**1**	-0.08
SI	**0.50**	-0.02	-0.17	**0.22**	0.11	**-0.29**	**0.40**	**0.48**	**-0.50**	**-0.49**	**0.45**	**-0.24**	**-0.25**	**0.25**	**0.29**	**1**

Note: CAI: Current annual increment [m^3 ha^{-1} yr^{-1}]; P_Br : Phosphorus Bray and Kurtz2 [ppm]; SWC: Soil water content [1m, mm]; Elev: altitude [m]; Lat : Latitude [° South]; Ppgs: Rainfall during growing season [mm yr^{-1}]; Ppt: Annual rainfall [mm yr^{-1}]; VPD: Vapor pressure deficit [bar]; Tmax: Annual maximum mean temperature [°C]; WI: Water deficit index [mm yr^{-1}] ; PET: Potential evapotranspiration [mm yr^{-1}]; LAI: Leaf area index [m^2 m^{-2}]; T_APAR: Annual intercepted active radiation [TJ ha^{-1} yr^{-1}]; SI: Site index [m, 20 yr old].

Table 6. Correlation coefficients for all environmental and stand variables, for year 2009 (top) and period 2005-2009 (bottom). Bold numbers represents significance with $\alpha = 0.05$.

	CAI	C	N	OM	P_Ol	P_Br	K	Ca	Mg	Al_ex	SWC	Sand	Silt	Clay	Elev	Lat	Lon	Dist	Ppgs	Ppt	VPD	Tmax	Tmin	WI	PET	Trans	T_PAR	LAI	T_APAR	Age	N	SI
CAI	**1**	0.19	0.12	0.19	0.04	**0.18**	-0.08	-0.02	-0.02	0.15	**0.39**	-0.04	0.10	-0.03	**0.30**	**-0.37**	-0.21	-0.18	**0.65**	**0.68**	**-0.70**	**-0.73**	0.09	**0.65**	**-0.38**	**-0.40**	0.03	**0.46**	**0.33**	-0.02	-0.23	**0.78**
C	**0.20**	**1**	**0.98**	**1.00**	-0.07	**-0.44**	0.10	**0.55**	0.13	**0.97**	-0.02	**-0.59**	**0.78**	0.16	-0.01	-0.16	0.01	0.06	0.15	0.08	-0.06	-0.16	0.27	-0.05	0.12	0.13	**-0.37**	0.26	0.01	0.33	0.34	-0.09
N	0.14	**0.98**	**1**	**0.98**	-0.03	**-0.50**	0.14	**0.54**	0.09	**0.96**	-0.06	**-0.54**	**0.77**	0.09	-0.01	-0.15	0.04	0.10	0.15	0.11	-0.03	-0.13	0.23	-0.06	0.11	0.12	-0.29	0.25	0.04	**0.39**	0.34	-0.17
OM	**0.20**	**1.00**	**0.98**	**1**	-0.07	**-0.44**	0.10	**0.55**	0.14	**0.97**	-0.02	**-0.59**	**0.78**	0.16	-0.01	-0.16	0.01	0.06	0.15	0.08	-0.06	-0.17	0.27	-0.05	0.12	0.13	**-0.37**	0.26	0.01	0.33	0.34	-0.09
P_Ol	-0.04	-0.08	-0.02	-0.08	**1**	**0.53**	**0.59**	0.27	-0.04	-0.15	-0.28	0.01	0.06	-0.08	0.30	0.09	-0.02	-0.05	0.04	0.13	0.00	0.05	-0.17	-0.06	-0.03	-0.04	0.12	0.24	0.24	0.11	0.09	0.02
P_Br	0.00	**-0.44**	**-0.44**	**-0.44**	**0.53**	**1**	-0.27	-0.21	**-0.57**	-0.42	0.14	**0.70**	**-0.60**	**-0.66**	-0.22	0.07	-0.28	-0.38	-0.27	-0.10	-0.04	0.11	-0.01	**0.49**	**-0.55**	**-0.55**	0.36	**0.65**	**0.70**	0.21	**-0.53**	0.36
K	0.04	**0.26**	**0.31**	**0.26**	**0.48**	**-0.21**	**1**	**0.40**	0.31	0.02	-0.25	**-0.50**	**0.36**	**0.45**	**0.64**	0.02	0.20	0.22	0.18	0.17	0.06	0.03	-0.27	-0.19	0.25	0.25	0.00	-0.21	-0.17	-0.19	**0.55**	-0.24
Ca	-0.04	**0.23**	**0.28**	**0.23**	**0.57**	-0.19	**0.89**	**1**	**0.70**	**0.44**	-0.02	**-0.70**	**0.66**	**0.47**	0.12	-0.10	-0.05	-0.03	0.05	-0.04	-0.03	-0.09	0.07	-0.17	0.30	0.30	**-0.38**	0.19	-0.05	-0.02	0.07	-0.05
Mg	-0.02	-0.02	0.00	-0.02	**0.40**	**-0.39**	**0.74**	**0.88**	**1**	0.02	0.20	**-0.66**	**0.41**	**0.67**	-0.01	-0.10	-0.16	-0.14	0.08	-0.08	-0.10	-0.16	-0.11	-0.09	**0.36**	**0.35**	-0.28	-0.17	-0.25	-0.30	-0.08	0.14
Al_ex	**0.18**	**0.96**	**0.95**	**0.96**	**-0.18**	**-0.35**	0.12	0.08	**-0.18**	**1**	-0.08	**-0.54**	**0.73**	0.14	0.03	-0.14	0.08	0.16	0.12	0.07	-0.01	-0.12	0.29	-0.10	0.13	0.14	**-0.41**	0.17	-0.08	0.31	**0.39**	-0.15
SWC	**0.33**	-0.06	-0.09	-0.06	**-0.38**	0.11	**-0.23**	**-0.30**	-0.14	-0.08	**1**	0.11	-0.18	0.01	**0.29**	-0.27	-0.01	0.02	**0.42**	**0.42**	-0.19	**-0.29**	0.07	**0.59**	0.04	0.04	**0.28**	0.18	**0.30**	**0.35**	**-0.43**	**0.36**
Sand	**-0.20**	**-0.63**	**-0.57**	**-0.63**	**0.19**	**0.62**	**-0.53**	**-0.47**	**-0.40**	**-0.56**	0.11	**1**	**-0.82**	**-0.81**	-0.18	0.08	-0.23	-0.23	-0.20	-0.04	-0.02	0.10	0.12	0.22	**-0.42**	**-0.42**	**0.50**	0.20	**0.41**	**0.35**	**-0.42**	0.09
Silt	**0.17**	**0.77**	**0.76**	**0.77**	0.00	**-0.47**	**0.51**	**0.50**	**0.33**	**0.72**	**-0.21**	**-0.85**	**1**	0.32	0.06	-0.09	0.17	0.20	0.21	0.13	-0.03	-0.14	0.05	-0.18	0.31	0.31	-0.31	0.03	-0.13	-0.05	**0.42**	-0.05
Clay	0.15	**0.21**	0.12	**0.21**	**-0.34**	**-0.62**	**0.35**	**0.25**	**0.32**	**0.17**	0.06	**-0.79**	**0.35**	**1**	0.24	-0.05	0.21	0.16	0.11	-0.07	0.07	-0.01	-0.25	-0.17	**0.38**	**0.38**	-0.51	**-0.35**	**-0.54**	**-0.53**	0.27	-0.09
Elev	**0.14**	**-0.30**	**-0.31**	**-0.30**	**-0.19**	**0.37**	**-0.46**	**-0.40**	**-0.44**	-0.12	**0.31**	**0.27**	**-0.40**	-0.01	**1**	-0.04	**0.35**	**0.45**	**0.33**	**0.36**	-0.08	-0.12	-0.13	0.22	-0.01	-0.01	-0.03	-0.07	-0.07	0.00	**0.31**	0.19
Lat	**-0.42**	-0.12	-0.10	-0.12	0.06	**-0.33**	0.16	0.04	0.01	-0.12	**-0.35**	0.03	0.00	-0.06	0.1	**1**	**0.49**	-0.10	**-0.67**	**-0.53**	**0.30**	**0.53**	**-0.37**	**-0.77**	**0.63**	**0.61**	-0.03	**-0.34**	-0.20	-0.23	0.04	-0.24
Lon	**-0.21**	**0.18**	**0.19**	**0.18**	-0.11	**-0.55**	0.14	0.05	-0.07	**0.27**	-0.10	**-0.30**	**0.27**	**0.23**	**0.55**	**0.55**	**1**	**0.68**	-0.12	-0.15	**0.54**	**0.56**	**-0.54**	**-0.41**	**0.52**	**0.53**	-0.05	**-0.28**	-0.19	-0.17	**0.35**	**-0.35**
Dist	**-0.19**	0.13	0.13	0.13	-0.08	**-0.32**	-0.10	-0.01	-0.10	**0.28**	-0.09	**-0.19**	**0.18**	0.13	**0.45**	0.05	**0.70**	**1**	0.04	-0.07	**0.51**	**0.41**	-0.22	-0.04	0.03	0.06	-0.03	-0.17	-0.11	-0.06	**0.54**	**-0.34**
Ppgs	**0.48**	0.14	0.13	0.14	-0.10	-0.01	-0.10	-0.06	-0.05	0.15	**0.36**	-0.07	0.07	0.05	0.07	**-0.72**	**-0.31**	**-0.14**	**1**	**0.94**	**-0.41**	**-0.61**	-0.11	**0.71**	-0.26	-0.26	0.09	**0.35**	0.26	0.15	-0.10	**0.47**
Ppt	**0.50**	0.11	0.11	0.11	-0.08	0.11	-0.14	-0.10	-0.10	0.14	**0.32**	-0.01	0.04	-0.04	0.07	**-0.66**	**-0.37**	**-0.22**	**0.82**	**1**	**-0.52**	**-0.64**	-0.12	**0.71**	**-0.29**	**-0.30**	0.17	**0.39**	**0.35**	0.22	-0.20	**0.52**
VPD	**-0.53**	-0.09	-0.06	-0.09	0.15	**0.20**	-0.07	0.02	-0.06	-0.06	**-0.25**	**0.24**	-0.10	**-0.31**	-0.02	**0.23**	**0.36**	**0.53**	**-0.39**	**-0.48**	**1**	**0.93**	-0.25	**-0.59**	**0.53**	**0.56**	-0.05	**-0.33**	-0.24	0.07	**0.36**	**-0.73**
Tmax	**-0.57**	**-0.16**	-0.12	**-0.17**	0.14	0.13	0.01	0.02	-0.05	-0.12	**-0.35**	**0.23**	-0.13	**-0.26**	0.01	**0.47**	**0.43**	**0.47**	**-0.55**	**-0.58**	**0.89**	**1**	**-0.31**	**-0.70**	**0.54**	**0.56**	-0.06	**-0.36**	-0.26	-0.01	**0.29**	**-0.74**
Tmin	**0.16**	-0.14	**-0.18**	-0.14	-0.02	**0.40**	**-0.27**	**-0.33**	**-0.36**	-0.13	-0.02	**0.30**	**-0.35**	-0.12	**-0.14**	**-0.20**	**-0.39**	**-0.25**	0.09	0.10	**-0.21**	**-0.20**	**1**	0.23	**-0.38**	**-0.37**	-0.09	0.06	-0.03	**0.30**	0.01	0.10
WI	**0.50**	-0.04	-0.07	-0.04	**-0.16**	**0.42**	**-0.35**	**-0.31**	**-0.24**	-0.02	**0.59**	**0.19**	**-0.25**	-0.04	**0.19**	**-0.80**	**-0.45**	-0.11	**0.79**	**0.72**	**-0.43**	**-0.57**	**0.31**	**1**	**-0.73**	**-0.72**	0.24	**0.44**	**0.43**	**0.30**	**-0.38**	**0.60**
PET	**-0.22**	**0.19**	**0.21**	**0.19**	-0.03	**-0.63**	**0.47**	**0.40**	**0.40**	0.15	-0.02	**-0.43**	**0.47**	**0.22**	0.00	**0.61**	**0.55**	0.08	**-0.30**	**-0.36**	**0.22**	**0.27**	**-0.56**	**-0.66**	**1**	**-0.62**	0.13	**0.33**	**-0.29**	0.19	-0.14	**0.55**
Trans	**-0.22**	**0.20**	**0.22**	**0.19**	-0.03	**-0.63**	**0.46**	**0.41**	**0.41**	**0.16**	-0.01	**-0.43**	**0.48**	**0.21**	0.00	**0.59**	**0.55**	0.09	**-0.30**	**-0.36**	**0.23**	**0.27**	**-0.57**	**-0.66**	**1.00**	**1**	-0.12	**-0.36**	**-0.30**	-0.14	0.15	**-0.40**
T_PAR	-0.03	**-0.34**	**-0.27**	**-0.34**	**0.22**	**0.27**	0.02	0.01	0.10	**-0.39**	0.11	**0.39**	**-0.28**	**-0.37**	**-0.20**	-0.10	**-0.44**	**-0.35**	0.03	0.12	-0.11	-0.08	0.11	0.13	-0.16	**-0.17**	**1**	-0.37	**0.76**	-0.13	0.17	-0.42
LAI	**0.43**	**0.36**	**0.33**	**0.37**	0.00	**0.31**	0.00	-0.01	-0.12	**0.32**	**0.31**	-0.08	0.11	0.02	0.10	**-0.60**	**-0.35**	-0.13	**0.58**	**0.45**	**-0.30**	**-0.36**	**0.24**	**0.66**	**-0.51**	**-0.51**	0.06	**1**	**0.82**	0.09	**-0.22**	**0.14**
T_APAR	**0.34**	0.11	0.12	0.11	0.13	**0.39**	0.01	-0.01	-0.06	0.05	**0.30**	0.16	-0.07	-0.21	-0.03	**-0.52**	**-0.51**	**-0.28**	**0.46**	**0.40**	**-0.29**	**-0.32**	**0.27**	**0.60**	**-0.52**	**-0.52**	**0.56**	**0.85**	**1**	**-0.02**	-0.23	0.78
Age	0.00	0.07	0.07	0.07	-0.03	**0.24**	-0.09	-0.16	**-0.21**	0.05	**0.14**	0.14	-0.08	**-0.16**	0.07	0.04	0.04	-0.02	**-0.26**	**-0.34**	**0.15**	0.11	0.00	**-0.15**	0.00	0.02	-0.06	0.13	0.10	**1**	-0.35	0.41
N	-0.04	**0.34**	**0.29**	**0.34**	**-0.40**	-0.12	**-0.35**	**-0.35**	**-0.43**	**0.43**	**-0.28**	**-0.17**	**0.22**	0.04	**0.19**	**0.19**	**0.50**	**0.52**	**-0.14**	**-0.19**	**0.29**	**0.24**	**-0.14**	**-0.22**	0.11	0.12	**-0.36**	**-0.14**	**-0.30**	0.05	**1**	**-0.08**
SI	**0.50**	-0.02	-0.09	-0.02	0.01	-0.17	0.03	0.06	**0.20**	-0.04	**0.22**	**-0.21**	0.13	**0.23**	0.11	**-0.29**	**-0.32**	**-0.28**	**0.40**	**0.48**	**-0.50**	**-0.49**	**0.16**	**0.45**	**-0.24**	**-0.25**	**0.19**	**0.25**	**0.29**	**-0.59**	**-0.34**	**1**

Note: CAI: Volume growth [m^3 ha^{-1} yr^{-1}]; C: Soil organic carbon [%]; N: Soil total nitrogen [%]; OM: Soil organic matter[%]; P_Ol: Phosphorus Olsen [ppm]; P_Br: Phosphorus Bray and Kurtz2 [ppm]; K: Soil potassium [ppm]; Ca: Soil calcium [ppm]; Mg: Soil magnesium [ppm]; Al_ext: Aluminum extractable [ppm]; SWC: Soil Water Holding Capacity [mm]; Sand: Sand texture [%]: Clay: Clay texture [%]; Elev: Elevation [m a.s.l]; Lat: Latitud [˚South]; Lon: Longitude [˚West]; Dist: Distance from Pacific ocean [km]; Ppgs: Growing season rainfall [mm yr^{-1}]; Ppt: Annual rainfall [mm yr^{-1}]; VPD: Vapor pressure deficit [bar]; Tmax: Averaged maximum temperature [˚C]; Tmin: Averaged minimum temperature [˚C]; WI: Water deficit index [mm yr^{-1}]; PET: Potential evapotranspiration [mm yr^{-1}]; Trans: Transpiration [mm yr^{-1}]; T_PAR: Annual Photosyntetically Active Radiation [TJ ha^{-1} yr^{-1}]; LAI: Leaf Area Index [m^2 m^{-2}]; T_APAR: Annual Intercepted Photosyntetically Active Radiation [TJ ha^{-1} yr^{-1}]; Age: [years]; N: Stocking [trees ha^{-1}]; SI: Site Index [m, averaged height 100 tallest trees]. Bold numbers have p-values <0.05.

Table 7. Select variables using linear regression procedures having Volume Growth [m^3 ha^{-1} yr^{-1}] as the dependent variable and the independent variables structured by soil, climatic, canopy and stand type categories for 2009 measurement.

Category	Independent variables	Regression	R^2
Soil	SWC, Lat	-57.9 + 0.03SWC - 2.07Lat	0.17 (P = 0.0154)
Climatic	Tmax , Rain	50.6 - 1.1Tmax + 0.006Rain	0.58 (P < 0.001)
Canopy	LAI	5.6 + 7.3LAI	0.19 (P = 0.0046)
Stand	SI	-11.9 + 1.2SI	0.60 (P < 0.001)
All	Tmax, LAI, Rain	329.4 + 4.1LAI - 22.7Tmax - 0.5 Rain + 0.4 $Tmax^2$ + 0. 04TmaxRain - 0.0007$Tmax^2$Rain	0.73 (P < 0.001)

Note: SWC: Soil Water Holding Capacity [mm]; Tmax: Averaged maximum temperature [˚C]; Lat: Latitud [˚South]; Rain: Annual rainfall [mm yr^{-1}]; LAI: Leaf Area Index [m^2 m^{-2}]; SI: Site Index [m, averaged height 100 tallest trees]

Table 8. Select variables using linear regression procedures having Volume Growth [m^3 ha^{-1} yr^{-1}] as the dependent variable and the independent variables structured by soil, climatic, canopy and stand type categories for period 2005-2009.

Category	Independent variables	Regression	R^2
Soil	Lat, SWC	-104.0 - 3.3Lat + 0.02SWC	0.20 (P < 0.0001)
Climatic	Tmax, WI	72.6 - 1.2Tmax - 0.012IWI	0.36 (P < 0.001)
Canopy	LAI	5.5 + 7.8LAI	0.18 (P <0.002)
Stand	SI	-0.2 + 0.7SI	0.25 (P < 0/0001)
All	Tmax, LAI, Rain	447.6 + 4.6LAI - 29.8Tmax - 0.5 Rain + 0.5 $Tmax^2$ + 0. 03TmaxRain - 0.0006$Tmax^2$Rain	0.48 (P < 0.001)

Note: SWC: Soil Water Holding Capacity [mm]; Tmax: Averaged maximum temperature [˚C]; Lat: Latitud [˚South]; Rain: Annual rainfall [mm yr^{-1}]; WI: Water deficit index [mm yr^{-1}]; LAI: Leaf Area Index [m^2 m^{-2}]; SI: Site Index [m, averaged height 100 tallest trees].

Table 9. Water and light supply, use, capture and use efficiency for conditions with high, medium or low availability of these site resources for period 2005 – 2009.

Resource	Water deficit index [mm yr-1]	Volume growth [m^3 ha^{-1} yr^{-1}]	Supply		Use	Capture	Use efficiency	
			Annual Rainfall [mm yr^{-1}]	Growing Season [mm yr^{-1}]	PET [mm yr^{-1}]	[%]	[m^3 m^{-3}]	[kg m^{-3}]
Water	Low [<-250]	29.1	1,720	646	682	0.40	0.0043	1.643
	Medium [-250-500]	22.6	931	238	717	0.77	0.0031	1.211
	High [<-500]	13.2	656	108	1,036	1.58	0.0013	0.492
			Annual PAR [TJ ha^{-1} yr^{-1}]		APAR [TJ ha^{-1} yr^{-1}]		[m^3 TJ^{-1}]	[g MJ^{-1}]
Light	Low [<-250]	29.1	32		22	0.69	1.32	0.50
	Medium [-250-500]	22.6	32		19	0.59	1.19	0.45
	High [<-500]	13.2	34		16	0.47	0.83	0.31

Note: Water use efficiency expressed by m^3 of wood per m^3 of water can be converted to [m^3 mm^{-1}] of water multiplying by 10. Volume growth was transformed to biomass using wood density values from Mora (2001).

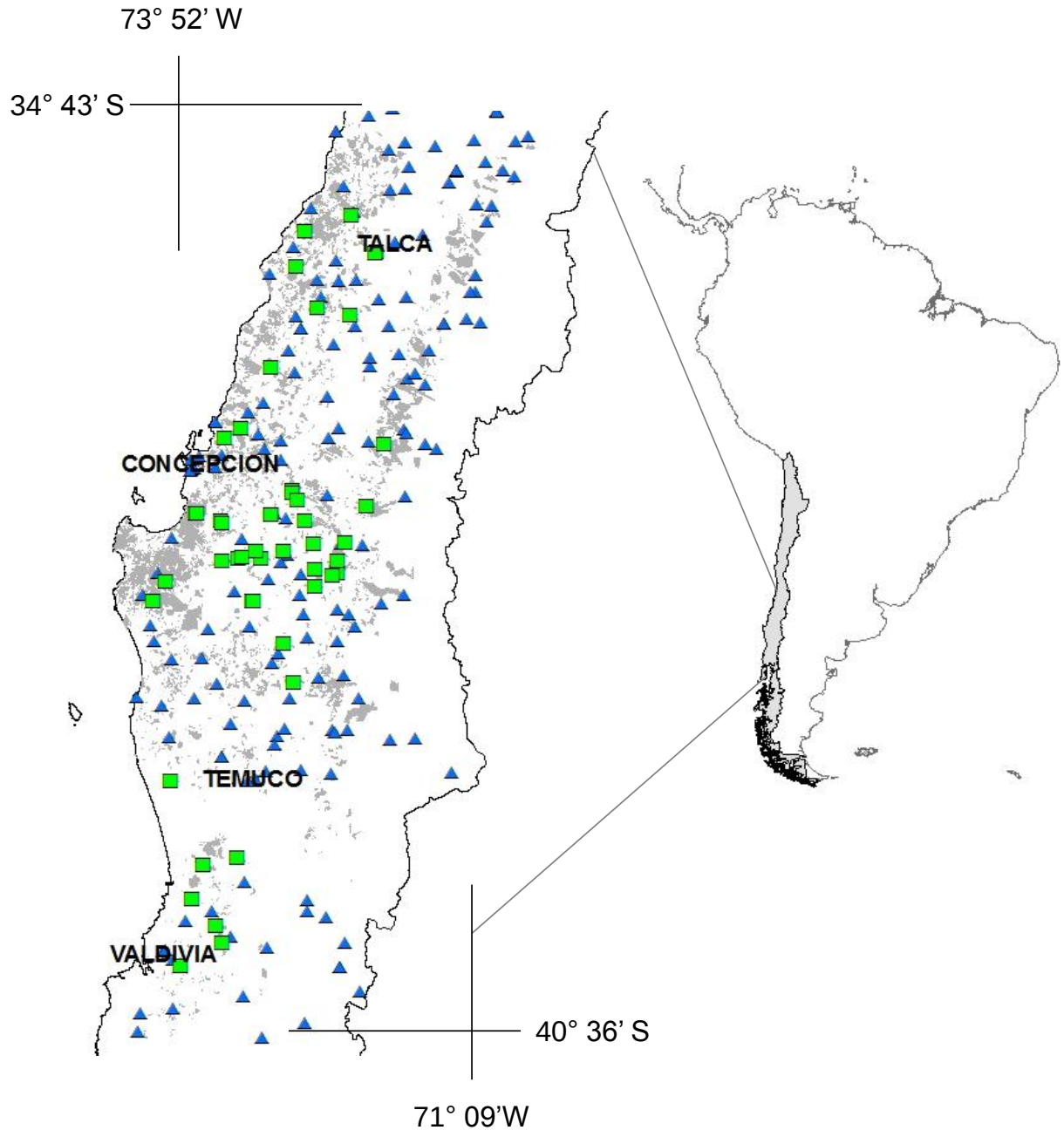

Figure 1. Study area in Chile, including forest plantations, location of permanent sample plots of Modelo Nacional de Simulación de Pino radiata de Chile, and the network of weather stations (networks of weather stations in blue; plot selected for analysis in green; and forest plantations in grey).

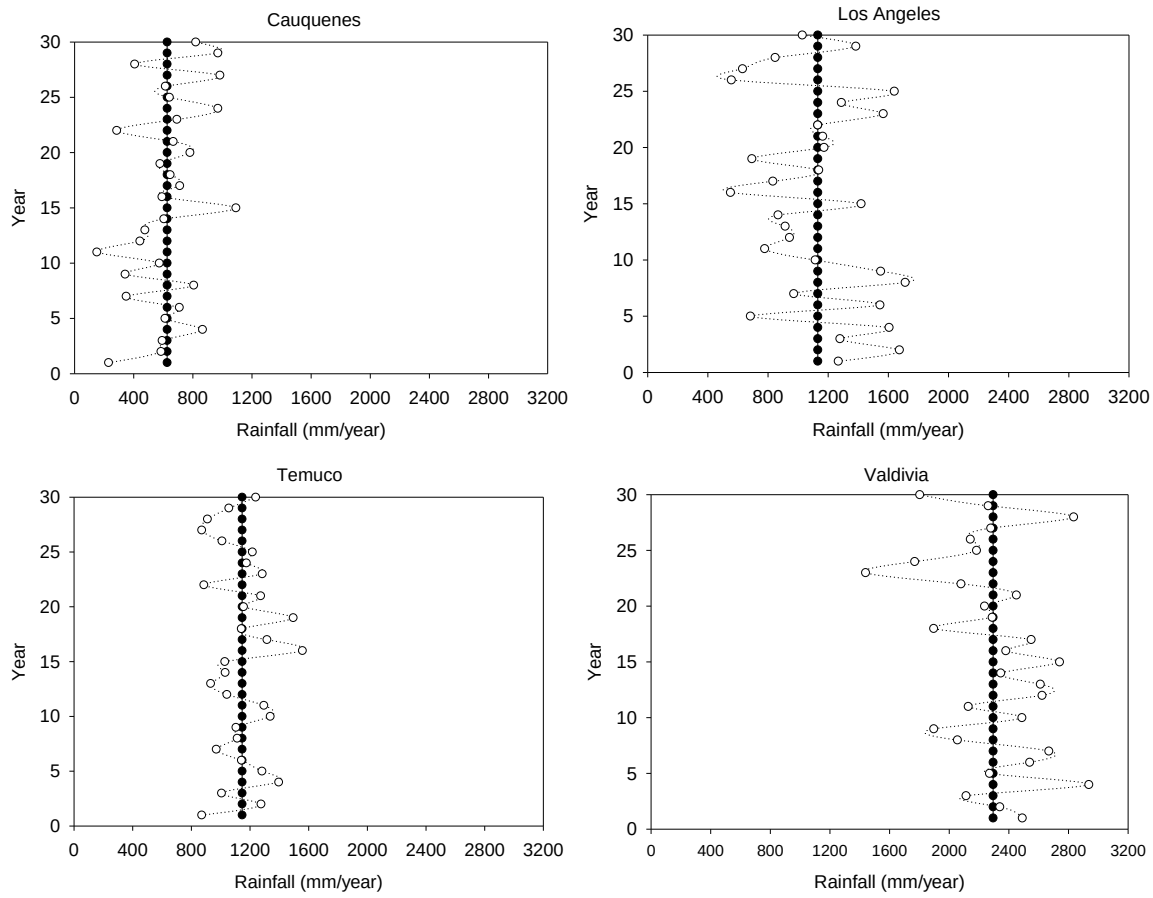

Figure 2. Variability of annual rainfall in north (Cauquenes), central (Los Angeles), south (Temuco), and southern-coast (Valdivia) of research area.

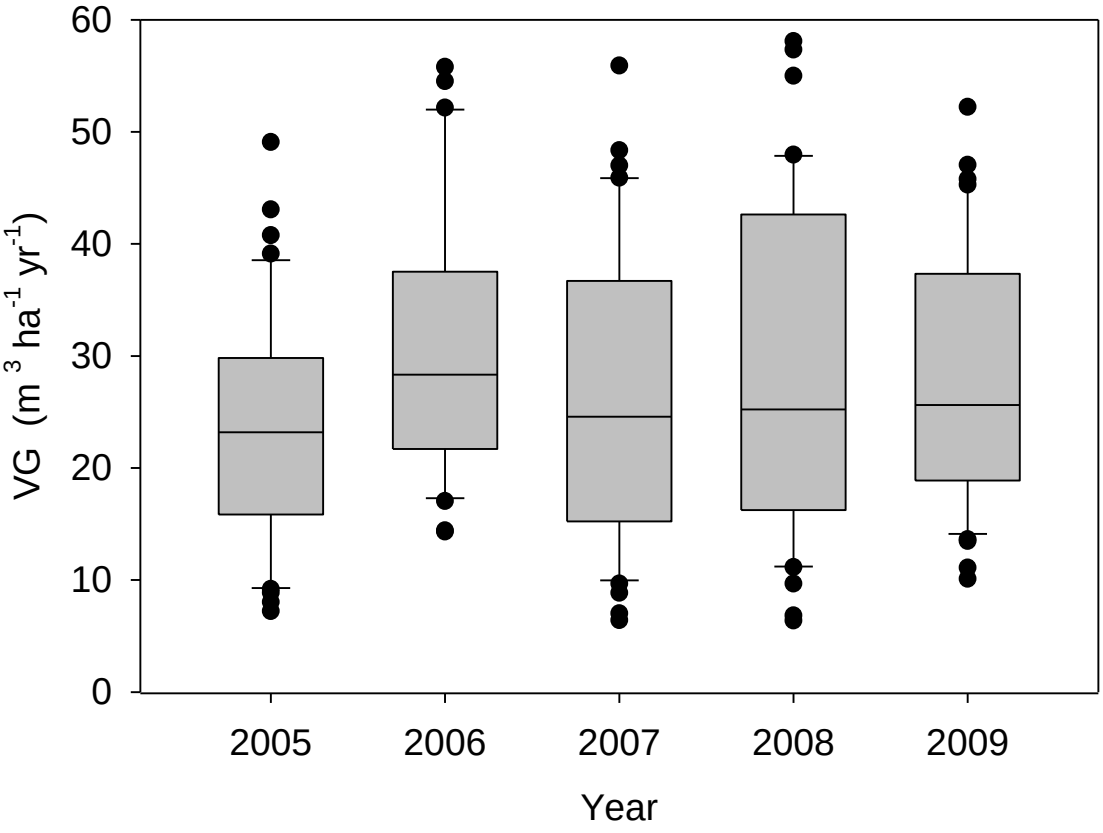

Figure 3. Volume growth per selected plots for period 2005 to 2009.

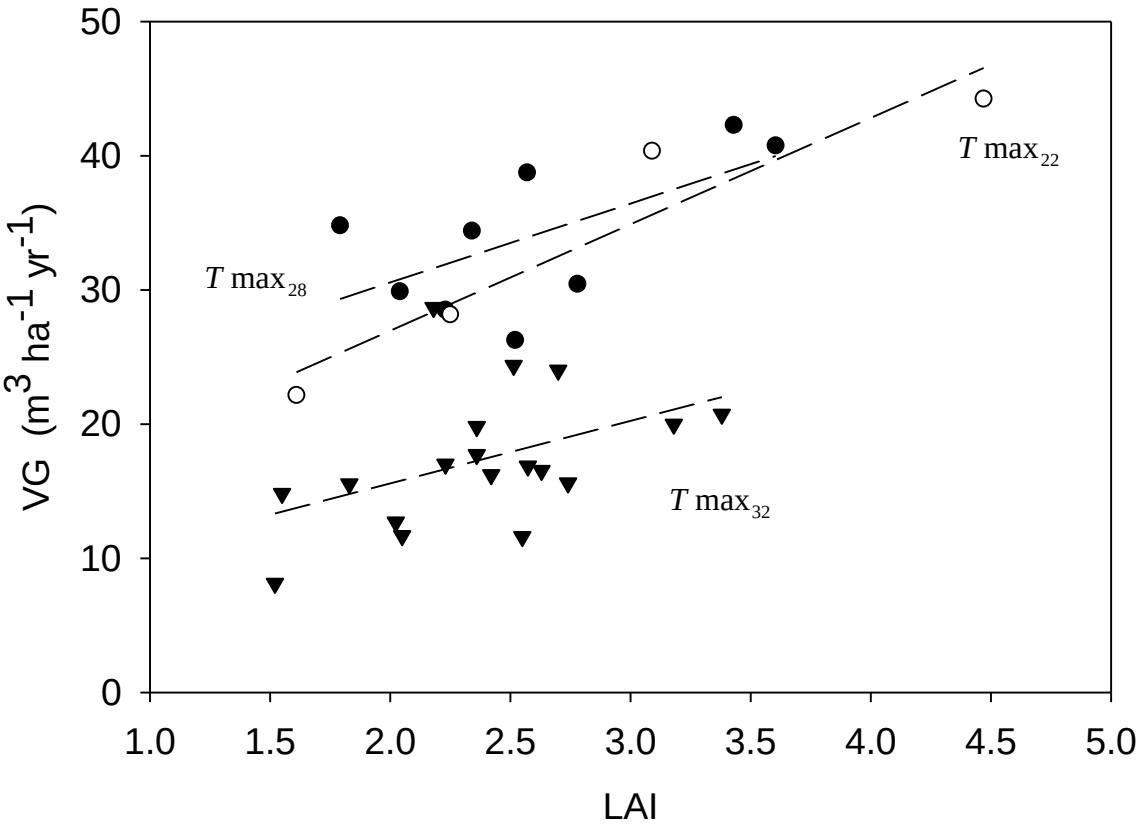

Figure 4. Relationship between volume growth and LAI under different levels of maximum temperature (Tmax) (● $Tmax_{22}$°C; ○ $Tmax_{28}$°C; ▼ $Tmax_{32}$°C) for 2009 measurement.

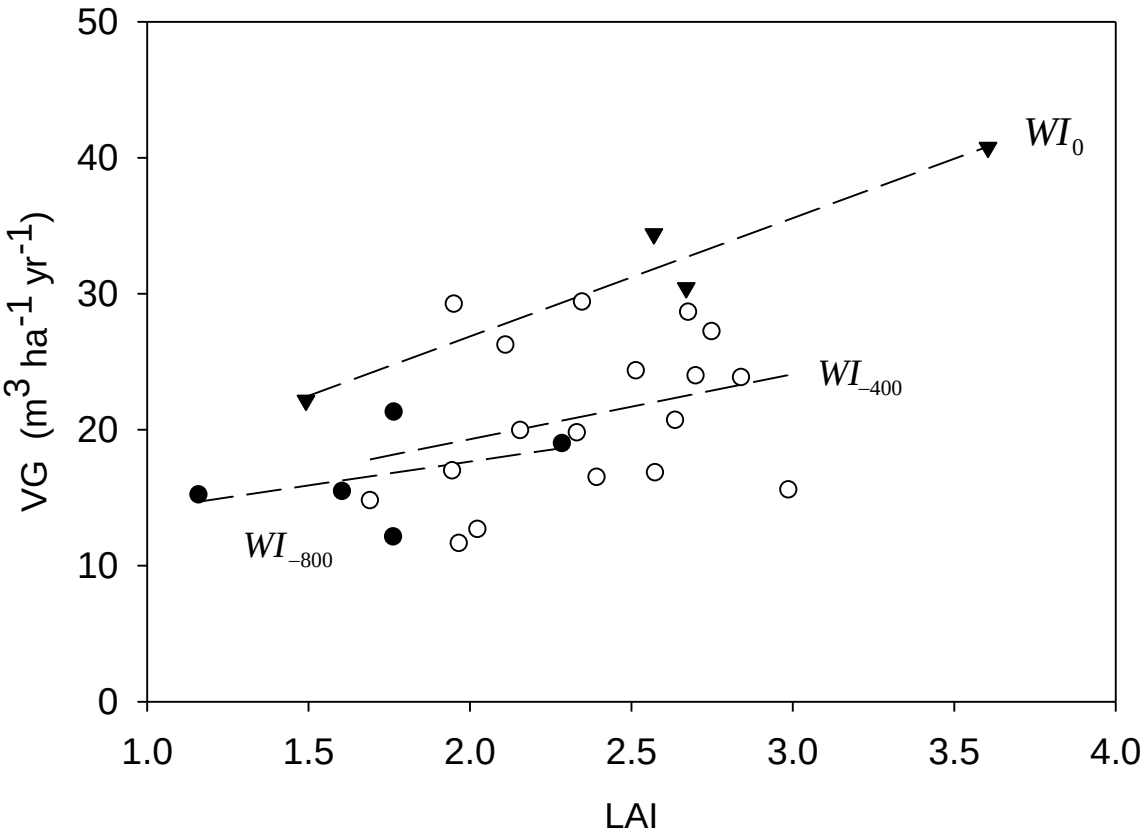

Figure 5. Relationship between volume growth and LAI under different levels of water deficit index (WI) (● WI_{-800} mm; ○ WI_{-400} mm; ▼ WI_0 mm) for 2009 measurement.

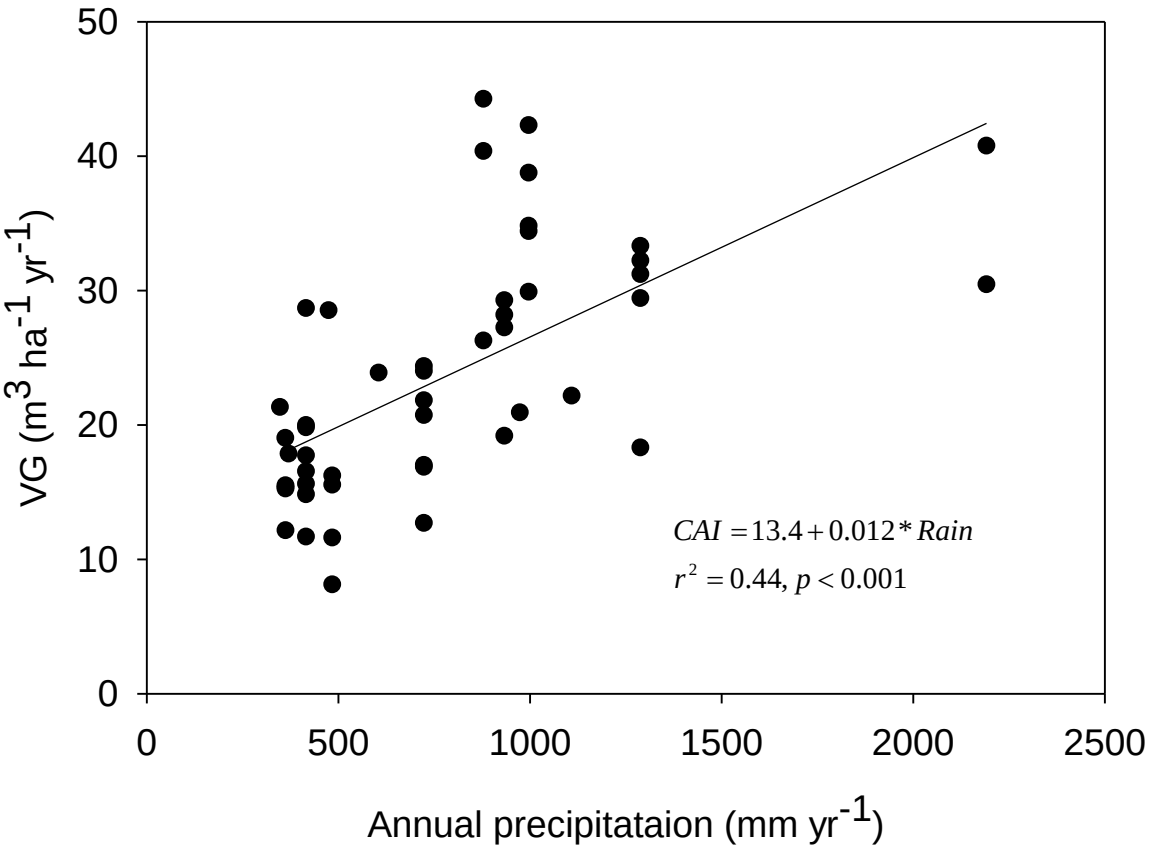

Figure 6. Relationship between stand growth volume and annual precipitation for 2009 measurement.

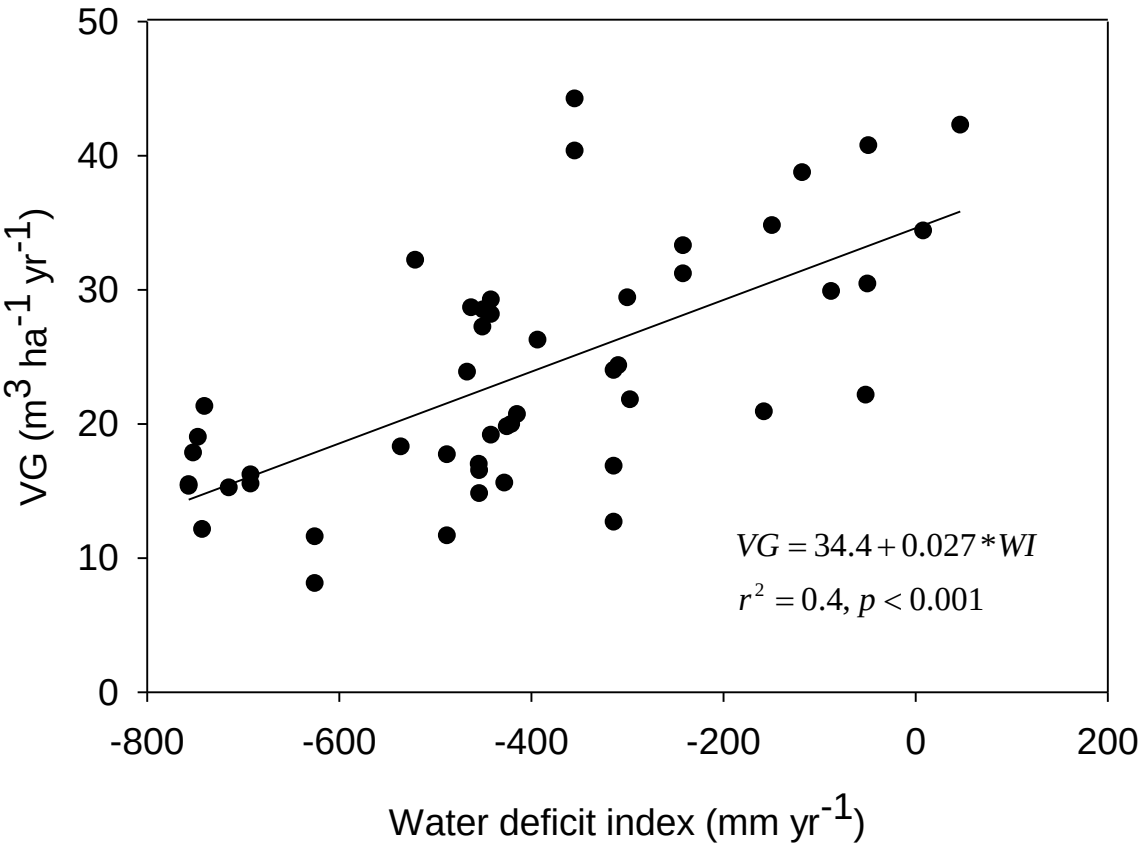

Figure 7. Relationship between volume growth and water deficit index for the 48 plots for 2009 measurement.

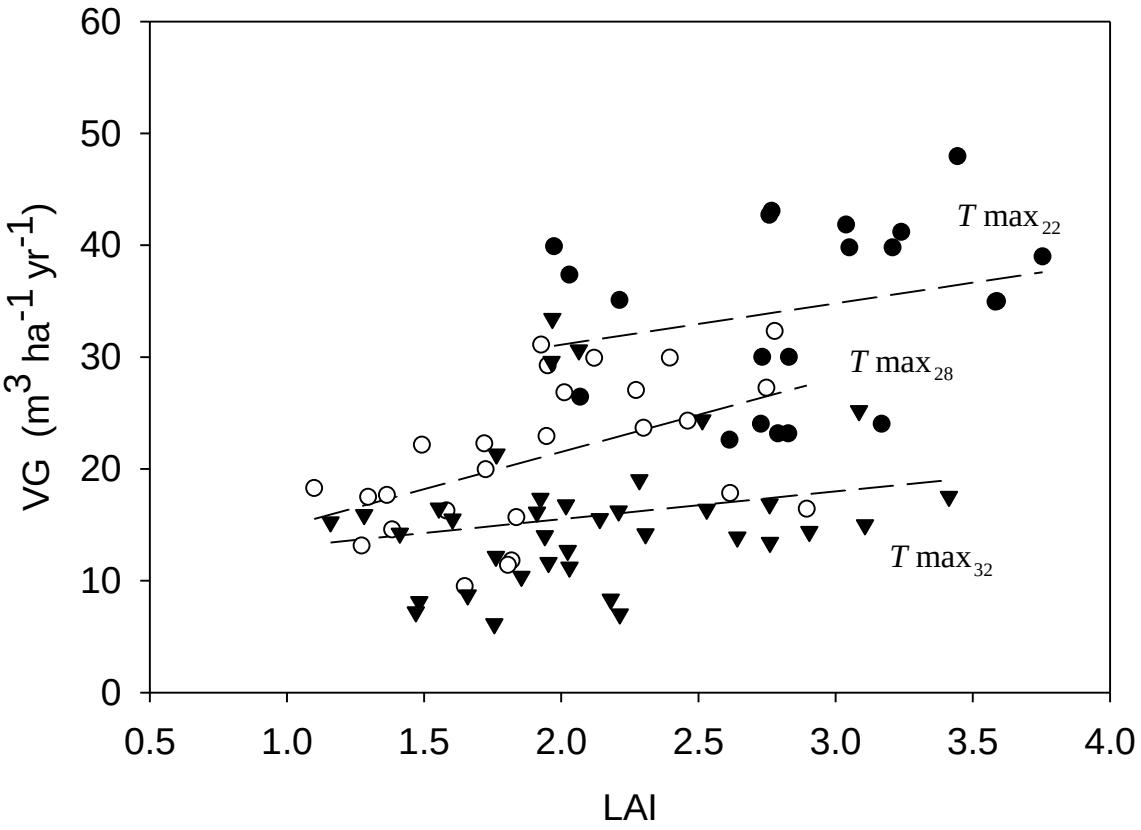

Figure 8. Relationship between volume growth and LAI under different levels of maximum temperature (Tmax) (● $Tmax_{22}$°C; ○ $Tmax_{28}$°C; ▼ $Tmax_{32}$°C) for 2005-2009 measurements.

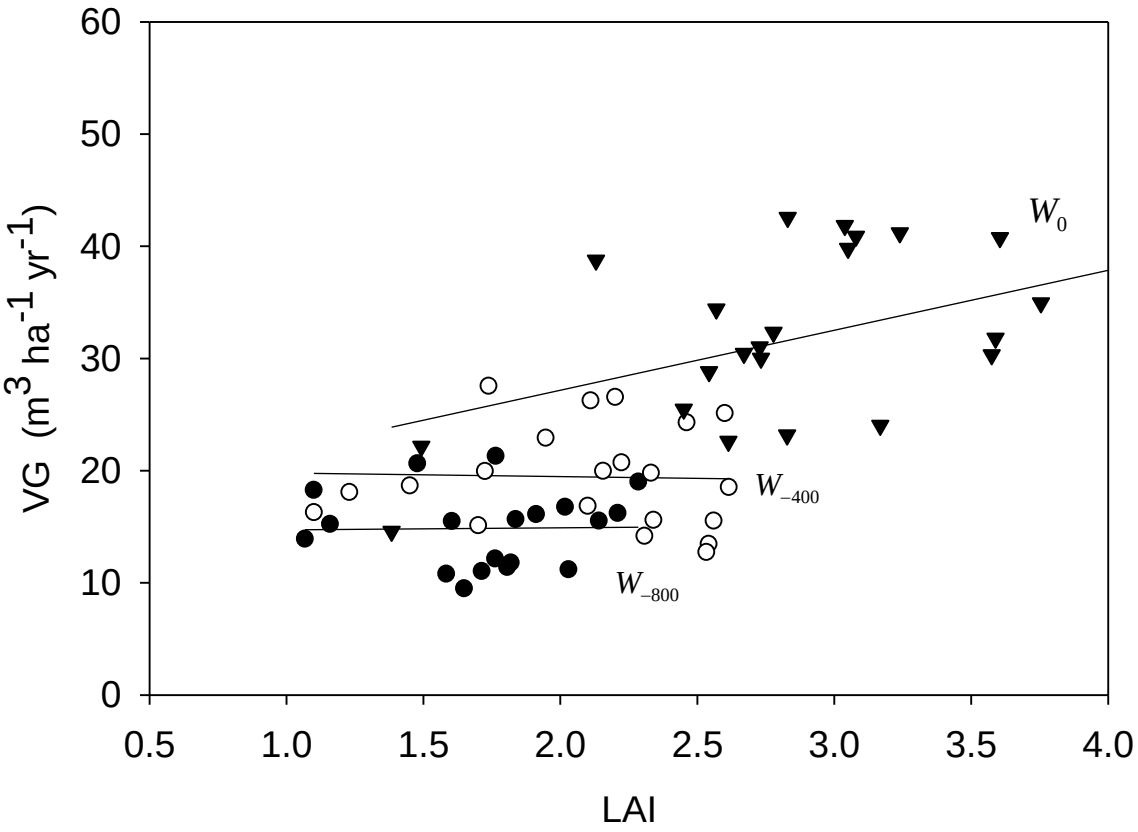

Figure 9. Relationship between volume growth and LAI under different levels of water deficit index (WI) (● WI_{-800} mm; ○ WI_{-400} mm; ▼ WI_0 mm) for 2005-2009 measurements.

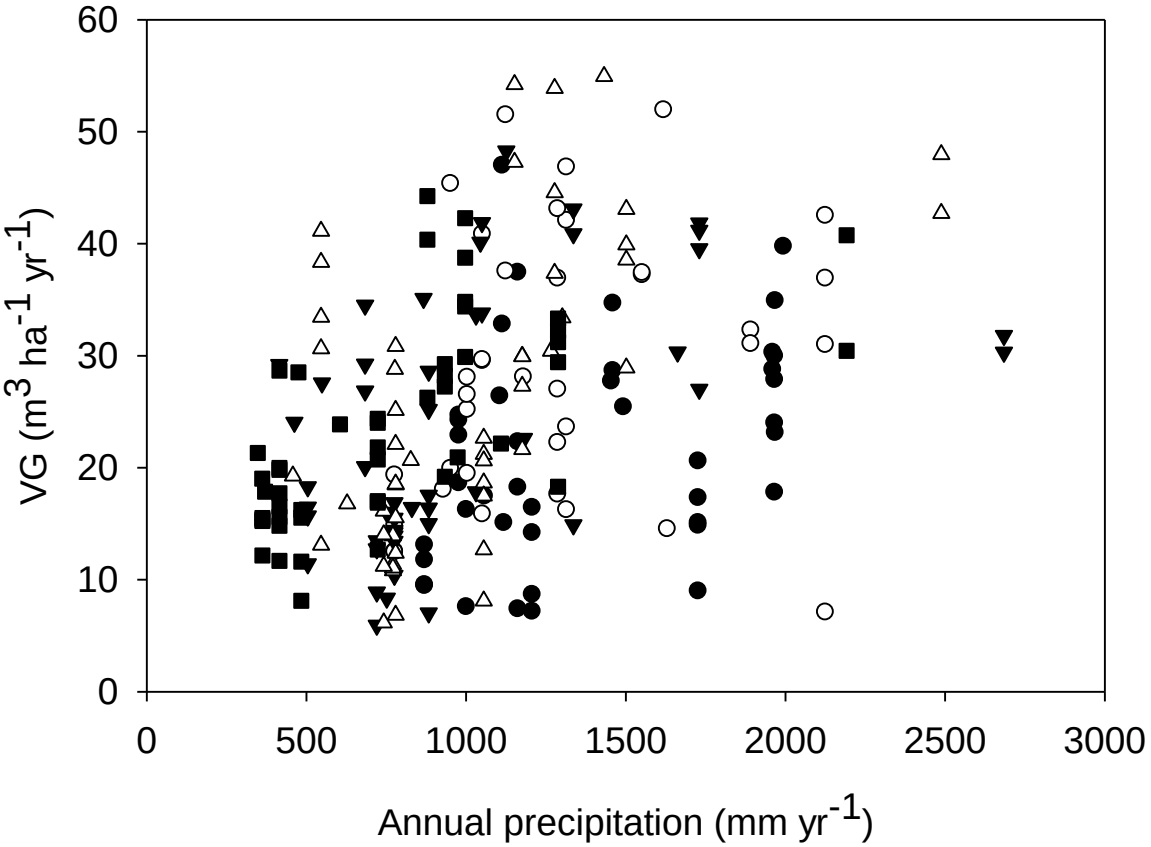

Figure 10. Relationship between volume growth and annual precipitation for years 2005 (●), 2006 (○), 2007 (▼), 2008 (Δ), and 2009 (■).

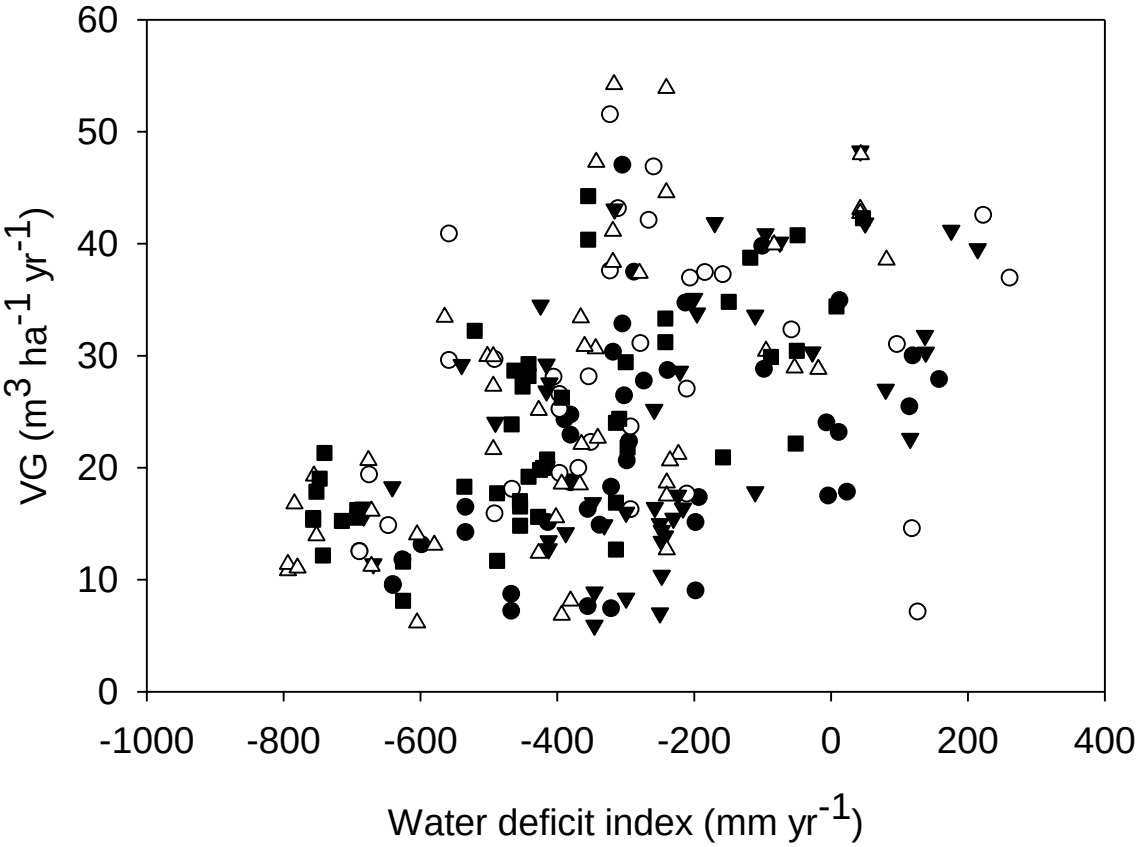

Figure 11. Volume growth and water deficit index for years 2005 (●), 2006 (○), 2007 (▼), 2008 (Δ), and 2009 (■).

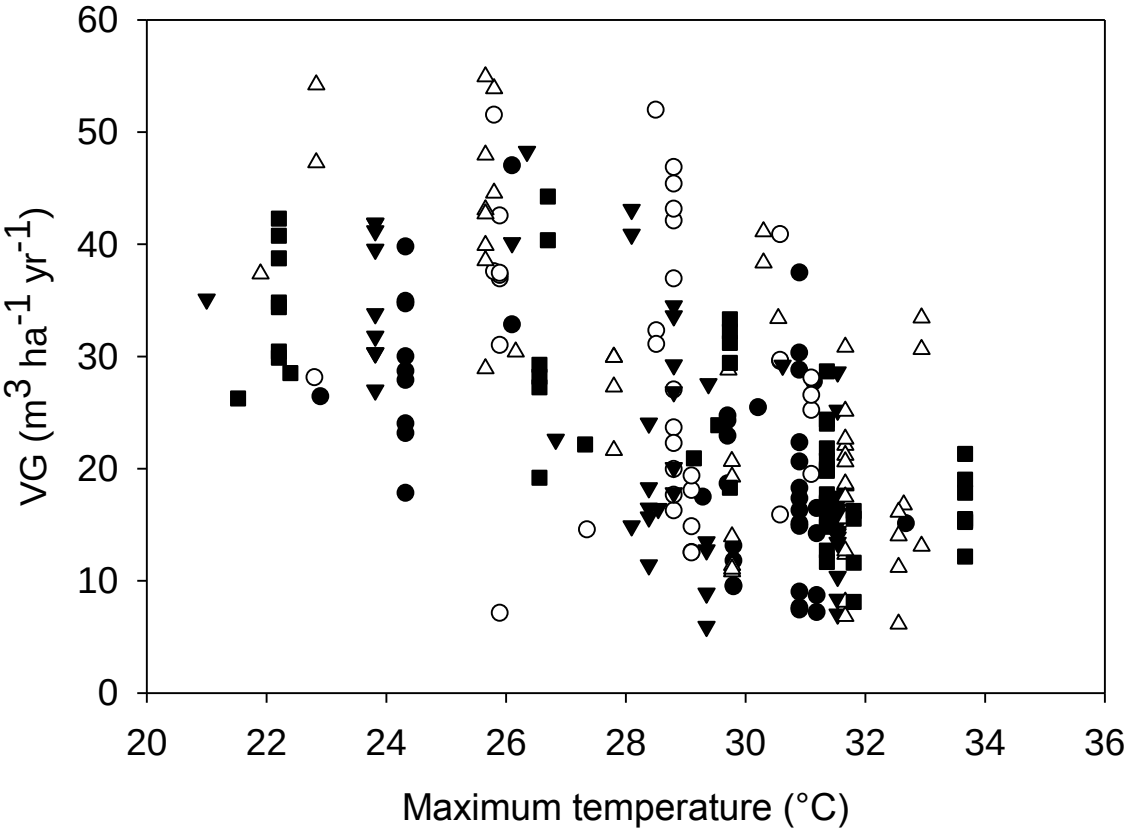

Figure 12. Relationship between volume growth and maximum temperature for years 2005 (●), 2006 (○), 2007 (▼), 2008 (Δ), and 2009 (■).

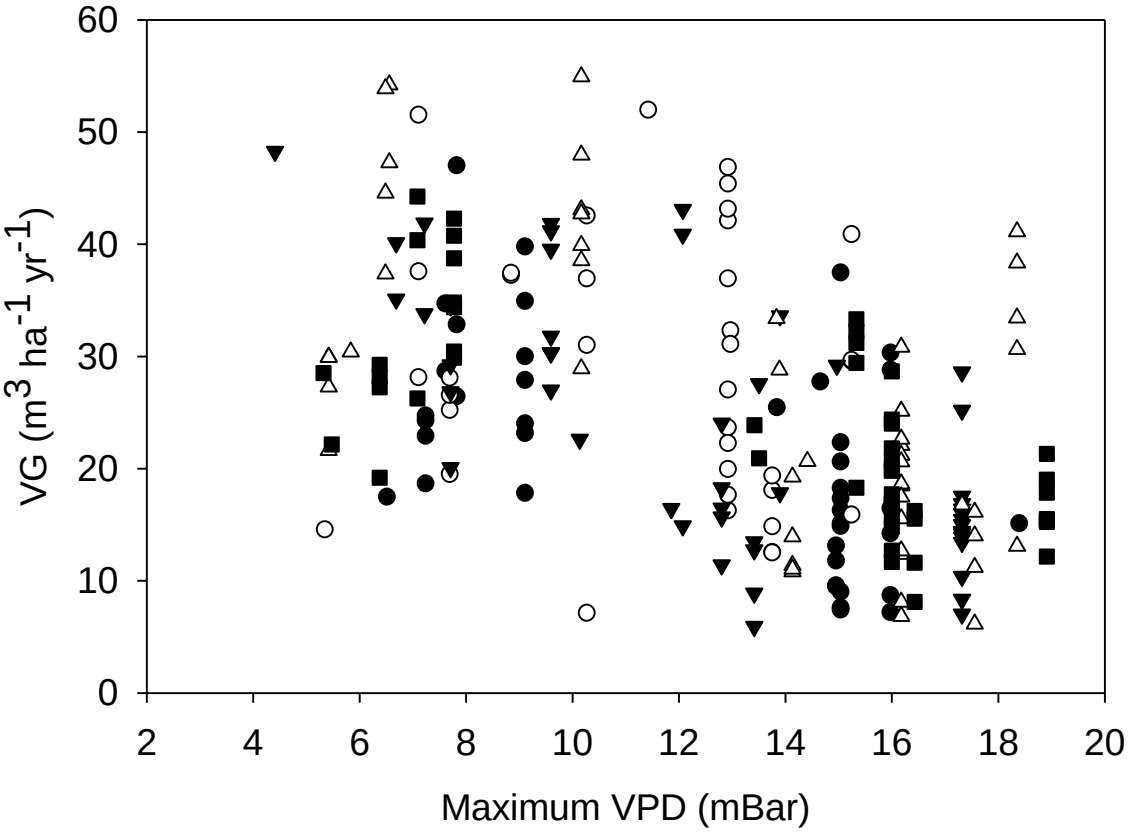

Figure 13. Relationship between volume growth and maximum VPD during the growing season for years 2005 (●), 2006 (○), 2007 (▼), 2008 (Δ), and 2009 (■).

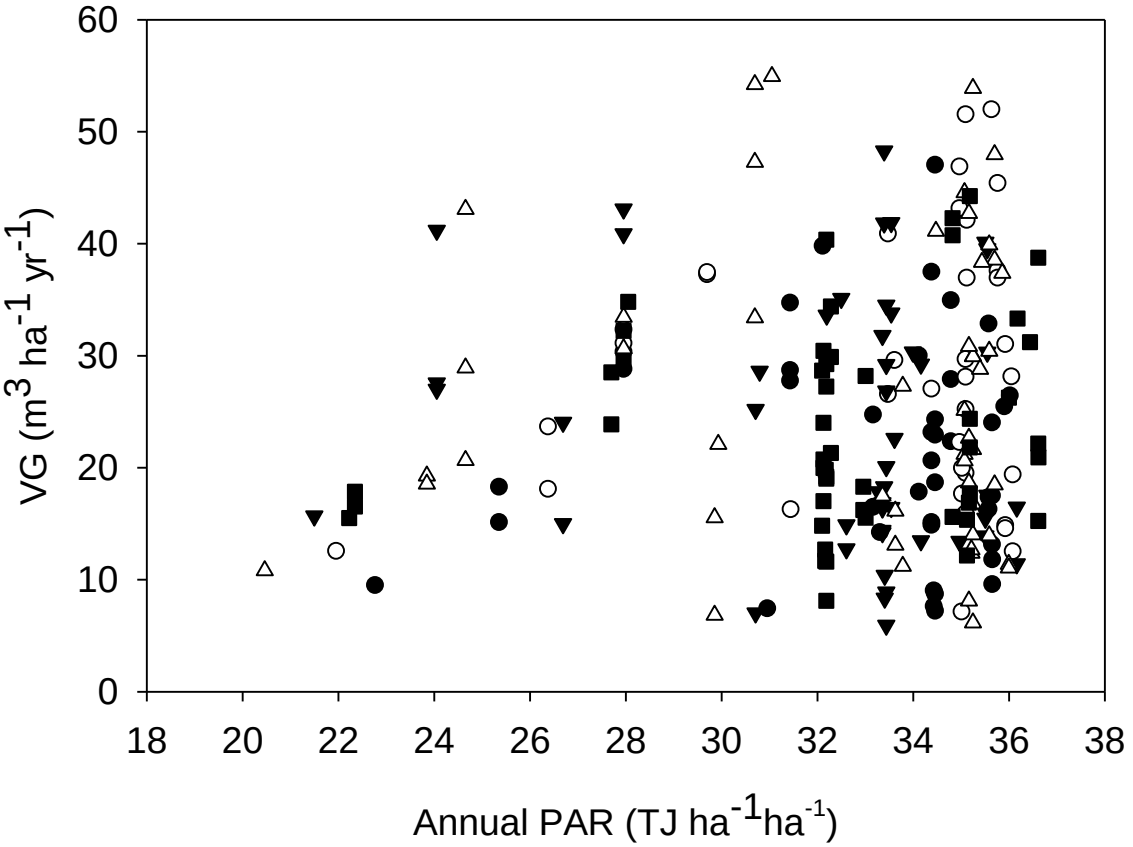

Figure 14. Relationship between volume growth and annual PAR for years 2005 (●), 2006 (○), 2007 (▼), 2008 (Δ), and 2009 (■).

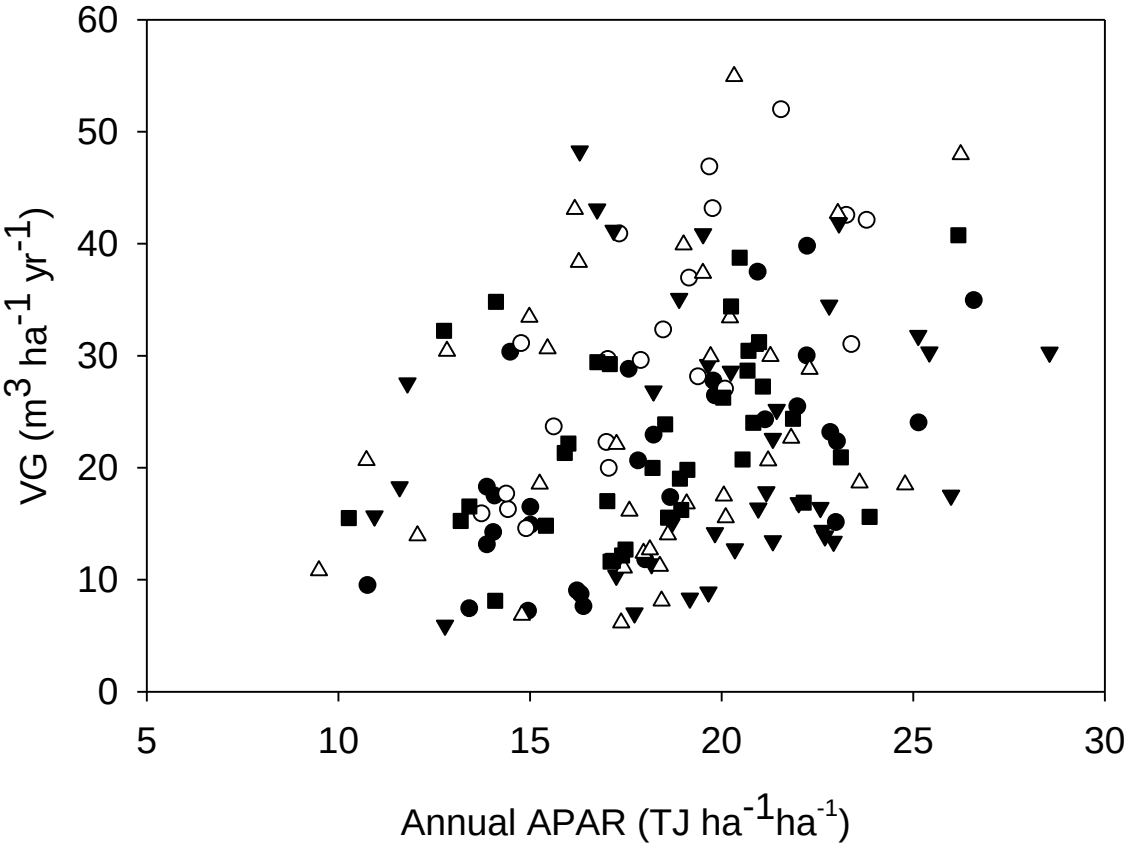

Figure 15. Relationship between volume growth and annual APAR for years 2005 (●), 2006 (○), 2007 (▼), 2008 (Δ), and 2009 (■).

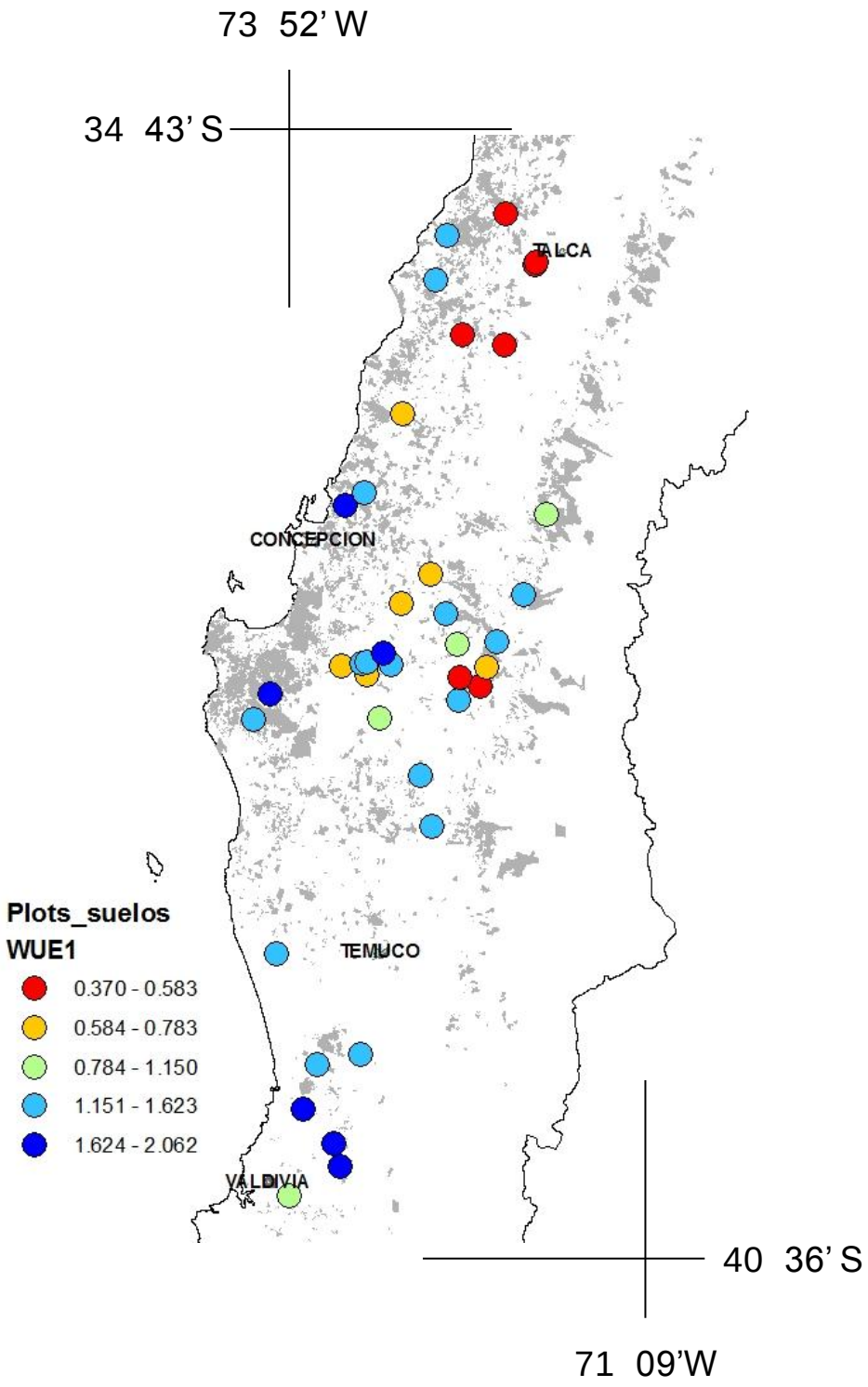

Figure 16. Average water use efficiency [kg stem biomass m^{-3} potential evapotranspired water] for period 2005-2009.

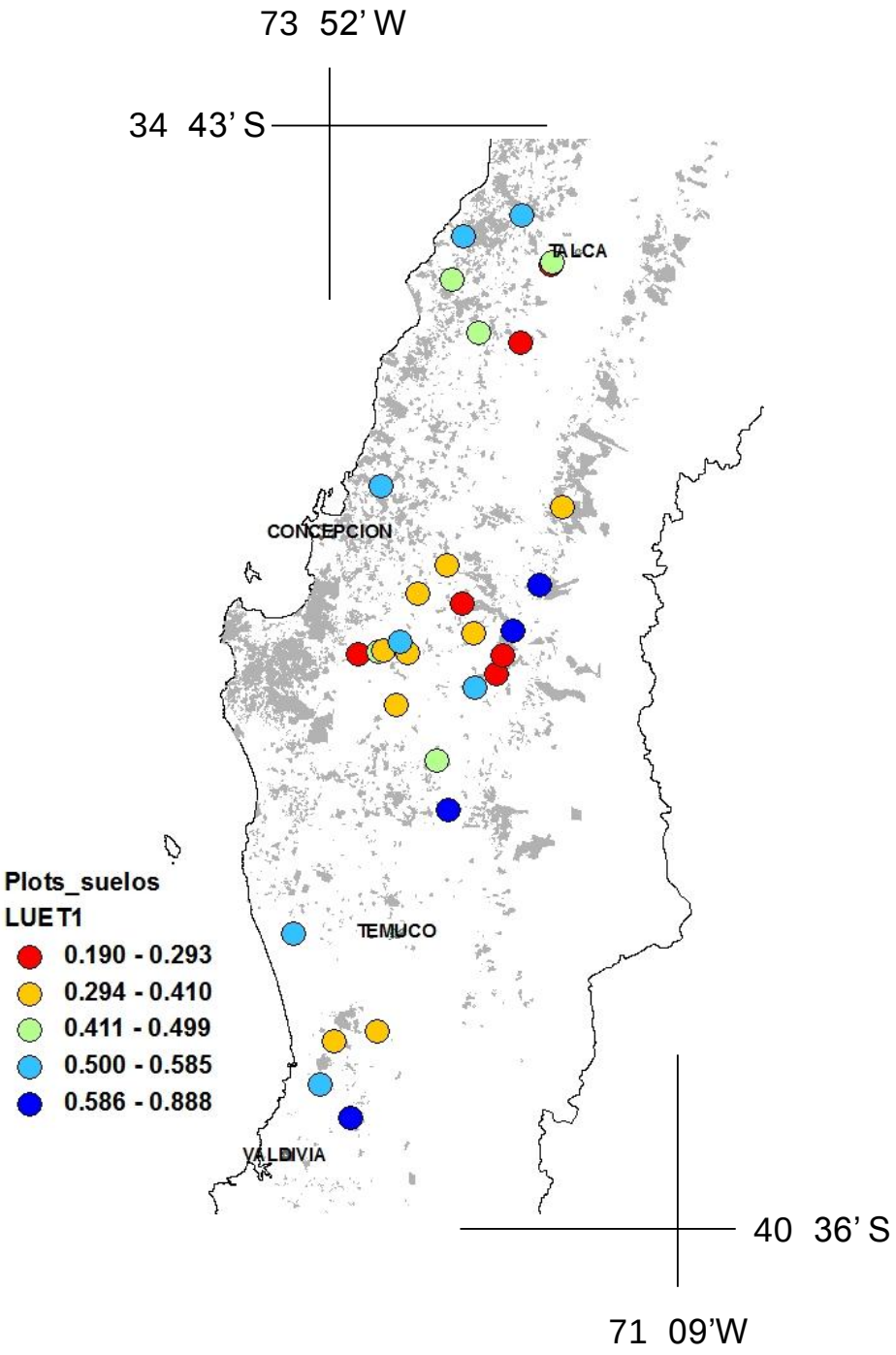

Figure 17. Average light use efficiency [g MJ^{-1}] for period 2005-2009.